

IVO SIBUL

Ground-penetrating radar in Estonia:
from fieldwork to open data reuse



IVO SIBUL

Ground-penetrating radar in Estonia:
from fieldwork to open data reuse



UNIVERSITY OF TARTU

Press

Department of Geology, Institute of Ecology and Earth Sciences,
Faculty of Science and Technology, University of Tartu, Estonia

Dissertation was accepted for the commencement of the degree of *Doctor philosophiae* in geology at the University of Tartu on 6 February 2023, by the Scientific Council of the Institute of Ecology and Earth Sciences, University of Tartu.

Supervisor: Assoc. Prof. Jüri Plado
University of Tartu, Estonia

Opponent: Asst. Prof. Jānis Karušs
University of Latvia, Latvia

Commencement: Estonia, University of Tartu, Chemicum, Ravila 14A, room
1019, on 22 May 2023 at 10.15

Publication of this thesis is granted by the Institute of Ecology and Earth Sciences, University of Tartu, and by the Doctoral School of Earth Sciences and Ecology created under the auspices of the European Social Fund.

ISSN 1406-2658 (print)
ISBN 978-9916-27-166-7 (print)
ISSN 2806-2310 (pdf)
ISBN 978-9916-27-167-4 (pdf)

Copyright: Ivo Sibul, 2023

University of Tartu Press
www.tyk.ee

CONTENTS

LIST OF ORIGINAL PUBLICATIONS	6
ABBREVIATIONS.....	7
1. INTRODUCTION.....	8
2. BACKGROUND.....	11
3. MATERIAL AND METHODS	15
3.1 Description of the study areas.....	15
3.2 Ground-Penetrating Radar	18
3.2.1 Principles	18
3.2.2 Data processing.....	22
3.2.3 Applications.....	24
3.2.4 Estonian experiences.....	27
3.2.5 Four case studies.....	30
4. RESULTS AND DISCUSSION	32
4.1 Superficial deposits	32
4.1.1 Peatlands.....	32
4.1.2 Coastal and aeolian environments	35
4.2 Carbonate bedrock	38
4.3 (Glacio)tectonic activities	40
5. RAISING THE EFFICIENCY OF THE GPR STUDIES.....	43
5.1 Geological mapping	43
5.2 Resource assessment.....	45
5.2.1 Peat	46
5.2.2 Aggregates	48
5.3 GPR antennas and carriers	50
5.4 Data processing and management.....	51
5.5 Data sharing	52
6. CONCLUSIONS.....	54
REFERENCES.....	56
SUMMARY IN ESTONIAN	77
ACKNOWLEDGEMENTS	80
PUBLICATIONS	81
CURRICULUM VITAE	137
ELULOOKIRJELDUS.....	139

LIST OF ORIGINAL PUBLICATIONS

This thesis is based on the following published papers, which are referred to in the text by their Roman numerals.

- Paper I Plado, J., **Sibul, I.**, Mustasaar, M., Jõelet, A. 2011. Ground-penetrating radar study of the Rahivere peat bog, eastern Estonia. *Estonian Journal of Earth Sciences*, 60(1), pp. 31–42.
- Paper II Muru. M., Rosentau, A., Preusser, F., Plado, J., **Sibul, I.**, Jõelet, A., Bjursäter, S., Aunap, R., Kriiska, A. 2018. Reconstructing Holocene shore displacement and Stone Age palaeogeography from a foredune sequence on Ruhnu Island, Gulf of Riga, Baltic Sea. *Geomorphology*, 303, pp. 434–445.
- Paper III **Sibul, I.**, Plado, J., Jõelet, A. 2017. Ground-penetrating radar and electrical resistivity tomography for mapping bedrock topography and fracture zones: a case study in Viru-Nigula, NE Estonia. *Estonian Journal of Earth Sciences*, 66(3), pp. 142–151.
- Paper IV Jõelet, A., **Sibul, I.**, Mustasaar, M., Plado, J. 2022. Bedrock deformations in northeastern Estonia based on ground-penetrating radar data. *Estonian Journal of Earth Sciences*, 71(4), pp. 189–200.

Author's contribution:

- Paper I The author participated in the fieldworks and data analyses. The paper was induced by the master's thesis of the author.
- Paper II The author participated in the fieldworks, data analyses and writing the manuscript.
- Paper III The author participated in the fieldworks, was responsible for the GPR data analyses, writing and submitting the manuscript.
- Paper IV The author participated in the data analyses and writing the manuscript.

ABBREVIATIONS

CMP	common midpoint
DEM	digital elevation model
GA	Geological Archive of Estonia
Geo3D	Estonian Land Board's 3D strategy
EGD	Engineering Geology Database
ELB	Estonian Land Board
EM	electromagnetic
ERT	electrical resistivity tomography
GIS	geographic information system
GBM	Geological Base Map of Estonia (1:50 000)
GPR	ground-penetrating radar
GSE	Geological Survey of Estonia
GPS	Global Positioning System
LiDAR	light detection and ranging
ML	machine learning
MR	Mineral Registry of Estonia
ns	nanosecond
OSL	optically stimulated luminescence
TWT	two-way traveltime
UT	University of Tartu
UXO	unexploded ordnance
VDZ	Vaivara Deformation Zone
WARR	wide angle reflection and refraction

1. INTRODUCTION

Geological studies frequently result in different scale maps and cross-sections. Estonian geologists have systematically assembled subsurface data during the last two centuries (Kirsimäe et al. 2020). In the light of today's understanding, the earliest maps (Engelhardt and Ulprecht, 1830; Schmidt, 1858) seem rather rudimentary. Besides reflecting the historical *status quo* of the Earth sciences, they also formed a foundation for the following map releases. Afterwards, our geological knowledge has continuously expanded due to thousands of core sections supplementing the outcrops' descriptions.

In the middle of the 20th century, extensive mapping campaigns were induced by the need for new mineral and water resources. At the same time, geophysical methods (gravimetric, magnetometric, electrometric, borehole geophysical logging) were broadly introduced (Klein, 2012). By the 1970s, the whole country was covered with maps at the scale of 1:200 000. Since the 1980s, mapping has been focused on the scale of 1:50 000. Currently, the Geological Survey of Estonia (GSE) compiles the Geological Base Map (GBM) at the same scale (1:50 000) for western and central Estonia (GSE, 2022a).

Before the deep mapping projects, Estonian bedrock was treated as a simple subhorizontal homocline. According to the present insight, structural activities, Late Pleistocene glaciations and other post-depositional processes have modified the geologic column significantly (Rõõmusoks et al., 1997). Quaternary succession has often been affected by the bedrock's layout and topography. Buried valleys, faults and karst features can change the subsurface properties considerably at a relatively short distance (Rattas and Kalm, 2004; Pirrus, 2007; Vaher et al., 2010).

During the last couple of decades, non-invasive geophysical techniques like ground-penetrating radar (GPR), electrical resistivity tomography (ERT), seismic sensing, measurements of the gravity and magnetic fields, palaeomagnetic analyses etc., have been increasingly applied for characterising the subsurface structures (Vaher et al., 2013; Plado et al., 2016, Dmitrijeva et al., 2018; Plado et al., 2020). Despite diverse digital outputs and models that have been developed recently (Rautenberg et al., 2015; Gorlach et al., 2015; Ani and Meidla, 2020), the mapping process itself has not changed much. On the field, drilling and test pitting have remained the conventional choices for obtaining new data. Yet these approaches have a few limitations:

- (a) direct measurements are expensive and time-consuming,
- (b) boreholes and trial pits can not provide continuous data flow laterally,
- (c) at some locations (rough terrain, environmental restrictions), drilling and pitting may contravene safety or legislation.

As an employee of the Estonian Land Board (ELB), the author has been dealing with geological maps since 2005. The constant demand for enhancing mapping speed and quality encouraged to set up the current thesis. Grasmueck et al. (2005) express:

Geoscientists, archaeologists, and engineers require clear three-dimensional views of the shallow subsurface to see internal geometry and to understand how rock, soil, water, and life interact.

Ground penetrating radar (GPR) can provide such knowledge with quick data capture and high precision. According to the GPR practice in Estonia and abroad, the device works well in soft sediments like sand and peat. Similarly, good results have been achieved in detecting the bedrock top surface. However, until now all those individual findings have not been summarised. The author tries to put the previous Estonian GPR experiences into a broader context in order to motivate the future research.

The thesis is based on four case studies wherein the author has personally contributed. One case focuses on peat's lithological and volumetric description (the Rahivere Bog; Paper I), another on the development of coastal (foredune) ridges (the Ruhnu Island; Paper II). Two sites (Viru-Nigula; Paper III, and the Sillamäe-Narva area; Paper IV) are somewhat related. Both represent the bedrock successions in NE Estonia that were structurally reshaped afterwards. Nevertheless, the causes and consequences of the geological processes were substantially disparate in those regions. While Papers III and IV showed up from the unsolved mysteries, Papers I and II were triggered by more practical needs.

The GPR data were collected during several field campaigns in all the case studies. Therefore it was possible to analyse the results in the meantime, and densify the profiling network at certain locations. Papers I and II confirm coring is the best approach for supporting the radar soundings. Paper III reveals the benefits of combining the GPR and ERT methods in one survey. Paper IV also concedes GPR alone can not provide answers for all the questions. In any case, more transparent capabilities of GPR should favour the right decisions for the following research.

The shortcomings encountered during the PhD studies inspired the author to seek better ways for the radar utilisation. Recent advances in GPR and information technologies indicate both the fieldwork and data post-processing can be enhanced significantly. ELB has witnessed impressive prospects emerging from the open data philosophy. Hopefully the GPR fieldwork results, handled as standardised spatial data packages, can reinforce geological mapping and mineral resource estimation workflows.

The main aims of the thesis are:

- (a) to specify the GPR potential by using the method in various environments, and recommend additional applications,
- (b) to compile an overview of the GPR studies carried out in Estonia, and propose new procedures for increasing the data collection and management efficiency.

2. BACKGROUND

Estonia is located on the outskirts of the East-European Platform, bordered by the Fennoscandian Shield in the NW (Puura and Vaher, 1997; Tuuling and Flodén, 2016). Palaeo- and Mesoproterozoic rock complexes are overlain by 100–800 m thick Neoproterozoic and Palaeozoic sedimentary successions (All et al., 2004; Kirs et al., 2009; Meidla, 2014). According to a simplified concept, the sedimentary bedrock comprises Ediacaran, Cambrian and Lower Ordovician sandstones, siltstones, claystones, covered by carbonate rocks (limestones, dolostones, marls) of the Ordovician and Silurian periods and Devonian sand- and siltstones as the topmost bedrock strata. These layers have a gentle southern dip (average 0.10–0.20°, or 2–3.5 m per km, Soesoo et al., 2020). As a result of such inclination, the map represents younger successions southwards (Fig. 1). Hence, in northern Estonia and on bigger islands, the uppermost bedrock consists generally of limestones and dolostones. The bedrock is thicker in southern Estonia, where the carbonate rocks are covered with sandstones.

Throughout geological history, Estonian territory has undergone numerous periods of crustal instability (Puura and Klein, 1997). The signs of those activities were recorded in the rocks as faults and other deformations frequently associated with the Early Palaeozoic Caledonian orogeny (Puura and Vaher, 1997; Tuuling and Põldsaar, 2021). Due to comprehensive studies, more faults have been described in northern Estonia (Fig. 1). The upper surface of bedrock is articulated by ancient river valleys (Raukas and Tavast, 1987; Miidel et al., 2006), often reshaped by the Late Pleistocene glaciers. In northern Estonia, the valleys are typically parallel-oriented and aligned in the NW–SE direction, while within the Devonian sandstone area, their position and drainage system are more complicated (Rattas, 2007). Bedrock erodibility is reflected in the shape of the valleys, as well. Typically shallow and wide valleys have been developed on the carbonate bedrock, whereas in the Devonian district, the incisions have been carved deeper into the sandstones (Tavast and Raukas, 1982). Another outstanding bedrock landmark is the North Estonian Klint on the northern coast of Estonia. The Klint represents one of the longest continuous Cambrian-Ordovician escarpments in the world (Miidel and Raukas, 2005; Suuroja, 2006). Furthermore, the largest glaciotectonic dislocations have been concentrated just south of the eastern part of the Klint (Rattas and Kalm, 2004).

Quaternary glaciations have vastly sculptured Estonian topography. The main direction of the glacial advance has been from the northwest (Kalm, 2012). At least three stadials and two interstadials have been distinguished in the Pleistocene (Kalm et al., 2011). The thickness of the Quaternary overburden is usually less than 5 m in northern and western Estonia (Fig. 2) and less than 10 m in the south (Raukas and Kajak, 1997; Rattas and Kalm, 1999; Kalm 2009). In alvars, superficial deposits are missing, whereas in some buried valleys, the filling may exceed 100 m (Raukas and Kajak 1995). Glacial, glaciofluvial and glaciolacustrine deposits prevail in the Quaternary succession (Kalm et al., 2011).

As the top strata beneath the pedosphere, Late Pleistocene glacial deposits coat nearly 40% of the country (Fig. 3). Till covers vast plain areas, occasionally stacked into positive landforms like hills, ridges and drumlins. Glaciofluvial eskers, kames, deltas and outwash plains frequently provide suitable material for the aggregate industry. Conversely, in most cases, glaciolacustrine varved clays, fine-grained and loamy sands are economically insignificant (Räägel, 1997). On top of the Late Pleistocene strata, postglacial wetland, coastal, aeolian, lacustrine, fluvial and technogenic deposits are generally exposed (Fig. 3). Regarding the topics discussed later in the thesis, peat and coastal deposits require an upcoming preface.

Sometimes organic-rich layers have been described in the sections of the Late Pleistocene interstadials (Kalm et al., 2009). The overwhelming majority of peat deposits have accumulated after the retreat of the last glaciation. The average accumulation rate in Holocene has been 1 mm yr^{-1} (Ilomets, 1994; Punning and Koff, 1997). Areas where peat has been found (regardless of its thickness) are called peatlands. These are terrestrial ecosystems where plant production exceeds (or has exceeded) the decomposition due to the local hydrologic conditions. About 20% (9 150 km²) of Estonia is blanketed with peatlands. According to Tanneberger et al. 2017, Estonia is the third most prosperous country after Finland and Ireland, concerning the peatland coverage in Europe.

Active peatlands (where peat is being deposited) are called mires. Three main mire development scenarios have been recognised, regarding the shift to drier conditions: (a) infilling in open water, (b) primary peat formation, and (c) paludification of mineral soils (Rydin and Jeglum, 2006). Local terrain, geological background, and the hydrological regime are the key factors controlling mire development (Comas et al., 2005; Hiiemaa et al., 2014; Stivrins et al., 2017; Pezdir et al., 2021). Typical mire evolution starts with a minerotrophic fen stage, where feeding comes from groundwater. Environmental changes ultimately lead the mire transition to the ombrotrophic bog, where precipitations are the primary water source (Orru and Orru, 2008; Paal and Leibak, 2011; Blaus et al., 2021).

Besides encompassing organic material of various decomposition rates, peatlands are also known as fresh water storages and natural carbon stocks. Mining and drainage cause the rapid release of carbon that has accumulated into peat over thousands of years (Stivrins et al., 2017; Minasny et al., 2019; Carless et al., 2019). In Estonia, extensive drainage of mires was carried out between the 1950s and 1980s (Paal et al., 2016), influencing the groundwater regime of most of the mires (Küttim et al., 2018). Drainage systems have decreased the total area of fens more than ten times (Paal and Leibak, 2011). The average thickness of peat in Estonian mires is 3–4 m (Orru, 1995).

After melting the Fennoscandian Ice Sheet, the Baltic Sea basin and adjacent areas have ascended significantly. Currently, the average glacioisostatic uplift is $1\text{--}3 \text{ mm yr}^{-1}$; nevertheless, earlier in Holocene, the rise was a lot brisker (Rosentau et al., 2012; Vassiljev et al., 2015; Kall et al., 2021). Hence the shoreline of the Baltic Sea has shifted, new islands and coastal landforms have emerged

continuously. The present length of the Estonian coastline (with islands) is 3800 km, placing the country in the world ranking top 30 (WIKI, 2022a).

Relic dune ridges subparallel to the sea shore, created during the regressive-transgressive fluctuations of the sea level and reshaped by wind, are frequently called foredunes. They are valuable indicators of past shoreline position and sea-level oscillations (Otvos, 2000; Tamura, 2012). Occasionally the foredunes may exhibit a particular storm event; however, most of the ridges can be associated with certain periods in the development of the Baltic Sea. Starting from the oldest, these stages are (a) Baltic Ice Lake, (b) Yoldia Sea, (c) Ancylus Lake, (d) Litorina Sea, and (e) Limnea Sea (Björck, 1995; Andrén et al., 2000; Saarse and Vassiljev, 2010). During the glacioisostatic uplift, coastal ridges gradually retreat from the seashore. Consequently, aeolian processes get control over reshaping the scenery (Mauz et al., 2013; Suursaar et al., 2019).

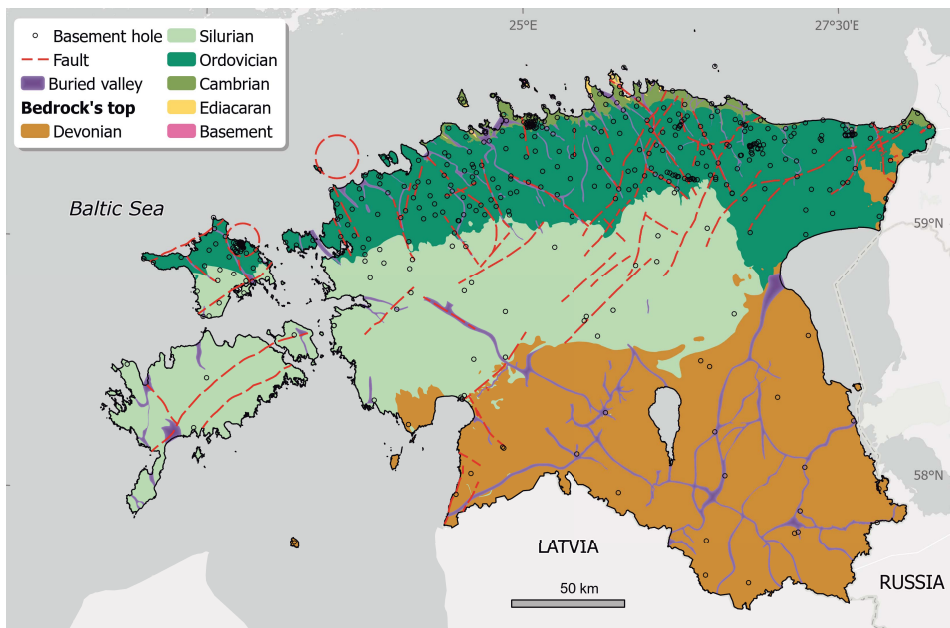


Figure 1. Estonian topmost bedrock units with main faults, buried valleys and boreholes penetrating the crystalline basement [GSE, 2022b (the generalised Map of Bedrock 1:200 000); ELB, 2022b (boreholes)].

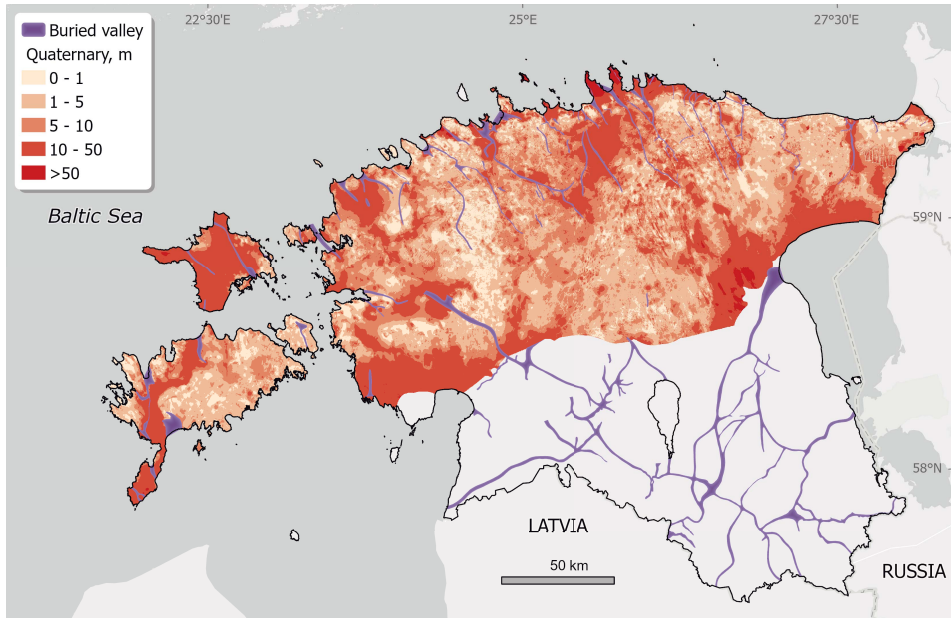


Figure 2. Total thickness of the Quaternary deposits in northern Estonia [the rock head DEM (Ani and Meidla, 2020) was subtracted from the LiDAR DEM (ELB, 2022c)].

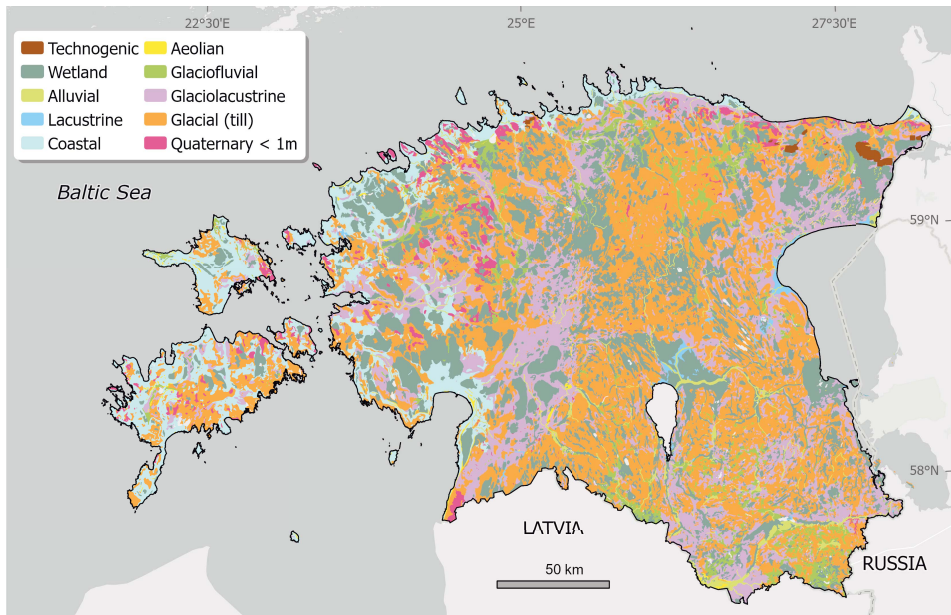


Figure 3. Estonian topmost Quaternary sediments (ELB, 2022d, the Map of Quaternary deposits).

3. MATERIAL AND METHODS

3.1 Description of the study areas

Four case studies were chosen for the thesis. These were performed in the Saadjärve Drumlin Field in eastern Estonia, Ruhnu Island, Viru-Nigula, and Sillamäe-Narva (Fig. 4). The Viru-Nigula and the Sillamäe-Narva quadrangles in NE Estonia cover relatively large and variable territories, whereas the other two localities are more specific.



Figure 4. Location of the study areas: (a) Rahivere (Paper I), (b) Ruhnu (Paper II), (c) Viru-Nigula (Paper III), and (d) Sillamäe-Narva (Paper IV) on the LiDAR DEM (ELB, 2022c).

The Rahivere study characterises a typical bog development, with preconditions provided by the Late Pleistocene glaciers. Rahivere Bog is located in a trough between the drumlins in eastern Estonia, about 40 km north of Tartu (Figs. 4a and 5a). Creation of the Saadjärve Drumlin Field between Lake Võrtsjärv and Lake Peipsi depressions was induced by the Pandivere Upland, where heights reach 130 m a.s.l. The upland, located NW from Rahivere (Fig. 4), comprises Ordovician and Silurian carbonate rocks. The drumlins were formed in the SE periphery of the upland, which acted as an obstacle for the Late Pleistocene ice streams. Heights within the Saadjärve Drumlin Field are generally 50–100 m a.s.l. (Rattas, 2004). Drumlins have been dated to the Sakala ice-marginal zone (around 14 cal. ka BP, Kalm et al., 2011). At about the same time, Lake Peipsi flooded large areas and reached the Lake Võrtsjärv basin (Rosentau et al., 2007).

Palaeozoic bedrock in the Vooremaa Drumlin Field consists of the Silurian dolostones and Devonian sand- and siltstones, usually covered by the Late Pleistocene tills. Thickness of the superficial deposits (till, glaciolacustrine, glaciofluvial beds) at the drumlin assemblages may extend to 70 m (Rõuk and Raukas, 1989). For example, in Borehole No. 73 (Fig. 5a), Devonian (the Pärnu Formation) sandstones are overlain by 52 m of Quaternary cover (ELB, 2022b). During the Holocene, clay, silt, fine sand, and organics were deposited within the lakes squeezed between the drumlins. In some larger troughs, lakes have been preserved, whereas most of the smaller depressions have been filled up with lacustrine deposits and peat (Rattas, 2004). A small remnant water body in the Rahivere Bog is an evidence of such mire evolution (Allikvee and Orru, 1979). Within the bog, the Rahivere Deposit, with total peat reserves of 97 000 tons, has been designated (Fig. 5a). In the Estonian Mineral Registry (MR), the area of the Rahivere Deposit is 0.54 km², and the average peat thickness is 2 m (ELB, 2022a).

Ruhnu Island with an area of 12 km² is located in the middle of the Gulf of Riga in the Baltic Sea (Fig. 4b). The highest point is 30 m a.s.l. at the eastern part of the island, where several series of subparallel coastal foredunes have been developed. The western part of the island is lower, without remarkable landforms (Fig. 5b). The island's territory has been increasing continuously in the Holocene, the average land uplift is currently 1.5 mm yr⁻¹ (Kall et al., 2021). The island is elongated in the NW–SE direction. It lies on a 30 km long and 10 km wide feature with a similar orientation. This ridge can be observed on the DEM (Fig. 4b) as a shoal cut in half by a narrow channel. According to Kask et al. (1994), the island's core is a relic bedrock rise that was more persistent to glacial erosion. The uppermost part of the island's bedrock belongs to the Middle-Devonian Narva Formation. In general, dolomitic marl, dolostone, clay, siltstone and sandstone can be distinguished within this lithostratigraphic unit (Kleesment and Mark-Kurik, 1997). A lot of information about the island's geology has been gained from the 787 m deep Ruhnu (No. 500) borehole (Fig. 5b), which has the thickest sedimentary bedrock succession (777 m) of all the Estonian boreholes (Pöldvere, 2003). Bedrock is mainly coated with the Late Pleistocene tills, Holocene coastal and aeolian sands. At the highest dunes, the total thickness of the overburden exceeds 10 m (Kask et al., 1994; ELB, 2022b).

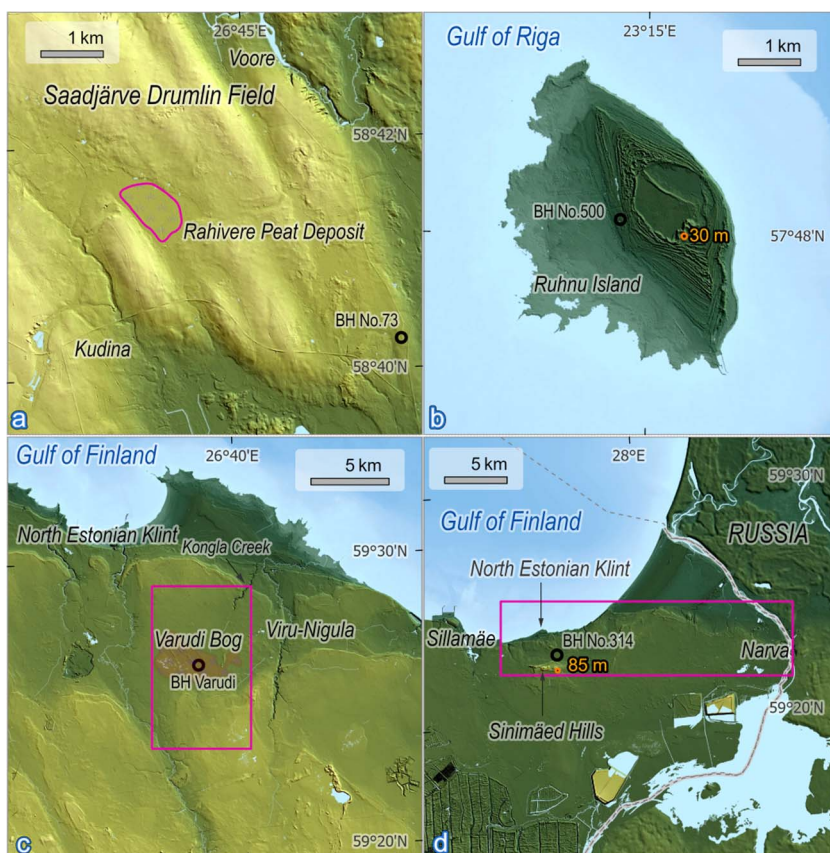


Figure 5. A closer look at the study areas: (a) Rahivere Bog and the related Rahivere Peat Deposit (Paper I), (b) Ruhnu Island (Paper II), (c) Viru-Nigula (Paper III), and (d) Sillamäe-Narva (Paper IV) on the LiDAR DEM (ELB, 2022c).

Additional geophysical surveys were conducted close to the Viru-Nigula Borough in NE Estonia, 5–15 km south of the Gulf of Finland and the North Estonian Klint (Figs. 4c and 5c). The ground surface is between 20–70 m a.s.l. there, rising southwards. In the NE part of the region, the Kongla Creek Valley has been carved into the terrain, whereas southwards the ravine disappears (Fig. 5c). The uppermost bedrock consists of the Middle Ordovician limestones and dolostones (Väo and Kõrgekallas Formations). In the centre of the region lies the currently exploited Varudi Bog, where peat (thickness typically 2 m) is underlain by gyttja (0.5 m), glaciolacustrine deposits (1.5 m) and glacial till (Veldre, 1994; ELB, 2022a). Generally, the total thickness of the Quaternary succession does not exceed 5 m in the study area. The core of the borehole drilled into the Varudi Bog (Fig. 5c) revealed an exceptionally thick (30 m) overburden on top of the Lower Ordovician bedrock. Atypical configuration of the bedrock’s morphology has been associated with the buried valley incised in NE–SW direction beneath the Varudi Bog (Suuroja et al., 2006).

The Sillamäe-Narva study area is also in NE Estonia, about 70 km eastwards from Viru-Nigula (Fig. 4d). The area is bordered by the Klint in the north and Sinimäed Hills in the south. The highest point is 85 m a.s.l. at the easternmost (Pargimägi) hill (Fig. 5d). As the bedrock's topmost unit, the same Vao Formation extends here likewise. However, the geological development has been unusual compared to the rest of northern Estonia. Abnormally thick piles of Cambrian clays have been described in several boreholes. For example, if the typical thickness of the Lükati Formation is 10–15 m, a four times thicker sequence has been noticed in Borehole No. 314 (Fig. 5d). Thus the mappers of the GSE have concluded that, due to increased water content, Lower Palaeozoic clay beds started to shift upwards as diapirs under the glacial overpressure. The origin of the Sinimäed Hills has been related to clay diapirism and the relocation of the overlying bedrock blocks (Suuroja and Ploom, 2016). Between the Sillamäe and Narva towns, the Late Pleistocene glaciers occasionally folded and tilted the Ordovician carbonate bedrock blocks. Geophysics allows shedding more light on the areal distribution of the glaciotectonic deformations, ranging from little inclination changes to impressive fault systems.

3.2 Ground-Penetrating Radar

3.2.1 Principles

Ground-penetrating radar is a non-destructive geophysical method using a set of transmitter and receiver antennas connected to the central radar unit, battery and computer. While the antennas are towed along the profiles, the data are recorded to the laptop's hard drive at constant traces for further processing (Neal, 2004).

In principle, high-frequency (10–1000 MHz) electromagnetic (EM) waves are continuously sent into the ground by the transmitting antenna. After reflecting back from different surfaces, the receiver registers the EM pulses. Following Maxwell's theory, the EM propagation velocity can be calculated by Eq. 1:

$$v = \frac{c}{\sqrt{\epsilon_r}} \text{ (m ns}^{-1}\text{)} \quad \text{In which } v \text{ is velocity, } c=0.3 \text{ m ns}^{-1} \text{ (the speed of light),}$$

and ϵ_r is the relative permittivity (dielectric constant).

Equation 1.

The time interval from the EM pulse launch to capture is called a two-way travel time (TWT). By measuring TWT (in nanoseconds, ns), the distance from the ground surface to the reflecting surface can be calculated if the propagation speed of the EM pulse in the material is known (Davis and Annan, 1989; Annan, 2009). A contrast in their physical properties must occur to distinguish materials from each other. The EM signals behave differently due to variations in electrical conductivity, magnetic permeability and relative permittivity of the sediments (Daniels, 2004; Neal, 2004; Cassidy, 2009a).

Electrical conductivity characterizes free charge movement (creating electric current) when an electric field is present. Magnetic permeability describes how intrinsic atomic and molecular magnetic moments respond to a magnetic field. Relative permittivity characterizes displacement of charge constrained in a material structure to the presence of an electric field. (Annan, 2009).

Some common relative permittivity values are shown in Table 1. In general, high permittivity values diminish the quality of the study results due to greater EM signal attenuation.

Ground-penetrating radar systems may be sled-mounted, or on wheels, handled by manpower or vehicle-driven, and location data may be gained by internal or external GPS. An odometer wheel may be appended into or behind the antennas to increase the measurements' accuracy. Some antennas are in direct contact with the ground surface, while others operate up to 1 m above the surface (Zajícová and Chuman, 2019). The antenna configurations are divergent as well: multi-frequency, multi-channel, wired and wireless etc. Generally, GPR data are collected in four antenna arrangements: common offset, common midpoint (CMP) common source, and common receiver (Fig. 6).

Most frequently, common offset method is applied, where the distance between the transmitter and receiver antenna is fixed during the antenna dragging on the ground (Fig. 6a). CMP technique enables to determine the EM velocities and relative permittivity. During a CMP survey, two antennas (one acting as a transmitter and the other as a receiver) are constantly moved apart from each other (Fig. 6b). The distance between the antennas is known, as well as the point of reflection in the ground; hence the EM signal velocity can be calculated (Nakashima et al., 2001; Neal, 2004; Annan, 2009). A common source application (also known as WARR: wide angle reflection and refraction) means the receiver is moved apart from the fixed transmitter stepwise (Fig. 6c; Huisman et al., 2003; Zajícová and Chuman, 2019).

Compared to the traditional common offset sounding, the WARR has several advantages like increased penetration depth and velocity estimation. Several "WARR-machines" have been developed, enabling data acquisition at normal profiling speeds (Annan and Jackson, 2017; Diamanti et al., 2018). Forte and Pipan (2017) classify the GPR systems into single-fold and multi-fold categories. Common offset is a single-fold system where typically, besides constant transmitter-receiver spacing, the antenna orientation is also fixed. Hence, data are collected from a single wavefront for each subsurface point. Conversely, multi-fold systems enable data compilation from multiple wavefronts. Most promising are the devices where an array of antennas with different frequencies is concurrently used (Linford et al., 2010; Phelan et al., 2014; Forte and Pipan, 2017).

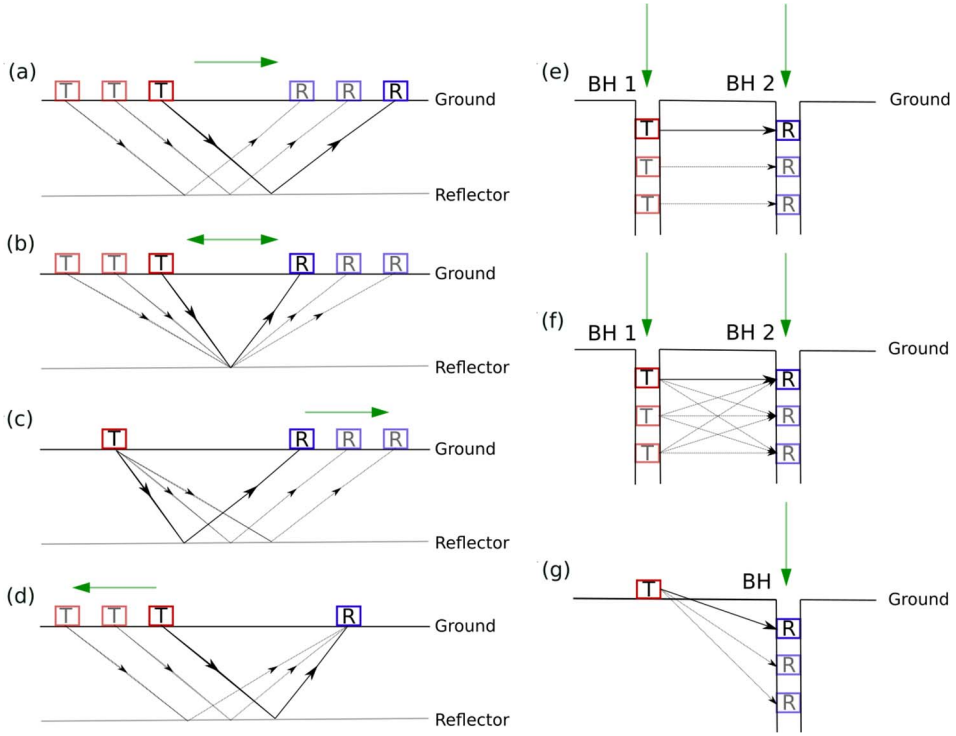


Figure 6. Main types of ground-penetrating radar surveys: (a) common offset, (b) common midpoint (CMP), (c) common source/wide angle reflection and refraction, (d) common receiver. Borehole GPR surveys typically involve (e) zero-offset, (f) multi-offset, and (g) vertical radar measurements. Transmitters (T) and receivers (R) are moved in the directions shown with green arrows. Modified from Neal (2004) and Liu et al. (2019).

Specific GPR devices have been designed for borehole studies. To get as much data as possible, generally low frequency (<100 MHz) thin dipole antennas are slid into the boreholes (Slob et al., 2010). Three techniques for borehole inspection are usually applied: zero-offset, multi-offset, and vertical radar (Fig. 6). During a zero-offset (Fig. 6e) study, the transmitter and receiver are simultaneously moved in two boreholes at the same depths and steps. A multi-offset study (Fig. 6f) implies that the transmitter is fixed at a certain depth in one borehole, while the receiver is moved in another. Vertical radar profiling (Fig. 6g) requires only one borehole, normally with the transmitter fixed on the ground surface and the receiver descending into the borehole (Tosti and Slob, 2015; Liu et al., 2019). Hence, the zero-offset method applied in boreholes is similar to the common offset method implemented on the ground. In contrast, the others (multi-offset and vertical radar) resemble the WARR technique.

Moisture plays a significant role in the EM propagation. EM velocities up to 0.2 m ns^{-1} have been registered for dry sand, whereas in water-saturated strata, 2–3 times slower values occur. Therefore, relative permittivity (Table 1) can vary remarkably within the same material (Cassidy, 2009a; Daniels, 2004; Huisman

et al., 2003; Neal, 2004). Experiments conducted by Topp et al. (1980) encouraged the development of various applications targeted at measuring the soil's moisture content (Chapter 3.2.3).

Table 1. Typical relative permittivity ϵ_r and static conductivity* for some materials at an antenna frequency of 100 MHz (Daniels, 2004; Cassidy, 2009a), and 80–120MHz (Neal, 2004).

Material	ϵ_r (Daniels, 2004)	ϵ_r (Neal, 2004)	ϵ_r (Cassidy, 2009a)	Conductivity, Sm^{-1} (Cassidy, 2009a)*
Air	1	1	1	0
Asphalt, dry	2–4			0.01–0.1 ^D
Asphalt, wet	6–12			0.001–0.1 ^D
Clay, dry	2–6	3–5	2–20	1–100
Clay, wet	5–40	15–40	15–40	100–1000
Concrete, dry	4–10		4–10	1–10
Concrete, wet	10–20		10–20	10–100
Freshwater	81	80	78–88	0.1–10
Freshwater ice	4		3	0.00001–1
Granite, dry	5		5–8	0.001–0.00001
Limestone, dry	7		4–8	0.001–0.0000001
Limestone, wet	8		6–15	10–100
Peat (freshwater)		57–80		<40 ^N
Sand, dry	2–6	3–8	3–6	0.0001–1
Sand, wet	10–30	20–32	10–30	0.1–10
Sandstone, dry	2–5		4–7	0.001–0.0000001
Sandstone, wet	5–10		5–15	0.01–0.001
Seawater	81	80	81–88	4000
Sea-water ice	4–8			0.01–0.1 ^D
Snow firm	6–12			0.000001–0.00001 ^D
Soil (average)			16	5
Till, dry		7–21		2.5–10 ^N
Till, wet		24–34		2–5 ^N

*In case Cassidy (2009a) has not listed some materials, conductivity values published by Daniels (2004): ^D and Neal (2004): ^N are given.

Another axiom states lower frequency antennas have longer wavelengths and deeper subsurface penetration (Annan, 2009; Bristow, 2009). Relations between frequency, velocity of the EM pulse and wavelength are shown in Eq. 2.

$\lambda = \frac{v}{f}$ In which λ is wavelength, v is velocity, and f is frequency.

Equation 2.

Thus, for example, a 100 MHz antenna enables one to study deeper beds than the 200 MHz one. However, concurrently some loss of resolution is inevitable with lower frequencies. Resolution determines the ability to visualise strata. Vertical resolution is generally around 0.25 of the wavelength (Annan, 2009). Resolution is closely related to EM transmission velocity through moisture. Bristow (2009) demonstrates that theoretical resolution in wet sand (0.15 m, with a 100 MHz antenna) is more than two times higher than in dry sand.

3.2.2 Data processing

Before going to the field with GPR, a few profiling settings (in addition to the suitable antenna selection) must be determined. Commonly the following parameters have to be specified (Annan, 2009; Bristow, 2009):

- (a) time window (ns) should be generally set to ~ 1.5 times larger than the maximum depth of interest (finding later that a reflector runs off the bottom of the image may be frustrating),
- (b) sampling interval (ns). Annan (2009) suggests the time interval between points for the output should be approximately six times the frequency of the used antenna. Hence, the maximum sampling interval for a 100 MHz antenna might be 1.67 ns,
- (c) step size (m) is the distance between each point where a measurement is made along a profile. For a 100 MHz antenna, a minimum step size of 0.25 m is recommended (Bristow, 2009), and
- (d) stacking is the process of averaging a set of repeated EM pulses for reducing noise.

Data acquisition at the site usually involves some basic filtering. During the sounding process, the GPR operator gets real-time information on the laptop's display; if necessary, adjustments in the profiling settings can be made promptly.

Successful GPR fieldworks result in radar images, which resemble continuous geological cross-sections. Yet, it is always important to remember that GPR images reveal only distinctive reflective surfaces of the EM energy, not the true stratigraphic sequence (Cassidy, 2009a). Images can be two-dimensional (2D; Davis and Annan, 1989) or three-dimensional (3D). The latter enables to recognise details in different orientations and identify the shape of the objects more accurately (Grasmueck et al., 2005; Kelly et al., 2021).

Cassidy (2009b) points out that the data post-processing at a desk should be as simple as possible – no super algorithm can make a miracle out of low-quality data. Still, the common workflow includes quite a few steps:

- (a) removing poor data, migrating files,
- (b) dewow (correction of low frequency and other distortions),
- (c) time-zero correction (matching the start time with surface position),
- (d) filtering to improve the signal-to-noise ratio and visual quality,
- (e) determining EM wave velocities,
- (f) topography adjustments,
- (g) converting the TWTs into depths, and
- (h) selecting appropriate gains for data display and interpretation.

Depending on the GPR proprietary software, some of these procedures can be applied for all the output files automatically and/or concurrently. Together with useful data, always some background noise (e.g., from traffic, power poles, mobile phones etc.) is recorded. *Background removal* generally enhances the result. However, if used without caution, it can also remove continuous flat reflectors by mistake. Simple spatial filters are particularly suitable for geological studies where the reflectors are low-angled and extensive (Cassidy, 2009b).

Ground-penetrating radar transmitter antenna sends EM waves in all directions. Thus, reflections are registered by the receiver before and after the antenna is towed over the underground object. The precept that the shortest TWT is measured precisely above the object results in a series of hyperbolas, where the vertices mark the horizontal location of the anomalies (Huisman et al., 2003).

For converting the radar images to depth scale, the average subsurface velocity must be assessed by drilling/test pitting (i.e. ground truthing), CMP surveys and/or hyperbolic velocity analysis. The last can be done by matching the ideal form of a velocity-specified hyperbolic function to the shape of the observed data (Cassidy, 2009b). TWTs can be converted to depths according to Eq. 3:

$$d = \frac{v t}{2} \text{ (m)} \quad \text{in which } d \text{ is depth, } v \text{ is velocity, and } t \text{ is TWT.}$$

Equation 3.

Electromagnetic energy is not directed vertically downwards on slopes, but has an additional horizontal component that escalates with an increasing slope dip (Neal, 2004). Radar images can be supplemented with LiDAR elevation data, which help to locate the GPR traces more precisely.

Gains improve the layout of the radar images. Usually, both noise and coherent signals are amplified together. Like spatial filters, gains may alter the data structure, not always in the best way (Cassidy, 2009b).

3.2.3 Applications

Wai-Lok Lai et al. (2018) divide GPR systems into three main categories based on the antenna frequency: (a) 10–100 MHz range is suitable for imaging deep structures on the tens of metre scale, (b) 100–1000 MHz can be used on the metre scale, and (c) GPR's in the 1000–5000 MHz range for the centimetre scale. Depending on the configuration, the device can be applied for various purposes (Davis and Annan, 1989; Daniels, 2004; Neal, 2004; Wai-Lok Lai et al., 2018; Zajícová et al., 2019):

- (a) agriculture,
- (b) archaeology,
- (c) borehole inspection,
- (d) civil engineering and geotechnics,
- (e) environmental geophysics,
- (f) forensics,
- (g) geology and geophysics,
- (h) hydrogeology,
- (i) military,
- (j) mining,
- (k) permafrost, glaciology, ice, snow, and
- (l) planetary.

This list is far from being complete; furthermore, every subject has several subdivisions.

Although geology and geophysics are more highlighted in the thesis, all the labels deserve a short overview:

- (a) for decades, GPR has been used in agriculture for mapping subsurface drainage systems (Koganti et al., 2021) and estimating soil water content (Lunt et al., 2005; Benedetto, 2010). Soil moisture mapping, using a wide-band antenna on a drone, was applied in Belgium (Wu et al., 2019),
- (b) numerous publications and books (Leckebusch, 2003; Goodman and Piro, 2013; Conyers, 2016) confirm archaeologists highly appreciate GPR as a

non-invasive method for detecting and studying ancient settlements and artefacts. If needed, GPR enables to describe the development of a specific palaeoenvironment in 4D (Corradini et al., 2020),

- (c) a borehole GPR operates in a single borehole, between two boreholes, from a borehole to the surface, or from a borehole to a mine tunnel. Borehole GPR antennas and the radar's main unit are typically enclosed in the same cylindrical casing (Slob et al., 2010). Tronicke et al. (2002) describe a study in a gravel pit where the outcrop analysis was integrated with GPR profiling and cross-hole tomography,
- (d) civil engineering (and geotechnics, as its subdivision) must cope with various challenges. A considerable coring capacity has been essential for the transportation infrastructure to acquire adequate subsurface knowledge. In densely populated areas making new boreholes may be problematic due to local restrictions. The exact location of old power lines and other underground infrastructure objects may be ambiguous. A myriad of GPR solutions supports pre-construction, ordinary maintenance and post-damage decision-making (Saarenketo and Scullion, 2000; Wai-Lok Lai et al., 2018). GPR can be used as a quality control tool for general (Prego et al., 2017; Bianchini Ciampoli et al., 2017) or very high precision void/ reinforcement detection (Maierhofer, 2003; Agred et al., 2018; Sánchez-Aparicio et al., 2019) afterwards,
- (e) GPR has been applied to detect landfill debris (Paap et al., 2011), buried tanks, and contaminated fluids. Besides safety issues, abandoned military devices frequently represent a severe environmental concern (Peters et al., 1994),
- (f) human remains, other organic materials, valuable items, explosives etc., can be revealed in the ground, beneath floors and within walls (Ruffell et al., 2014). In the United Kingdom, the gravesites of the victims of a serial murderer were discovered under concrete, using GPR (Daniels, 2004),
- (g) Neal (2004) provides an array of sedimentological environments (with references) where GPR can be used: fluvial, glaciofluvial, glacial, coastal, aeolian, delta, alluvial fan, lake, peatland, slope, carbonates, volcanic, faults, joints and folds. The British Geological Survey has used GPR in the mapping program (Busby et al., 2004). Similarly, the method enabled to specify the local geological development in Ireland (Pellicer and Gibson, 2011), the Netherlands (van Overmeeren; 1998; Bakker and van der Meer, 2003) and adjacent areas (Demagnet et al., 2001), Denmark (Overgaard and Jakobsen, 2001; Møller and Vosgerau, 2006; Høyer et al., 2013), Poland (Hirsch et al., 2015), Latvia (Lamsters et al., 2020), Norway (Eilertsen et al., 2011; Janocha et al., 2021), United States (Smith and Jol, 1995), Canada (Diallo et al., 2019). Many papers describe the detection of karst cavities and other types of caves (Chamberlain et al., 2000; Anchuela et al., 2009; Zajc et al., 2014; Bermejo et al., 2020),

- (h) in hydrostratigraphy and aquifer modelling, GPR has been used as the main application (Asprion and Aigner, 1999) or alongside other geophysical tools (Tronicke et al., 1999; Martel et al., 2018). Doolittle et al. (2006) note GPR can be engaged in locating new wells and reducing the number of wells needed for groundwater monitoring. Doetsch et al. (2012) suggest GPR results can significantly enhance the resolution of the ERT models. Satish Kumar et al. (2016) and Costall et al. (2020) used both GPR and ERT to locate saline water intrusion into freshwater aquifers,
- (i) abandoned land mines and other unexploded ordnance (UXO) are the legacy of many countries from war-time. With GPR, even low/no metal content mines can be discovered (Daniels, 2004). Prado and Marquez (2015) fused metal detectors' and GPR data to increase the probability of UXO discoveries and decrease false alarms. To raise the correct detection rate, Frigui and Gader (2009) propose an automated algorithm,
- (j) coal and salt deposits were surveyed with GPR already in the 1970s (Annan, 2002). In Canada, GPR surveys are regularly conducted for kimberlitic diamond exploration. Similarly, GPR can be used for studying laterites, bauxites, iron ore, limestone, and aggregates (Francke, 2012). Porsani et al. (2006) used GPR to specify the best localities for ornamental granite extraction. According to Rey et al. (2015), GPR can be used for selecting suitable decorative stone blocks for monuments. GPR is also an appropriate tool for peat thickness estimations and peatlands' inventories (Warner et al., 1990; Hänninen, 1992; Rosa et al., 2009; Parry et al., 2014); hence volume calculations for peat deposits can be gained with high accuracy,
- (k) GPR has been implemented for locating frozen ground, massive ice, and ice-rich sediments in Antarctica (Campbell et al., 2018). Sjöberg et al. (2015) combined GPR and ERT surveys in a peatland permafrost study in Sweden. Andreassen et al. (2015) used GPR to estimate ice thicknesses and volumes for Norwegian glaciers,
- (l) in February 2021, NASA's Mars 2020 Rover (Perseverance) landed on the Red Planet. The Rover seeks possible life signs from the rocks and is equipped with a drill for collecting samples and a GPR known as RIMFAX. With the antenna frequency range of 150–1200 MHz, the GPR image resolution can be modified from the Earth. Lower frequencies enable getting data from a depth of more than 10 m (RIMFAX, 2022).

A couple of cases show the boundaries between the above-described GPR application fields are somewhat vague:

- (a) GPR can be applied for detecting abandoned mine shafts (Pilecki et al., 2021); hence the application can be classified into either the civil engineering or mining category,

- (b) Moorman et al. (2003) point out that melting of the permafrost may cause severe geotechnical problems.

Ground-penetrating radar has been particularly useful in combination with other geophysical tools (Gourry et al., 2003; Paap et al., 2011; Høyer et al., 2013). If several subjects are discussed in one study, specialists from different disciplines must go into action. For example, multidisciplinary studies where archaeologists work alongside geologists (Zhao et al., 2013; Corradini et al., 2020) are increasingly favoured. Incorporating optically stimulated luminescence (OSL) dating for analysing marine and aeolian sedimentary environments enables to estimate past sedimentation velocities, and make some predictions for the future landscape morphodynamics as well (Bristow and Pucillo, 2006; Clemmensen et al., 2012; Tamura, 2012; Choi et al., 2014). Peatland studies were previously concentrated on the geological background and/or mineral resource assessments (Warner et al., 1990; Rosa et al., 2009). Today, peatlands are more underlined as natural carbon stocks (Minasny et al., 2019; Carless et al., 2021). Thus, while uncovering past events, GPR can contribute to coping with global climate change through environmental, glacial/permafrost, coastal, and peat surveys.

Davis and Annan (1989) emphasise good spatial resolution and almost instant sounding results are the major GPR advantages compared to the other geophysical methods. Getting more coherent data with less human effort is one of the tasks the GPR community has been tackling from the beginning. Until the 1990s, GPR was considered merely as a niche equipment. The golden era started with digital data processing. From the clumsy and power-consuming device GPR once was (Annan, 2002), a flexible and multi-purpose tool has evolved. Since 1986, GPR user meetings have been organised every 2 years (Annan, 2002; Wai-Lok Lai et al., 2018; GPR 2022). Using novel data collection and processing practices has opened new horizons for GPR. The author's thoughts concerning the possible future applications and overall potential of GPR are exposed in Chapter 5.

3.2.4 Estonian experiences

The first local GPR studies were carried out at the end of the 20th century for archaeological purposes (Vissak and Vunk, 1996). The Department of Geology at the University of Tartu (UT) obtained a Zond 12e GPR system in 2006. Since then, besides scientific papers and survey projects, more than ten thesis of different levels have been devoted to GPR applications (UT, 2022). Tallinn University (TLU) has been using a SIR 3000 GPR system primarily for coastal studies (TLU, 2022). Probably hundreds of GPR projects from various fields have been accomplished in Estonia. In the thesis, GPR studies are organised into three main categories: (a) peat, (b) coastal/aeolian, and (c) carbonate rocks. Following the same classification concept, the publicly available Estonian GPR works are presented in Fig. 7. Scientific publications with references are listed in Table 2.

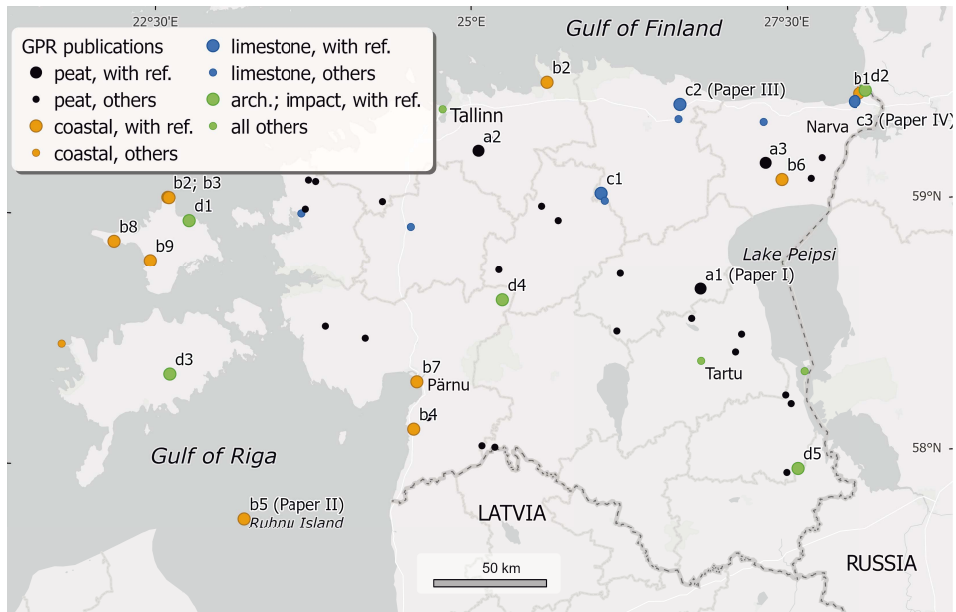


Figure 7. Estonian ground-penetrating studies are classified into four categories: (a) peat, (b) coastal/aeolian, (c) limestone, and (d) other studies (archaeological, impact etc.). Larger dots indicate the scientific studies with references listed in Table 2. Smaller dots are related to students' thesis and survey reports (Kull et al., 2013; GA, 2022; EGLD, 2022; ELERMO, 2022; UT, 2022; EGDB, 2022).

As revealed by Fig. 7, peat has been studied rather broadly; generally, these surveys are associated with students' thesis and various survey reports (Kull et al., 2013; GA, 2022; EGLD, 2022; UT, 2022). Besides Paper I, just a couple of scientific papers concentrate on peat. One of them was initiated by a hint about a possible impact crater (Mustasaar et al., 2013), while the other was triggered by the oil-shale mines approaching the protected wetlands (Hiiemaa et al., 2014). Coastal sedimentation has been analysed along the Estonian coastline (Fig. 7). Some studies (Rosentau et al., 2013; Vilumaa et al., 2013; Vilumaa et al., 2016; Suursaar et al., 2022) were focused on continuous coastal evolution from the geological and ecological perspectives. Another group of studies engaged archaeologists in interdisciplinary projects describing the composition of the subsurface and looking for ancient habitats concurrently (Tšugai et al., 2014; Habicht et al., 2017; Kriiska et al., 2018; Paper II; Nirgi et al., 2020; Rosentau et al., 2020). Holocene aeolian processes in relation to the glaciolacustrine sedimentation are highlighted by Kalińska et al. (2019).

Table 2. Estonian ground-penetrating radar publications. Labels are used on Fig. 7, showing the locations of the respective study areas.

Category	Label	Reference	Antennas (MHz)
(a) peat	a1 (Paper I)	Plado et al., 2011	300 (500)
	a2	Mustasaar et al., 2013	300
	a3	Hiiemaa et al., 2014	300
(b) coastal; aeolian	b1	Rosentau et al., 2013	300
	b2	Vilumaa et al., 2013	100 (270)
	b3	Vilumaa et al., 2016	270
	b4	Habicht et al., 2017	300
	b5 (Paper II)	Muru et al., 2018	300
	b6	Kalińska et al., 2019	300
	b7	Nirgi et al., 2020	300 (100)
	b8	Rosentau et al., 2020	270
	b9	Suursaar et al., 2022	270
(c) carbonate rocks	c1	Mustasaar et al., 2012	100, 300, 500
	c2 (Paper III)	Sibul et al., 2017	300
	c3 (Paper IV)	Jõelegt et al., 2022	300 (100)
(d) archaeology; impact studies	d1	Jõelegt and Plado, 2010	100
	d2	Tšugai et al., 2014	300
	d3	Wilk et al., 2016	300
	d4	Kriiska et al., 2018	300, 500, 900
	d5	Losiak et al., 2020	300

Naturally, carbonate studies are focused on northern Estonia, where limestone and dolostone beds are closer to the ground. One study conducted in a limestone quarry represents different approaches for determining EM propagation velocity in carbonate rocks (Mustasaar et al., 2012). The other limestone cases seek explanations for the genesis of some prominent geological features (Papers III and IV). In several works (Mustasaar et al., 2013; Jõelegt and Plado, 2010; Wilk et al., 2016; Losiak et al., 2020), GPR has provided additional data for characterising the proved or probable impact events. According to Table 2, 100–300 MHz antennas have been generally used for geological, archaeological and impact studies.

Since 2000, the Technical Center of Estonian Roads Ltd. (TCER) has been operating GPR for (a) surveys before road constructions, (b) quality checking after road construction, (c) measuring ice thickness on the temporary ice roads, and (d) studying subsurface anomalies (TCER, 2022). At least one private company has conducted GPR surveys mainly for civil engineering in larger cities (ELERMO, 2022). Some of these projects are the initiatives of the City of Tallinn,

aiming to create a 3D model for infrastructure by employing GPR (TALLINN, 2019). For mapping the infrastructure, antennas emitting frequencies of 400–2300 MHz are typically used (TCER, 2022; ELERMO, 2022).

3.2.5 Four case studies

Geologically, Estonia is a multiform country (Figs. 1–3). Changes in the composition of rocks and sediments may occur swiftly in a short distance. For the thesis, GPR was considered a suitable tool for identifying such key locations. Besides characterising the subsurface composition, it is essential to explain the development of the relevant depositional environments (Kettridge et al., 2012; Tamura, 2012). Following the Estonian experiences (Chapter 3.2.4) and considering the possible benefits for geological mapping, four survey sites were proposed.

For all the studies indicated in the Original List of Publications (Papers I–IV), GPR field data were collected with a Latvian (RADSYS) „Zond 12e“ ground-penetrating radar, generally with a common offset co-polarized sledge-mounted 300 MHz antenna. In addition, 500 MHz and 100 MHz antennas were occasionally applied. A 500 MHz antenna was used together with a 300 MHz antenna in the Rahivere Bog (Paper I). A 100 MHz antenna was applied to obtain data about greater depths for the Sillamäe-Narva study (Paper IV). Distances were always measured using an odometer wheel attached to the sledge’s rear. Transects were located with a portable GPS unit (AltinaGGM309; position accuracy 5–25 m) connected to the radar equipment. Generally, the GPR sounding was carried out in summer. Only the Rahivere survey (Paper I) was mainly accomplished in winter on the partly frozen ground covered with snow. Altogether, nearly 300 km of GPR transects were obtained during the four studies.

The data were processed and topographically corrected with Prism2 software. As a rule, time-zero correction, band-pass filtering (for removing low-frequency induction effects), and gain control (for amplifying deeper reflections) were applied during post-processing. Relief heights were determined by LiDAR data, which also helped to adjust horizontal positioning afterwards, together with topographic maps. Additional improvements were occasionally (Papers II–IV) enforced according to the depth of the groundwater level (table) observed in the radar images. Defining the groundwater level makes it possible to examine individually dry and water-saturated beds (Huisman et al., 2003; Doolittle et al., 2006; Takahashi et al., 2012).

An essential step was detecting the significant radar reflection patterns by tracking them along all the radar images. Prominent reflections were annotated as line features in Prism2 with a vertex interval of 5–10 m. For the identified radar facies, appropriate relative permittivities and EM propagation velocities are needed (Annan, 2009; Cassidy 2009b). Hence, for every study (Papers I–IV), hyperbola fitting was implemented in the GPR images, which resulted in the averaged EM wave velocities. Next, after the velocity calibration, the TWTs were

converted into depth (using Eq. 3). In Rahivere, the CMP technique was additionally employed. In two cases (Table 3), manual coring supported the EM velocity estimation. After processing the radar images in Prism2, CorelDRAW or Inkscape was used to achieve the final radar image design. Geographic information system (GIS) analyses and map production were carried out in MapInfo or ArcGIS.

In general, the task was to collect as much field data as possible – it is better to have more data than to be in a shortage. This principle becomes particularly relevant if the study site is not easily reachable (e.g., the Island of Ruhnu). Wherever possible, natural outcrops and previously published geological data were juxtaposed with new GPR-sounding and coring results. To characterise deeper strata, ERT profiling was performed for the Paper III studies. The thesis focuses on GPR; more details about ERT, OSL, and coring procedures can be gained from the respective papers.

Table 3. Antennas, relative permittivities ϵ_r within interpreted beds, and other methods (besides common offset) used for the GPR case studies.

Paper	Antennas, MHz	Interpreted beds, ϵ_r	Other methods
I: Rahivere	300 (500)	peat: 70	CMP, coring
II: Ruhnu	300	sand, gravel: 7 (dry); 20 (wet)	OSL, coring
III: Viru-Nigula	300	limestone: 9; sand, gravel: 16; till: 32; peat: 70	ERT
IV: Sillamäe-Narva	300 (100)	limestone: 10	

4. RESULTS AND DISCUSSION

4.1 Superficial deposits

Till, as the most widespread glacial deposit in Estonia (Fig. 3), is often considered unsuitable material for GPR studies. The four case studies (Papers I–IV) and the overall Estonian GPR practice (Chapter 3.2.4) support this perception. Due to high conductivity and relative permittivity (Table 1), there is a bias in favour of EM signal attenuation in clayey sediments (Sutinen, 1992; Bristow and Jol, 2003; Looms et al., 2018). However, thin clay beds and sandy tills (Bakker, 2002; Møller and Jakobsen, 2002; Bakker and van der Meer, 2003) may be sufficiently penetrable (Weaver, 2006). Contrary to massive clayey succession, GPR can give excellent results in glaciofluvial and glaciolacustrine environments (Leclerc and Hickin, 1997; Beres et al., 1999; Lang et al., 2017).

Holocene fine-grained silts and clays are more challenging environments for the GPR than coarser sands and gravels. Unconsolidated river deposits are among the most studied sediment types in the world (Bristow and Jol, 2003). Although peat has a relatively high permittivity (Table 1), its moderate conductivity allows using GPR extensively for peatlands' investigations (Zajícová and Chuman, 2019).

4.1.1 Peatlands

The traditional method for peat surveying is manual coring. An extendable metal pole is pushed into the ground until it hits some resistance or mineral layer, while the thickness of layers and geographical location of the site are registered. The Russian peat borer has a chamber for peat sampling. The critical concerns with manual probing are that small-scale local variability may affect the results, and the measurement volume is relatively small (Minasny et al., 2019). Ground penetrating radar has been applied in peatland studies for several decades (Hänninen, 1992; Comas et al., 2005; Rosa et al., 2009; Parry et al., 2014; Carless et al., 2021). Regarding the overall GPR fieldwork coverage, peat is the most studied substance in Estonia (Fig. 7). Peat profiling is discussed in Papers I and III. As Paper III focuses mainly on bedrock's topography and tectonics (Chapters 4.2–4.3), hence further discussion about peat concerns primarily Paper I.

Hänninen (1992) points out that peat properties (e.g., moisture content, bulk density, energy content) can vary greatly even within a very short distance. Kettridge et al. (2012) analysed GPR vertical resolution with different antennas and found higher frequency (>240 MHz) studies suitable for describing peat stratigraphy at 0.1 m precision. Such a resolution is required for characterising the dipping reflectors caused by the mineral soil microrelief. In suitable conditions, even 0.01 m precision is accessible (Comas et al., 2015).

For Paper I, a 300 MHz common offset GPR lineup was organised along with common midpoint (CMP) testing. Traditionally CMP technique has been applied

for estimating EM propagation velocity and calibrating peat's total thickness (Warner et al., 1990; Slater and Reeve, 2002; Lowry et al., 2009; Comas et al., 2017). Based on 15 references from different authors, Parry et al. (2014) calculated the mean peat's EM velocity (0.038 m ns^{-1}) and the respective relative permittivity (63). In Rahivere, CMP with simultaneous usage of 300 MHz and 500 MHz antennas performed in winter did not provide adequate results. Therefore, the survey was repeated in summer. For Paper I, the EM propagation 0.036 m ns^{-1} was measured, corresponding to the relative permittivity of 70. A radar configuration with 300 MHz antenna provided penetration depth down to 4 m, comparable with the maximum (4.5 m) peat thickness according to manual probing. Regarding the GPR resolution, propagation range, and mobility, a 300 MHz setup was a compromise for Paper I. In greater depths, antennas emitting lower frequencies are more relevant. *De facto*, the most common range for peatland studies has been 100–200 MHz (Hänninen, 1992; Slater and Reeve, 2002; Doolittle and Butnor, 2009; Rosa et al., 2009; Walter et al., 2016). Operating <100 MHz antennas is usually challenging due to their size and weight.

Peat is easily penetrable with manual coring. Ground truthing is essential for calibrating the GPR interfaces, hence peatland surveys are often supplemented with probing results (Rosa et al., 2009; Parry et al., 2014; Kennedy et al., 2018). In the original survey report of the Rahivere Peat Bog (Allikvee and Orru, 1979), 13 corings were used to calculate the resources of the Rahivere Deposit. During the Paper I studies, auxiliary 13 corings were achieved. Theimer et al. (1994) acknowledge that the typically detectable GPR interfaces are (a) the transition from the near-surface aerobic peat to the anaerobic one, and (b) the top surface of the mineral basement. In the latter case, the water content may decrease several times. Paper I shows GPR can be effectively used for tracking the contact between organic deposits, and the mineral ground. High contrast in radar images occurred on top of the sandy loam and clay. According to Warner's (1990) observations, a weaker response from the basal reflector is generally caused by clayey beds. GPR images in Rahivere revealed a lot more variations in the base topography of the deposit compared to the original survey data (Allikvee and Orru, 1979), thus contributing to larger peat volume estimation.

The logging data (Allikvee and Orru, 1979; Paper I) demonstrate peat is occasionally underlain by gyttja. The interface between peat and lacustrine lime or gyttja can be identified with GPR if bulk density and moisture content differ significantly in peat and the underlying succession (Warner et al. 1990; Hänninen 1992; Walter, 2016). Otherwise, gyttja remains undetectable in the radar images (Lowry et al., 2009; Habicht et al., 2017). Distinguishing gyttja as a separate layer in the Rahivere Bog was also complicated due to its relatively thin bedding (<0.4 m) and similar properties with the overlying peat.

Hänninen (1992), Hiiemaa et al. (2014), and Walter et al. (2016) discuss the possibility of splitting distinctive peat types while interpreting the GPR profiling results. In ombrotrophic bogs, greater penetration depths can be typically achieved than in the minerotrophic fens. While bogs get fed by precipitation, fens inherit more nutrients, higher conductivity and pH values from groundwater (Doolittle

and Butnor, 2009). In general, ombrotrophic peat can be characterised by corrugated and intermittent patterns in radar images. Due to the higher decomposition rate, minerotrophic peat produces a more continuous subparallel layout without distinctive minor reflections (Theimer et al., 1994).

The cluster of undecomposed tree stumps in-between different peat types usually generates an array of strong reflections in the radar images. In larger mires where the minerotrophic phase is constantly thick (>2m), the tree-stump interval is a valuable indicator for peat classification. However, the contact between ombrotrophic and minerotrophic phases may be rather transitional (Hiimaa et al., 2014; Paat et al., 2020). Identifying peat types in the radar images was complicated in the Rahivere Bog (Paper I), as well. Missing the well-expressed tree stump horizon is typical to the small inter-drumlin bogs within the Vooremaa Drumlin Field (Jõeleht, A., personal communication, 2022).

According to Cassidy (2009a), electric conductivity and relative permittivity are remarkably higher in wet snow than in dry conditions. Thus, the sounding results of the same strata may vary substantially. After compiling the same GPR transects in autumn and winter, Hänninen (1992) does not recommend GPR fieldwork in winter. In his opinion, snow and the frozen surface of the peatland undermine the results considerably. To some extent, the author agrees with Hänninen (1992) by admitting the CMP sounding implemented in Rahivere in February was disrupted by snow and ice. On the other hand, peatlands may be more accessible in the cold season (Comas et al., 2005; Proulx-McInnis et al., 2013; Pezdir et al., 2021). Bog ponds that can not be studied in summer become reachable through the ice cover (Mellett, 1995; Paat et al., 2020). Water molecules begin to polarise before freezing, thus increasing the dielectric permittivity and enhancing the EM wave spreading (Ruffell and Parker, 2021). Therefore, lower temperatures positively impact the GPR-sounding results in peatlands.

The Rahivere Bog, a depression encircled by drumlins, was formed during lake infilling after the glacial retreat (Allikvee and Orru, 1979). In Paper I, some implications about the bog genesis are raised. Initially, there were probably several glacially incised elongated lows which were later integrated into one mire. Other authors (Rosa et al., 2009; Proulx-McInnis et al., 2013; Pezdir et al., 2021) have proposed similar peatland-forming mechanisms. Peat accretion speed can differ a lot, even in adjacent mires. Hiimaa et al. (2014) calculated the lateral mire expansion rate of 0.6 m yr⁻¹ in the Selisoo Bog (NE Estonia). Presumably, in smaller Vooremaa mires, peat accumulation has been intermittently even more intensive due to articulated relief that affects the hydrological regime and nutrient availability.

After the Second World War, Estonian peatlands were systematically drained for agricultural purposes (Kimmel et al., 2010). Environmental protection and mire restoration become ever more relevant with extending knowledge about the peatlands as important natural carbon reservoirs.

For organising further protection remedies, the information about mire evolution, composition, and groundwater regime is crucial (Parry et al., 2014; Comas et al., 2017; Carless et al., 2021). The Rahivere Bog has been a valuable reference

region for subsequent studies. The objective of Paper I was essentially scientific – to provide general insight into the peatland forming mechanisms, composition, and volume estimation perspectives. The denouement that the Rahivere Bog is minuscule, and its peat resources are economically unfeasible, is evident just by looking at the map. Nevertheless, the procedures used for re-evaluating the Rahivere Peat Deposit with the GPR data could be applied more broadly. Additional notions concerning the peatlands as mineral resources will be discussed in Chapter 5.2.1.

4.1.2 Coastal and aeolian environments

Coasts have been studied with GPR worldwide (Bristow et al., 2000; Nielsen et al., 2009; Choi et al., 2014; Tamura et al., 2019). Sand and gravel, the main components of the coastal landforms, are exquisite substances for GPR studies. Due to low conductivity and magnetic permeability (Table 1), they generally grant good resolution and penetration depths (Bristow, 2009). Continuous GPR surveys of the beach-ridge systems, in conjunction with ground truthing and OSL, support quantitative and chronological estimation of sediment accumulation. These studies often deliver input for the climate change discussion (Buynevich, 2009; Tamura, 2012).

Considering the scientific papers published about Estonia, coastal research outnumbers all the other types of GPR activities (Fig. 7, Table 2). Paper II summarises a multi-proxy study where GPR surveys accompanied GIS modelling, sedimentological analyses, and OSL dating. A few GPR profiles for the Paper IV study also reached the foredune plain near Narva-Jõesuu Town (NE Estonia). However, regarding the thesis, coastal and aeolian morphodynamics are central subjects only in Paper II.

The Island of Ruhnu is not always accessible, hence the aim there was to obtain sufficient raw GPR data for further analyses. Altogether more than 30 km of profiling was carried out, primarily in the SE part of the island. The main focus was laid on one 1.6 km long, S-N oriented profile (Fig. 8). This transect provides evidence of the island's gradual ascending. Moreover, OSL dating and manual coring were performed along the same line.

The ideal profiling network consists of lines parallel and perpendicular to the sedimentary dip direction (Bristow, 2009). On Ruhnu Island, profiling was guided by the location and orientation of the foredune ridges. The western part of Ruhnu Island is predominantly forested. Natural preconditions did not favour determining the true dip directions and angles. Only apparent dipping was estimated during the Ruhnu GPR data analysis.

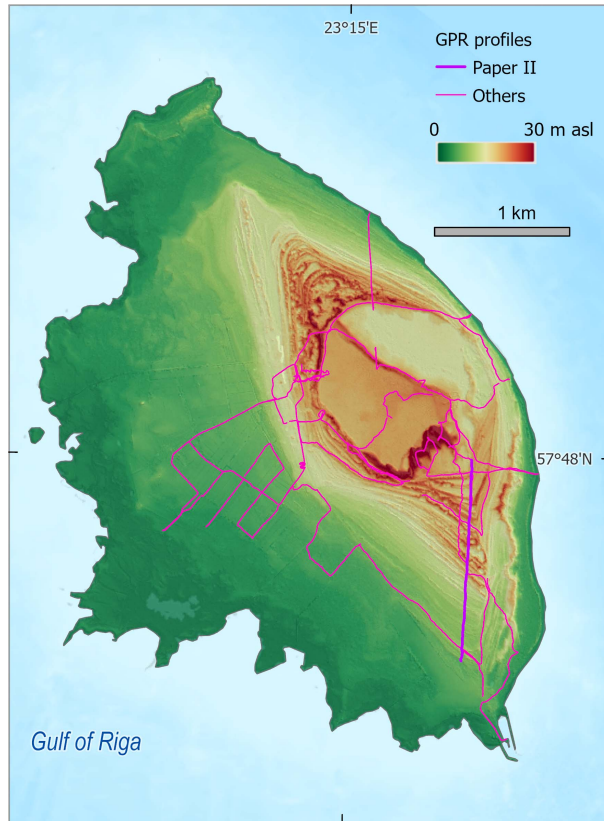


Figure 8. GPR profiles attained on Ruhnu Island. The S-N-oriented profile described in Paper II is shown with a thick purple line; all the others have thinner lines. LiDAR DEM (ELB, 2022c) represents the foredune successions and general topographic variability.

In Estonia, the most relevant GPR antenna frequencies for coastal studies have been 270–300 MHz (Table 2). For Paper II, a 300 MHz antenna set enabled visualising the stratigraphic sequences to the depth of 10 m. Relative permittivity was calculated by fitting the refraction hyperbolas. Permittivity values of 7 and 20 were used for estimating thicknesses above and below the groundwater table, respectively.

Four major radar facies were distinguished on Ruhnu Island, starting from the bottom:

- (a) Middle-Devonian sandstones and siltstones,
- (b) Late-Pleistocene till,
- (c) coastal sand and gravel, and
- (d) aeolian sand.

A rather similar geological cross-section has been described on Hiiumaa Island (Rosentau et al., 2020; Suursaar et al., 2022). In the Ruhnu radar images, the interface between the Devonian bedrock (presumably the Narva Formation) and till is generally well expressed. Till has greater permittivity and much higher conductivity than sandstone (Table 1). Occasionally signs of glacial diamicton consisting of variable grain sizes were observed in the radar patterns. Hyperbolic anomalies are often related to larger rocks and boulders within the finer-grained matrix (Moorman et al., 2007; Hausmann and Behm, 2011; Paper III). In the Ruhnu case, such hyperbolas may associate with boulders enclosed in till and its overburden. The acknowledgement of Kask et al. (1994) about till coating being <0.7 m thick was confirmed by the coring data (Paper II). In water-saturated sand, the theoretical vertical resolution of the GPR sounding was about 0.06 m ($\epsilon_r = 7$; see also Eq-s. 1–2). Occasionally till wedges were beyond the GPR resolution, indicating that glacial deposits may have been totally outwashed there (Kask et al., 1994).

Typically the GPR reflectors of the coastal successions have a gentle seaward dip with a flat or a minor concave-up design (Oliver et al., 2017). In the lithological context – sandy sub-parallel strata are superseded with coarser material. Gravelly intercalations that can be traced continuously over hundreds of metres in the longshore direction are relevant markers for documenting coevality (Lindhorst and Schutter, 2014; Tamura, 2018). According to the OSL datings (Paper II), the Ruhnu GPR images represent the deposits of the Litorina Sea. Pre-Litorina successions have been described in the central part of the island (Kask et al., 1994). Probably some of the ancillary GPR profiles (Fig. 8) characterise the Ancylus Lake period, as well. Nevertheless, without further sampling and dating, determining the bounding surfaces of the Baltic Sea stages remains inconclusive.

Beach development on the Island of Ruhnu has not always remained steady. Erosional surfaces and gravel beds coarsening at their landward extent may indicate abrupt storm events (Tamura, 2012). In the radar images, the storm deposits can be identified as planar high-amplitude reflections, occasionally amplified by high concentrations of heavy minerals (Buynevich et al., 2009; Cunningham et al., 2011).

Coastal sands between peat may refer to an ancient storm that carried coastal sands behind the ridges into a peatland (Buynevich, I.V., public lecture in UT, 2022). And vice versa, the sand bulk articulated by peat lenses occasionally exhibits a regressive episode (Habicht et al., 2017; Nirgi et al., 2019). GPR is an excellent tool for detecting peat lenses and estimating their vertical and lateral extent with high precision (Buynevich, 2009). Peat has been mapped in some depressions in the central part of Ruhnu Island (Kask et al., 1994). Earlier in the Holocene, the conditions for organic sedimentation were unsuitable. Hence peat was not discerned in-between the Ruhnu coastal deposits.

The topmost beds within the Ruhnu foredunes have been formed by wind activity, comprising mainly fine-grained sand. Contrary to the near-shore facies, the aeolian succession typically has landward dipping, larger dip angles and shorter wavelengths. Variable dip angles within the constantly well-sorted fine sand may

indicate changes in wind directions (Bristow, 2009; Lindhorst and Reimann, 2021). The sea-level oscillations induced mixtures of the marine and aeolian sediments, noticeable in the radar images.

Most of the Ruhnu GPR profiles were not presented in Paper II. However, they all provided valuable data for visualising the subsurface and describing the foredune progradation. Radar image analysis ensures a relative stratigraphic framework that can be used for selecting OSL sampling points (Bristow et al., 2005). Combined with coring and OSL dating, a more holistic understanding of the island's evolution was acquired. Knowing the forming mechanisms of the coastal landforms makes it easier to monitor the current processes and propose prediction models for sediment transportation.

4.2 Carbonate bedrock

Most carbonate bedrock research with GPR is related to karstification (Doolittle and Collins, 1998; Anchuela et al., 2009; Tao et al., 2022). Fewer papers have been published on faulting/fracturing (Chapter 4.3) and mineral surveys (Chapter 5.2.2). In NE Estonia, where the Palaeozoic limestones and dolostones are blanketed with a relatively thin layer of Quaternary sediments (Figs. 1–3), all the above-mentioned situations can be encountered. Besides Paper III (i.e. the biggest contributor to the current chapter), bedrock structures were also investigated in Paper IV. Henceforth, the issues associated with the bedrock relief and composition will be summarised, while the pre-Quaternary and glacial tectonism will be discussed later in Chapter 4.3.

Several GPR field campaigns were conducted for Paper III, with a total profiling length of 66 km. A 300 MHz antenna configuration granted the maximum survey depth of 4 m. One major disadvantage of GPR – confined penetration depth in conductive soils – can be surmounted with other techniques. Integrating several geophysical methods is a common practice (Slater and Reeve, 2002; Pellicer and Gibson, 2011; Comas et al., 2015; Diallo et al., 2019; Tao et al., 2022). In Viru-Nigula, the GPR survey was augmented with the ERT profiles (Paper III).

According to the hyperbolic anomalies observed in the GPR images, the average permittivity of 9 was assigned for the Ordovician bedrock. This value is in accordance with other limestone studies (Table 1; Mustasaar et al., 2012; Mount and Comas, 2014). Carbonate rocks and sands have similar relative permittivity values (Table 1), yet they have specific characteristics in the radar images. Typically the bedding planes of the carbonate shelf facies are represented by parallel subhorizontal reflections of several hundred metres in length (Papers III and IV). For Paper III, the best GPR results were obtained in places where the surficial deposits are thin (<2 m), and the Ordovician limestones directly underlie the Quaternary sands. In the Viru-Nigula study area, the basal part of the superficial sequence frequently comprises clayey till. Numerous hyperbolic reflections in the radar images are related to larger boulders within the lowermost portion of the till

body. Similar hyperbolas have also been detected at the other types of bedrock-till contact (Paper II and IV). Geologically, the hyperbolas can also be associated with local weathering, karst or faulting (Porsani et al., 2006; Grasmueck et al., 2013; Sellmann et al., 2022).

Even a relatively thin (<2 m) till layer can diminish the EM penetration depth substantially, thus the bedrock remains unreachable with GPR (Chapter 4.1). As expected, bedrock was not detected within the Varudi Bog, where the total thickness of the Quaternary deposits (predominantly till) reaches 30 m (Suuroja et al., 2006). In the radar images, the bedrock top surface was traced to 4 m, dispersed at greater depths, or remaining in the shadow zone because of the conductive overburden. Fortunately, even the absence of data may be useful. For example, in the northern part of the study area, the gap within the GPR-derived bedrock top surface was registered in several NW-SE-oriented radar images (Paper III). When these gaps are juxtaposed on the map, a rough estimation of the direction and inclination of the sought bedrock structure can be delivered.

The GBM displays a long buried valley running through the Varudi Bog in the S-N direction. On the western edge of the study area, another, more spacious valley (the Kunda Valley) has been outlined (Paper III). According to Rattas (2007), the bedrock valleys have been important pathways for subglacial meltwater. Presently, some valleys possess remarkable groundwater resources within the porous Quaternary aquifers. Geophysics provides valuable data for exploring the geometry, composition, and hydrogeological conditions of buried valleys (Wolfe and Richard, 1996; Sandersen and Jørgensen, 2003; Auken et al., 2009). The groundwater yield of the Varudi Valley is not remarkable due to its small dimensions. However, as the methodology allowed adjustment of the morphology of the bedrock incision, it can be treated as a success story and reiterated elsewhere.

In the Viru-Nigula study area, the GBM shows the general Estonian trend by representing younger bedrock formations southwards. In the northern part of the study area, the Middle Ordovician Vão and Kõrgekallas Formations have been mapped right beneath the Quaternary overburden. In the south, the top of the bedrock is represented by the Upper Ordovician sequences (ELB, 2022e). Perhaps the most remarkable of all these units, especially regarding mineral extraction, is the Vão Formation. According to Hints (1997), it consists of three members, (a) the Rebala Member (argillaceous limestone), (b) the Pae Member (dolostone), and (c) the Kostivere Member (thick-bedded hard limestone).

In Paper III, the mineral potential was not the primary target. However, as the GPR images reveal the Quaternary thickness, they can also be helpful for feasibility estimation. The Viru-Nigula study area has a partial overlap with a limestone perspective area. The same units mapped in the Viru-Nigula bedrock map are currently extracted from the nearby quarries (ELB, 2022e). Carbonate rocks, concerning mineral exploration, will get the spotlight in Chapter 5.2.2.

Dagallier et al. (2000) point out that the pattern characteristics (frequency, amplitude, continuity, geometry) of the GPR images can help to distinguish limestones by their facial origin. Even low-frequency antennas (50–100 MHz)

can provide enough details for detecting facial changes (Dekeyser et al., 2007). More porous/permeable carbonate rocks transfer stronger EM responses. However, due to the porosity variations and argillaceous interlayers within the lithological entities, correlating the radar facies directly with the stratigraphic ones is not explicit (Franseen et al., 2007; Knoph et al., 2010; Mustasaar et al., 2012).

As no direct core/outcrop inspection was carried out in Viru-Nigula (Paper III), it was complicated to identify the formations and members in the radar images. In some sections, the EM signal penetration decline might be associated with more argillaceous beds (Martinez et al., 1998; Mustasaar et al., 2012). Occasionally the bedrock reflections wedge out; these patterns may indicate the facial substitution. Ground truthing or new GPR studies at a nearby exploited quarry might be beneficial for better assurance.

The Viru-Nigula case (Paper III) is significant for the diverse geological setting. Previously, the region was quite realistically mapped (Suuroja et al., 2006). While geophysics typically precedes coring, it was the opposite way around this time. In the Varudi Bog, the cartographers of the GSE drilled precisely into the bedrock incision, proving that intuition is a substantial asset for geologists. However, the origin of the Varudi Buried Valley remained vague until the geophysical engagement. GPR and ERT surveys unmasked two fracture zones where the bedrock has been crushed, outwashed and replaced by the Quaternary sediments. Papers III and IV confirm that even if the bedrock structures lie too deep for complete depiction, GPR can be successfully applied for framing their indicative borders.

4.3 (Glacio)tectonic activities

As noted in the previous chapter, geophysics is often indispensable for acquiring data about tectonic features. Ground-penetrating radar has been widely used to map the shallow subsurface where glacial and pre-Quaternary dislocations may occur (Busby and Merritt, 1999; Overgaard and Jakobsen, 2001; Høyer et al., 2013; Sellmann et al., 2022). Northern Estonia has excellent preconditions for such investigations (Fig. 1, Papers III and IV). In the Viru-Nigula case, GPR was suitable for the primary identification of the bedrock faults (Paper III; Chapter 4.2). The Viru-Nigula study area is located next to the Aseri Fault System (Paper III; ELB, 2022e); hence, finding new pieces of faulting evidence is not surprising. The area between the Sillamäe and Narva towns is even more attractive, considering the overall density of the multi-scale ground displacements (Suuroja and Ploom, 2016). Therefore, the current chapter focuses mainly on Paper IV.

About 170 km of GPR profiling was done in the Vaivara Deformation Zone (VDZ) and farther eastwards, up to the Narva Old Town (Paper IV). Predominantly an antenna arrangement of 300 MHz was applied, with occasional support from the 100 MHz set. For the carbonate bedrock, an average EM wave velocity value of 0.093 m ns^{-1} was derived from the hyperbolic reflections (which corresponds to the relative permittivity of 10, according to Eq. 1). Both the

relative permittivity (10) and the maximum penetration depth (4 m) with a 300 MHz antenna in the VDZ (Paper IV) are similar to the respective values obtained in Viru-Nigula (Paper III).

One type of the radar facies – the constant, subhorizontal layout following the regional bedrock dip angle – has already been described in Chapter 4.2. Some Ordovician bedrock units remarked in Viru-Nigula (e.g., the Vão Formation) extend to the southern periphery of the VDZ. Lithostratigraphic units were not delineated in Paper IV due to the deficit of the direct measurements (see also Chapter 4.2). Besides the Ordovician limestones, the other types of bedrock are also mirrored in the radar images. Sandstones are typically represented by occasionally fluctuating patterns, at times similar to the limestones. Yet the reflective surfaces of the sandstones intersect and wedge out more often, illustrating the cross-bedding conditions of the tidal palaeobasin.

It is important to remember that the Estonian bedrock has repeatedly been under stress throughout the Phanerozoic. Põldsaar and Ainsaar (2015) present different liquefaction-induced deformations in the Cambrian outcrops along the North Estonian Klint, 200 km westwards from the VDZ. At first glance, dating any deformation is complicated in the outcrop, not to mention the indirect GPR inspection. However, a deformation visible in the outcrop can be linked with the relevant GPR image, and thus extended to the concealed space. For example, Fig. 6 in Paper IV provides such a bilateral view from the Udria Cliff.

Bedrock faults and fractures can be located with GPR due to different porosity and grain-size distribution within them, compared to the surrounding material (Tanner et al., 2020). In the VDZ area, numerous types of deformations were detected, indicating local variations in the sub-glacial pressure.

The deformations were grouped into three types:

- (a) subhorizontal wavy reflections, with modest (<3 m *per* 100 m) vertical undulations; occurs in the carbonate bedrock,
- (b) inclined reflections, with larger apparent dip angles (>3 m *per* 100 m), occur in the carbonate bedrock and may contain fold and fault elements; hence it is not easy to distinguish from type (c),
- (c) thrusts, folds; observable in present topography as elongated ridges.

Type (a) represents a relatively homogeneous architecture, while the others tend to associate with the collisional contacts between the adjoining bedrock blocks. Attempts were made to outline the margins of those blocks based on the radar interpretations, LiDAR DEM, and some topographic features (e.g., the drainage system). In some places, the blocks seem almost perceptible (e.g., between the Udria and Meriküla villages; Fig. 3B in Paper IV). However, in most of the study area, such block alignments would be too equivocal without additional data.

Despite the difficulties with the spatial depiction, the most outstanding blocks deserve at least a concise description. In Paper IV, the Sinimäed Hills, the Laagna

heights, the Udria Cliff, the Puhkova blocks, the Sõmerkallas Bank, the Pähkli-mäed Hills, and the Narva block, are provided with the GPR interpretations.

Paper IV delivers the first attempts of characterising the glaciotectionic deformations within the solid sedimentary bedrock, by applying GPR. The strengths and weaknesses of the method become evident. Occasionally the shape and structure of the deformed bedrock blocks can be derived from the radar images. Yet, for the proper structural mapping, additional geological/geophysical methods should be incorporated.

The region between the Sillamäe and Narva towns has been studied repeatedly (Suuroja and Ploom, 2016), whereas every succeeding survey sheds more light on the geological background. Several Middle-Ordovician bedrock blocks within the Lower Palaeozoic clay diapirs are currently shown in the GBM (ELB, 2022b). Paper IV and the following surveys obviously motivate updating the GBM. However, adjusting the map composed of numerous individual layers is rather complicated. Hopefully, such revisions can be made more smoothly in the future (Chapter 5.4).

5. RAISING THE EFFICIENCY OF THE GPR STUDIES

5.1 Geological mapping

As a relatively fast and accurate method, ground-penetrating radar has an excellent mapping potential (Chapter 3.2.3 (g)). It can be applied for acquiring new geological data, or verifying the integrity of existing maps (Schellentrager et al., 1988; Daniels, 2004). The Estonian case studies (Chapter 4) indicate that GPR can be used for mapping the composition of superficial deposits (peat, sand, gravel), bedrock relief, and deformations. Maximum penetration depth in different sediment types is visualised in Fig. 9. The GPR possible contribution to the GBM thematic maps (ELB, 2022b) is introduced below.

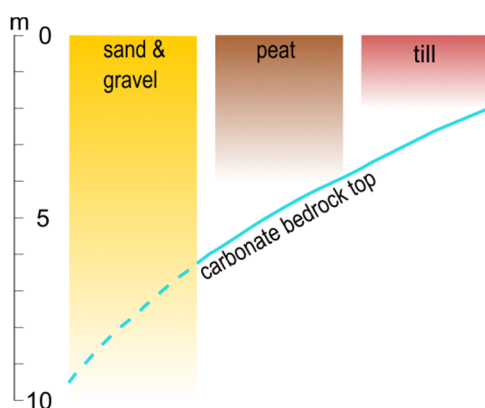


Figure 9. Maximum penetration depth in Quaternary sediments with the 300 MHz antenna, according to Papers I–IV. For the respective permittivity values, see Table 3.

Generally, the bedrock relief and the thickness of the Quaternary are the first GBM layers mapped by the GSE cartographers. According to Paper III (Chapter 4.2), the bedrock top can be tracked with GPR if (a) the thickness of superficial deposits is moderate (<4 m), (b) the clay/till bedding is limited (<2 m), and (c) the physical properties of the bedrock differ significantly from the superficial ones. The thickness of the Quaternary deposits does not exceed 1 m in about 2500 km² of northern Estonia (Ani and Meidla, 2020; Fig. 3). About half of those thin-Quaternary areas have not been mapped in the GBM yet (Fig. 10).

Thin Quaternary cover typically encourages the economic exploitation of the carbonate rocks (see also Fig. 12). Geological mapping should guide the mineral exploration to the areas of the most promising deposits and the least possible mining-induced stress. Mineral occurrences are mapped as points or polygons in the GBM (ELB, 2022b). Chapter 4 indicates that GPR could assist in locating the favourable peat, sand, gravel and carbonate deposits. With respect to the resource estimations, those materials will be further discussed in Chapter 5.2.

The best quality limestone for the construction industry is extracted from the Middle Ordovician Vão Formation (GSE, 2022c). Ani and Maido (2022) note that the previously mapped distribution of the Vão Formation perspective areas needs revision. Typically the overburden is thin in those areas (Fig. 10), thus, GPR can be used for getting more accurate thickness data. It might be even possible to trace the argillaceous beds by following the same stratification design visible in the quarries and cores (see also Chapter 4.2). According to Jorry and Bièvre (2011), the distinct lithological facies and bioherms can be recognised with GPR.

Bedrock faults, fractures and deformations are significant regarding mineralization, mining constraints, groundwater resources and protection. The faults in the Estonian bedrock are classified as (a) identified (confirmed with ground truthing), and (b) presumable (discovered primarily by the geophysical methods); (ELB, 2022b; Fig. 10). The fault zones and minor deformations are observable with GPR (Chapters 4.2–4.3). Hence the radar could be applied for updating the respective GBM feature classes. For example, adjusting the spatial extent of the bedrock faults within the Vão Formation perspective areas (Fig. 10) is relevant, regarding the possible quarrying developments.

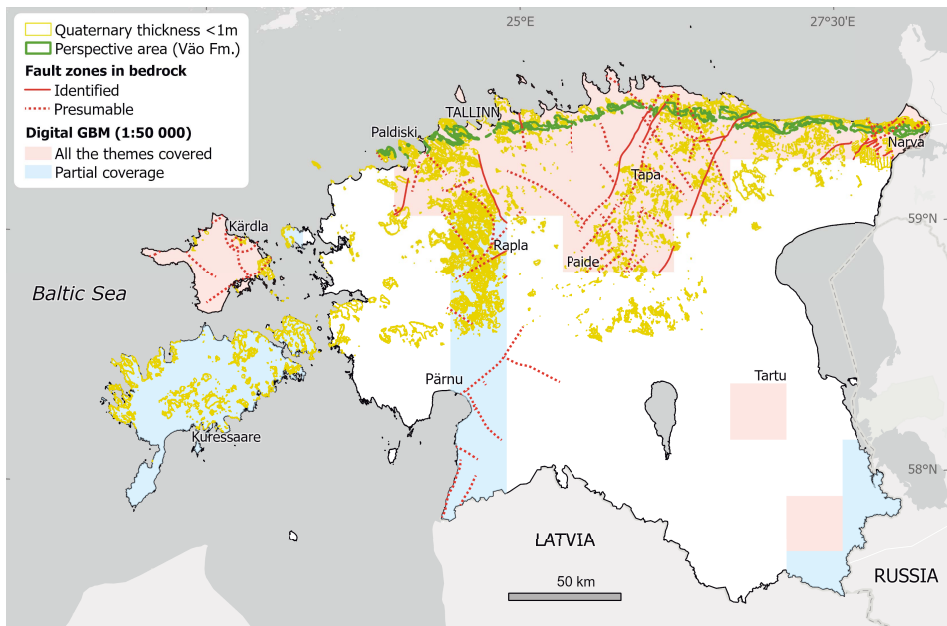


Figure 10. Light pink and blue sections are covered with full, or partial digital Geological Base Map (GBM), respectively. Red lines mark the bedrock fault zones (GSE, 2022b). Yellow polygons indicate the thin Quaternary cover (according to the GBM and the Fig. 2 derivation in the presently unmapped sheets). The spatial extent and feasibility of the Vão Formation limestone perspective areas (shown with green colour) need further assessment (Ani and Maido, 2022).

Dissolution of the carbonate bedrock is a relatively common phenomenon in northern Estonia (Pirrus, 2007), controlling the local hydrological regime and groundwater vulnerability. The case studies (Papers I–IV) confirm that the groundwater table is easily detectable with GPR (Chapter 3.2.5); occasionally, the signs of karstification were noticed in the radar images (Paper III). Up to now, karst has not been a critical subject in the Estonian GPR practice (Chapter 3.2.4). However, the foreign cases indicate that GPR is an effective method for mapping underground rivers, cavities, and small karst-related features (Chapter 3.2.3 (g)). Furthermore, GPR can assist in groundwater monitoring projects and positioning new wells (Chapter 3.2.3 (h)).

Sand and gravel can be easily distinguished and classified by grain size in the hand-made trial pits, which are typically about 1 m deep. Besides providing better vertical coverage, GPR can help to locate the bedding alterations between the pits. The mapping fieldwork would be even more effective if a lightweight hand auger or a shovel were conveyed during profiling. Perhaps the sampling from pits can be done right after observing essential changes in the GPR pattern. For sediment dating, occasionally, OSL sampling might be appropriate (Paper II). If the pitting must be postponed, the sites can be marked for the next time. When radar profiles overlap with ground-truthing, the mapping uncertainty can be reduced significantly.

In the Quaternary succession, many other lithological varieties can be mapped with GPR (Chapter 3.2.3 (g)). Paper I represents one approach for contouring the peat bottom. Although peat thickness can be estimated quickly and precisely with GPR (Chapter 4.1.1), developing a regular peat profiling grid for the Quaternary mapping plan is irrational. GPR is still a practical choice for a more specific need, like (a) validating the discordant mapping data, and (b) providing more nuanced resource estimations (Chapter 5.2.1).

5.2 Resource assessment

The Environmental Ministry Decree regulates Estonian mineral exploration and resource assessment. Mineral resources are divided into commodities according to mineral lithology and quality. The reserves are calculated separately for each commodity, while the reserves above and below the water table must be also distinguished. To establish proved mineral reserves for the extraction, sampling from the cores, outcrops, or trial pits must be carried out with sufficient density. Geophysics can also be engaged during the exploration, primarily for specifying the bedding conditions of the mineral material and its overburden (ENVIR, 2022a; Table 4). In the following two chapters, the possible contribution of GPR to the Estonian peat and aggregate resource estimation will be discussed.

Table 4. Mineral commodities, the size of the biggest survey grid allowed, and the reserve calculation unit with accuracy, according to the Environmental Ministry Decree (ENVIR, 2022a).

Mineral	Commodities	Survey grid	Unit
peat	undecomposed	200 m	10 ³ t*
	decomposed		
sand; gravel	construction	200 m	10 ³ m ³
	filling		
	technological**		
limestone; dolostone	high quality	50–400	10 ³ m ³
	low quality		
	filling		
	ornamental		
	technological	50–200 m	

* Volumes are converted to weight, using decomposition coefficients for 40% conditional humidity.

** Applies only for sand.

5.2.1 Peat

The MR embodies 3550 km² of peat deposits, where the peat thickness exceeds 0.9 m (ELB, 2022a; Fig. 11). GPR profiling in the Rahivere Deposit is discussed in Paper I. In this chapter, firstly the results of the Rahivere Deposit volume calculations are introduced, followed by some general comments, and a foreign use case.

The Rahivere Deposit (0.54 km²; for location, see also Figs. 4 and 5a), embodies 979 000 m³ (97 000 tons) of peat; the estimation is based on 13 manual corings (Allikvee and Orru, 1979). In the MR, these reserves are divided into undecomposed (77 000 m³) and decomposed (902 000 m³) commodities (ELB, 2022a). Those two types could not be differentiated in the radar images (Paper I). Even if the tree stump horizon favours such distinction in the other peat deposits (Chapter 4.1.1), the resulting surface remains rather indefinite.

However, Paper I demonstrates a superb alternative for the total resource estimation. In case the top surface of the mineral soil is articulated, GPR enables estimating the total peat volume more precisely than just coring. GPR sounding with a 300 MHz antenna provides the theoretical vertical resolution of 0.03 m, while the thickness accuracy for the reserve approval must not exceed 0.05 m. The 200 m radar profile spacing also satisfies the exploration requirements (ENVIR, 2022a; Table 4).

The valid peat extraction permits cover 220 km² (Fig. 11). The Rahivere Deposit is not presently exploited and probably will never be. The European

Union’s policy for reducing carbon emissions indicates that the pristine peatlands need more protection. Hence the Estonian Ministry of the Environment favours withdrawing the deposits from the previously exploited and later abandoned peatlands (ENVIR, 2022b; ENVIR, 2022c), covering 40 km² of the country (Fig. 11). In those areas, GPR can support remnant reserve calculations in the first order.

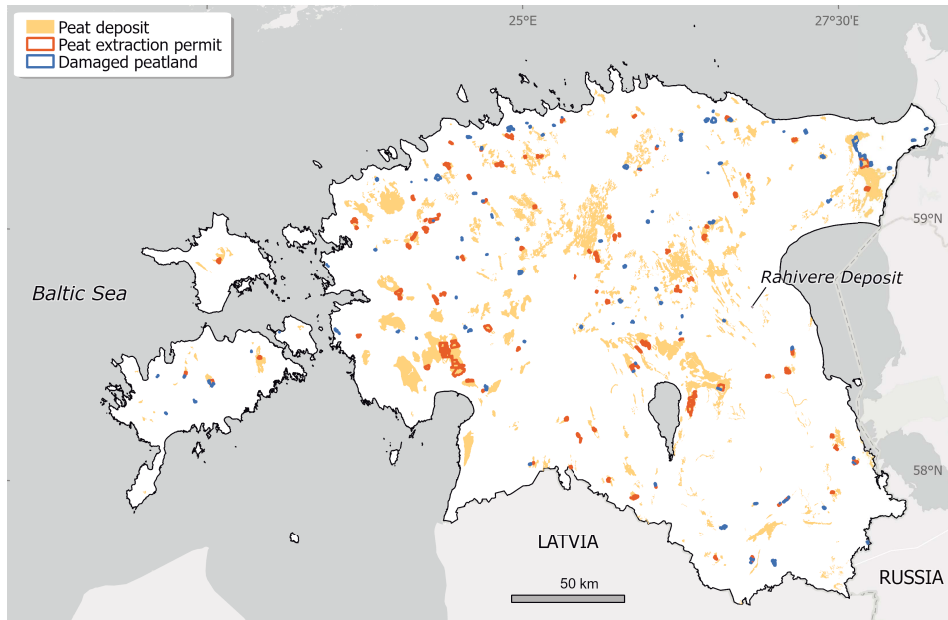


Figure 11. Peat deposits, extraction permits, and damaged peatlands according to the Mineral Registry of Estonia (ELB, 2022a) as of December 01, 2022.

The Geological Survey of Finland has conducted GPR studies in peat production areas for decades. With antenna frequencies of 100–250 MHz and profile spacing of 40 m, approximately 10 000 km of GPR lines (450 km²) have been accomplished. The results are used for (a) managing production fields, (b) applications for environmental permits, (c) mass calculations, and (d) peatland restoration (GSF, 2020).

In Estonia, GPR has shown excellent efficiency in larger mires, towed by an amphibious vehicle (Paat et al., 2020). The aforementioned Finnish experiences, as well as Paper I and Chapter 4.1.1, encourage using GPR for the total peat resource estimations. A 300 MHz frequency antenna is typically a good choice. Lower frequencies should also be considered if peat thickness exceeds 4 m. Along with the volumes, more insight can be achieved into the surrounding hydrological conditions. Regardless of the sounding purpose, the GPR studies should be accompanied by probing. Direct measurements assist both the EM velocity estimation and the radar facies recognition.

5.2.2 Aggregates

By the general definition, sand, gravel, and crushed carbonate rocks are called „aggregates“ if used in the construction industry. In this chapter, the mineral material is primarily considered as lithological bodies. Later on, some remarks will also be made on the ornamental carbonate rocks, which are essentially not aggregates but deserve some attention.

Sand is a granular substance where the ratio of particles >31.5 mm is less than 35%. Material exceeding this ratio is classified as gravel (ENVIR, 2022a). Frequently they coexist in one deposit. As of December 1, 2022, the valid permits for mining sand/gravel covered 56 km², while the reserves are evenly distributed throughout the country (Fig. 12; ELB, 2022a).

By genesis, the Estonian sand and gravel deposits are mostly of glaciofluvial origin; glaciolacustrine, aeolian and marine types cover $<30\%$. Yet even coastal landforms contain coarse sand and gravel that may be of economic interest locally (Räägel, 1997). Grain size within the glaciofluvial landforms (e.g., eskers) is quite variable. Occasionally the useful beddings are ruptured by clay or till wedges.

According to the coastal studies (Chapter 4.1.2), sand and gravel transmit distinctive radar signals, thus enabling their differentiation. GPR is considered valuable for sand and gravel resource evaluations (Busby et al., 2004). McCuaig and Ricketts (2004) claim GPR supports gravel quarry planning, while a 100 MHz antenna set can acquire data from depths to 30 m. Bērziņš et al. (2017) used two configurations in a sand quarry – with a 300 MHz antenna, the maximum survey depth of 10 m was achieved, whereas the 75 MHz one enabled somewhat better (10–15 m) coverage.

The previously mentioned examples indicate GPR can be used as a complementary tool for reserve calculations. In the Estonian case, the sand and gravel deposits must be probed with a certain density before quarrying (Table 4). GPR may be used (a) in the early stage of exploration for pinpointing the probing sites, (b) during the extraction to get more details about the lithological changes, or (c) repeatedly.

Two types of carbonate rocks are regarded as mineral resources in Estonia: (a) limestone, and (b) dolostone. As of December 1, 2022, valid permits for their mining covered 24 km². Due to the regional bedrock geology (Fig. 1), the carbonate quarries are assembled almost entirely in the north (Fig. 12; ELB, 2022a). Both the limestone and dolostone reserves are classified into several commodities (Table 4). For the ornamental stone (Fig. 12), the quality of the material is essential.

Papers III and IV present detectable fractures several metres below the ground. The studies conducted in different limestone quarries suggest GPR can provide more efficiency in mine planning (Sigurdsson and Overgaard, 1998; Chamberlain et al., 2000; Dagallier et al., 2000; Dekeyser et al., 2007; Zanzi et al. 2019; Elkarmoty et al., 2018).

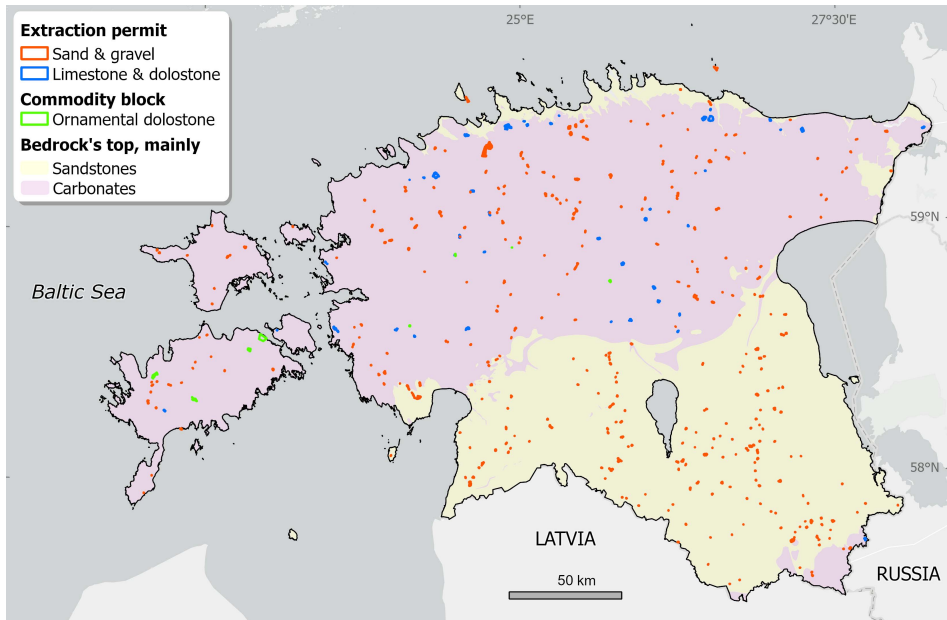


Figure 12. Locations of the aggregate extraction permits as of December 01, 2022, according to the Mineral Registry of Estonia (ELB, 2022a). The ornamental dolostone reserves are shown separately. Bedrock's topmost units are divided into sandstones and carbonates (as a derivation from the map displayed in Fig. 1).

Ground-penetrating radar sounding may be problematic in case the deposit is covered with till. Regardless of the thickness of the overburden, till has to be removed entirely before aggregate quarrying can start. Thus the time window between the till relocation and the mineral extraction is probably the best chance to engage GPR. During the extraction, the active face can also be sounded to locate the possible fracture zones and karst cavities ahead.

To summarise the outlooks for the aggregate resource estimation:

- (a) the borders between the GPR facies and the mineral commodity blocks are mostly discordant. Hence GPR alone does not allow classifying and estimating the reserves,
- (b) GPR can be applied before invasive procedures to specify the best borehole/pit locations,
- (c) GPR may reduce the drilling capacity in more complicated geological situations, and
- (d) GPR can contribute to selective mining in the working quarries. The lithological changes, karstification, and fractures observed in the GPR images may guide the active face advancement.

5.3 GPR antennas and carriers

Taking several antennas to an uncharted field may be a good idea. After some testing, the radar images reveal the best apparatus arrangement. The concern about the ideal frequency can be subdued, as the antennas emitting various frequencies simultaneously are also available (Chapter 3.2.1).

Until now, Estonian GPR studies (Chapter 3.2.4) have been performed only on the ground surface and ice, typically with 100–300 MHz antennas (Table 2). For surveys up to 10-km scale, pulling them with manpower is often the optimal technique. On roads, the antennas are towed by cars, while ATVs seem more appropriate in wild terrain (e.g., mires, forests). In fact, GPR usage is not fixed to these environments and carriers – additionally, the antennas may be lifted above the ground, submerged below the ground (Slob et al., 2010) or even water (Ruffell and Parker, 2021). Next, some GPR antenna configurations are introduced, which may be beneficial in the local context.

GPR application in mineral exploration is not limited to peat and aggregates (Chapter 5.2). Estonia's most intensive mining activities are related to oil shale extraction. For quarry development, more data are frequently required about the faults within the oil shale and its overburden (mainly limestone). A 50 MHz flexible 9 m long „snake“ antenna may increase the penetration depth to 30 m in limestone while the resolution (0.6 m) still upholds faults and larger fractures (Zanzi et al., 2019). In an underground limestone mine, a vertically positioned 200 MHz antenna enables to study karst cavities 5–10 m far from the active face (Baggett et al., 2020).

An unmanned aerial vehicle (UAV) may be the only way to collect data in rugged or otherwise complicated areas. For GPR data acquisition, different airborne platforms have been used (Noviello et al., 2022). In limestone quarries, for instance, UAVs equipped with lightweight GPR devices are applicable for mapping tectonic features (Saponaro et al., 2021; Zhao et al., 2022). Borehole GPR can accompany other logging methods during hydrogeological (Chang et al., 2006) and mineral (Bellefleur and Chouteau, 2001; Ma et al., 2016; Looms et al., 2018) research. Remotely controlled GPR robots are currently developed primarily for UXO detection (Bechtel et al., 2018). Safety restrictions, limited accessibility, and the need for higher productivity promote robot assistance more widely and much closer than Mars (RIMFAX, 2022).

5.4 Data processing and management

GPR users want to fill two needs with one deed – achieve adequate depth and maintain a reasonable resolution simultaneously. Multi-fold radar systems (Chapter 3.2.1) help to satisfy the demand, yet with a remarkable increase in the data volume. Regardless of the antenna setup, manual data processing is time-consuming. GPR studies are more productive if some procedures get automated.

Machine learning (ML) supported algorithms can be used for tracing the characteristic patterns in radar images. Various techniques have been proposed for the automatic detection and classification of hyperbolas (Chen and Cohn, 2010; Dou et al., 2017; Harkat et al., 2019; Yamaguchi et al., 2022). Numerous GPR tools are published as open-source packages (GitHub, 2022a); access to the radar images compiled by different proprietary GPR programs is also supported (RGPR, 2022).

Preferably, ML-assisted data processing should be launched already in the field. The author recommends the GPR vendors to upgrade their software with the option to integrate the LiDAR topography and drill logs into the radar images on the fly. Both data sets should be imported in standardised file formats (e.g., WIKI, 2022b; GitHub, 2022b). The additional window next to the radar image might show the radar location in the geological map/orthophoto/DEM. Extending the GIS capabilities with a GPR plug-in (e.g., De Angeli et al., 2022) is another way to put more efficiency into the data processing.

Blending the GPR interpretations from different field campaigns, collected by various radar operators, requires consistent interoperability. Essentially, the GPR data points might be handled similarly to the LiDAR points, assembled by airborne or terrestrial scanners, and classified into distinct groups (Gigli and Casagli, 2011; Park and Guldman, 2019). In the GPR programs, vertices (points) clicked to the bounding surfaces automatically gain the X, Y, and Z coordinates during the interpretation. The author would assign those points additional attributes, indicating the appropriate GPR radar surface (e.g., 1 for the peat bottom, 2 for the Quaternary bottom etc.). Then the GPR points characterising different radar surfaces can be exported simultaneously as one data set and compiled into a GIS database as 3D point clouds. Entirely new perspectives can be opened by fusing the GPR and LiDAR clouds into a coherent structure (Merkle et al., 2021).

In the coming years, the ELB's data collection, modelling and visualisation will move to the Geo3D mapping environment (ELB, 2022f). Among the other information (topography, infrastructure, property maintenance etc.), the GPR results verified by the core logs are an essential addition to the Geo3D underground module. The LiDAR, borehole, and GPR data fused into one national up-to-date 3D platform will hopefully lead to fantastic synergy. The proposed data flow between the GPR operator and the Geo3D host database is shown in Fig. 13.

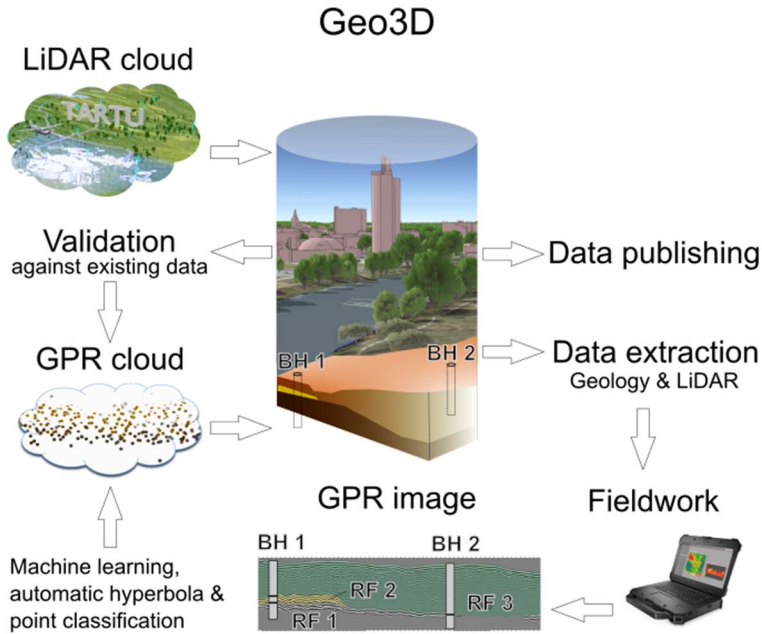


Figure 13. The proposed GPR data circulation with the Estonian Geo3D database (pictures taken from the ELB, 2022g, ELB, 2022h, Paper III, DELL, 2022; modified by the author). An extraction is made for a new survey project according to the spatial query from the host database. The surveyor gets LiDAR DEM and a geological model with the coring data for the study area. LiDAR relief and boreholes (BH) are plotted in the radar images automatically; machine learning tools assist radar facies (RF) recognition and classification. Vertices (i.e., points) of the radar bounding surfaces are the main interpretation results. The geological units in the Geo3D host database will be adjusted after the new GPR point cloud has passed the validation.

5.5 Data sharing

Every GPR surveyor obviously wants to get new data about the study object. After the results have been delivered, perhaps the data remains in one computer for a while and then disappears forever. Online scientific papers and exploration reports continue exhibiting text and figures without spatial data. Hence finding the necessary sources and associating the described objects with the correct positions is complicated afterwards.

European directive on open data and the re-use of public sector information (EU, 2019/1024) declares:

(27)

The volume of research data generated is growing exponentially and has potential for re-use beyond the scientific community. In order to be able to address mounting societal challenges efficiently and in a holistic manner, it has become crucial and urgent to be able to access, blend and re-use data from different sources, as well as across sectors and disciplines.

...

Open access helps enhance quality, reduce the need for unnecessary duplication of research, speed up scientific progress, combat scientific fraud, and it can overall favour economic growth and innovation.

The GPR profiles of the four case studies (Papers I–IV) are shown in the GBM (ELB, 2022i), while the web link to the proper paper is displayed with just a click. The author encourages all the GPR data owners to share their outcomes similarly. Besides the profiles, their interpretation points can also be displayed on the map, after being uploaded to the ELB web application (ELB, 2022j). Both feature classes are freely downloadable as open spatial data.

In the coming years, the GPR interpretations will help to frame the Geo3D subsurface domain. And then, the data, once collected with GPR on the field, enriched with the other Geo3D information, will serve the following surveys as the best possible input.

*We can only see a short distance ahead, but
we can see plenty there that needs to be done.*

Turing (1950)

6. CONCLUSIONS

The thesis is built up on four scientific papers, each focusing on a specific geological situation. The results confirm ground-penetrating radar (GPR) suitability for describing the near-surface strata in peatlands, sandy environments, and carbonate bedrock. Contrarily, the capability in the conductive clays and tills is rather limited. GPR can be used in the geological mapping process for the systematic validation of old data, and obtaining new data about:

- (a) bedrock relief and the total thickness of the Quaternary succession,
- (b) lithological properties of the Quaternary deposits,
- (c) hydrogeology – water table, karst features, groundwater vulnerability,
- (d) bedrock faults and other tectonic deformations, and
- (e) peat and aggregate perspective areas.

Estonian mineral exploration is based on sample collection and description. The author suggests GPR as a preparatory tool for assisting the sampling point placement. With smart integration of coring and EM sounding, more details about the mineral quantity, quality and mining constraints can be exposed. Such information is crucial for selective mining operations. GPR can potentially decrease exploration costs and increase extraction profits.

Although GPR enables to cover large areas with continuous data flow, the results remain ambiguous without direct measurements. Considering the data acquisition speed and cost-efficiency, GPR might be the first method to start with. After the preliminary data analysis, ground truthing (e.g., coring, test pitting) should follow wherever possible. Radar studies combined with other methods (e.g., coring, ERT, OSL) grant more comprehensive understanding of the sub-surface layout than just a single approach.

In Estonia, typically common offset radar surveys are organised, where the maximum penetration depth is limited to 5–10 metres. Foreign examples demonstrate the multi-frequency systems, “snake” antennas, and borehole instruments allow much deeper data acquisition. The manual workload of data processing can be reduced significantly as computers can be trained to recognise specific patterns in the radar images. GPR vendors are very welcome to implement the software upgrade ideas proposed by the author.

The thesis overviews the Estonian GPR studies conducted and published so far. The focus is mainly on geological and mineral studies; however, GPR is also indispensable in civil engineering, archaeology, and many other fields. As the spatial survey results are predominantly unavailable, the interpreted data reuse (e.g., for the map updates and machine learning activities) is complicated. The

author encourages all the data owners to share their GPR profiles and interpretation points in the Land Board's geoportal. Three-dimensional GPR points derived from the radar images can contribute to the up-to-date subsurface module of the future Estonian Geo3D mapping environment. Multilateral open data sharing ensures that for every new survey, the best geological insight will be available as a reliable source.

REFERENCES

- Agred, K., Klysz, G., Balayssac, J.-P. (2018). Location of reinforcement and moisture assessment in reinforced concrete with a double receiver GPR antenna. *Construction and Building Materials*, 188, pp. 1119–1127.
<https://doi.org/10.1016/j.conbuildmat.2018.08.190>
- All, T., Puura, V., Vaher, R. (2004). Orogenic structures of the Precambrian basement of Estonia as revealed from the integrated modelling of the crust. *Proceedings of the Estonian Academy of Sciences. Geology*, 53(3), pp. 165–189.
https://books.google.ee/books?id=9TbFL2OuWrcC&source=gbs_all_issues_r&cad=1
- Allikvee, H., Orru, M. (1979). *Report of the Search and Investigations at the Peat Deposits in the Jõgeva District*. Geoloogia Valitsus, Tallinn, 446 pp. GA No. 5182. [In Estonian]. <https://fond.egt.ee/fond/egf/5182>
- Anchuela, Ó. P., Casas-Sainz, A. M., Soriano, M. A., Pocoví-Juan, A. (2009). Mapping subsurface karst features with GPR: results and limitations. *Environmental Geology*, 58(2), pp. 391–399. <https://doi.org/10.1007/s00254-008-1603-7>
- Andreassen, L. M., Huss, M., Melvold, K., Elvehøy, H., Winsvold, S. H. (2015). Ice thickness measurements and volume estimates for glaciers in Norway. *Journal of Glaciology*, 61(228), pp. 763–775. <https://doi.org/10.3189/2015Jog14J161>
- Andrén, E., Andrén, T., Sohlenius, G. (2000). The Holocene history of the southwestern Baltic Sea as reflected in a sediment core from the Bornholm Basin. *Boreas*, 29(3), pp. 233–250. <https://doi.org/10.1111/j.1502-3885.2000.tb00981.x>
- Ani, T., Meidla, T. (2020). Rock head elevation model of northern Estonia. *Estonian Journal of Earth Sciences*, 69(2), pp. 109–120. <https://doi.org/10.3176/earth.2020.07>
- Ani, T., Maido, M. (2022). Adjusting the outcrop area of the Vão Formation in the 1:50 000 geological map, with regard to the preliminary feasibility estimation. Geological Survey of Estonia, Tallinn, pp. 1–41. GA No. 9621. [In Estonian].
<https://fond.egt.ee/fond/egf/9621>
- Annan, A. P. (2002). GPR—History, Trends, and Future Developments. *Subsurface Sensing Technologies and Applications*, 3(4), pp. 253–270.
<https://doi.org/10.1023/A:1020657129590>
- Annan, A. P. (2009). Electromagnetic Principles of Ground Penetrating Radar. In Jol, H. M. (Ed.), *Ground Penetrating Radar Theory and Applications* (pp. 3–40). Elsevier. <https://doi.org/10.1016/B978-0-444-53348-7.00001-6>
- Annan, A. P., Jackson, S. R. (2017). The WARR machine. In *2017 9th International Workshop on Advanced Ground Penetrating Radar (IWAGPR)* (pp. 1–4). Edinburgh, United Kingdom: IEEE. <https://doi.org/10.1109/IWAGPR.2017.7996106>
- Asprion, U., Aigner, T. (1999). Towards realistic aquifer models: three-dimensional georadar surveys of Quaternary gravel deltas (Singen Basin, SW Germany). *Sedimentary Geology*, 129(3–4), pp. 281–297.
[https://doi.org/10.1016/S0037-0738\(99\)00068-8](https://doi.org/10.1016/S0037-0738(99)00068-8)
- Auken, E., Sørensen, K. I., Lykke-Andersen, H., Bakker, M. A., ... Jokumsen, V. (2009). Buried Quaternary Valleys – a geophysical approach. *Zeitschrift Der Deutschen Gesellschaft Für Geowissenschaften*, 160(3), pp. 237–247.
<https://doi.org/10.1127/1860-1804/2009/0160-0237>
- Baggett, J., Abbasi, A., Monsalve, J., Bishop, R., Ripipi, N., Hole, J. (2020). Ground-Penetrating Radar for Karst Detection in Underground Stone Mines. *Mining, Metallurgy & Exploration*, 37(1), pp. 153–165. <https://doi.org/10.1007/s42461-019-00144-1>

- Bakker, M. A. (2002). Comparison of ground-penetrating radar facies and sediment characteristics in a Pleistocene push moraine in the Netherlands. In Koppenjan, S., Lee, H. (Eds.), pp. 317–322. Presented at the Ninth International Conference on Ground Penetrating Radar (GPR2002), Santa Barbara, CA.
<https://doi.org/10.1117/12.462304>
- Bakker, M. A. J., Van Der Meer, J. J. M. (2003). Structure of a Pleistocene push moraine revealed by GPR: the eastern Veluwe Ridge, The Netherlands. *Geological Society, London, Special Publications*, 211(1), pp. 143–151.
<https://doi.org/10.1144/GSL.SP.2001.211.01.12>
- Bechtel, T., Pochanin, G., Truskavetsky, S., Dimitri, M., Ruban, V., Orlenko, O., ... Capineri, L. (2018). Terrain Analysis in Eastern Ukraine and the Design of a Robotic Platform Carrying GPR Sensors for Landmine Detection. In 2018 17th International Conference on Ground Penetrating Radar (GPR) (pp. 1–4). Rapperswil: IEEE.
<https://doi.org/10.1109/ICGPR.2018.8441556>
- Bellefleur, G., Chouteau, M. (2001). Massive sulphide delineation using borehole radar: tests at the McConnell nickel deposit, Sudbury, Ontario. *Journal of Applied Geophysics*, 47(1), pp. 45–61. [https://doi.org/10.1016/S0926-9851\(01\)00046-5](https://doi.org/10.1016/S0926-9851(01)00046-5)
- Benedetto, A. (2010). Water content evaluation in unsaturated soil using GPR signal analysis in the frequency domain. *Journal of Applied Geophysics*, 71(1), pp. 26–35.
<https://doi.org/10.1016/j.jappgeo.2010.03.001>
- Beres, M., Huggenberger, P., Green, A. G., Horstmeyer, H. (1999). Using two- and three-dimensional georadar methods to characterize glaciofluvial architecture. *Sedimentary Geology*, 129(1–2), pp. 1–24. [https://doi.org/10.1016/S0037-0738\(99\)00053-6](https://doi.org/10.1016/S0037-0738(99)00053-6)
- Bermejo, L., Ortega, A. I., Parés, J. M., Campaña, I., Bermúdez de Castro, J. M., Carbonell, E., Conyers, L. B. (2020). Karst features interpretation using ground-penetrating radar: A case study from the Sierra de Atapuerca, Spain. *Geomorphology*, 367, 107311. <https://doi.org/10.1016/j.geomorph.2020.107311>
- Bērziņš, D., Karušs, J., Krievāns, M., Lamsters, K. Usage of ground penetrating radar for sand-gravel and sand deposit prospecting, Krizovka case study, eastern Latvia. (2017). In *Proceedings of the 17th International Multidisciplinary Scientific Geo-Conference SGEM2017*. <https://www.sgem.org/index.php/elibrary-research-areas?view=publication&task=show&id=2776>
- Bianchini Ciampoli, L., Tosti, F., Brancadoro, M. G., D’Amico, F., Alani, A. M., Benedetto, A. (2017). A spectral analysis of ground-penetrating radar data for the assessment of the railway ballast geometric properties. *NDT & E International*, 90, pp. 39–47. <https://doi.org/10.1016/j.ndteint.2017.05.005>
- Björck, S. (1995). A review of the history of the Baltic Sea, 13.0–8.0 ka BP. *Quaternary International*, 27, pp. 19–40. [https://doi.org/10.1016/1040-6182\(94\)00057-C](https://doi.org/10.1016/1040-6182(94)00057-C)
- Blaus, A., Reitalu, T., Poska, A., Vassiljev, J., Veski, S. (2021). Mire plant diversity change over the last 10,000 years: Importance of isostatic land uplift, climate and local conditions. *Journal of Ecology*, 109(10), pp. 3634–3651.
<https://doi.org/10.1111/1365-2745.13742>
- Bristow, C. S., Chroston, P. N., Bailey, S. D. (2000). The structure and development of foredunes on a locally prograding coast: insights from ground-penetrating radar surveys, Norfolk, UK. *Sedimentology*, 47(5), pp. 923–944.
<https://doi.org/10.1046/j.1365-3091.2000.00330.x>
- Bristow, C. S., Jol, H. M. (2003). An introduction to ground penetrating radar (GPR) in sediments. *Geological Society, London, Special Publications*, 211(1), 1–7.
<https://doi.org/10.1144/GSL.SP.2001.211.01.01>

- Bristow, C.S., Lancaster, N., Duller, G.A.T. (2005). Combining ground penetrating radar surveys and optical dating to determine dune migration in Namibia. *Journal of the Geological Society* 162, pp. 315–321. <https://doi.org/10.1144/0016-764903-120>
- Bristow, C. S., Pucillo, K. (2006). Quantifying rates of coastal progradation from sediment volume using GPR and OSL: the Holocene fill of Guichen Bay, south-east South Australia. *Sedimentology*, 53(4), pp. 769–788. <https://doi.org/10.1111/j.1365-3091.2006.00792.x>
- Bristow, C. (2009). Ground Penetrating Radar in Aeolian Dune Sands. In Jol, H. M. (Ed.), *Ground Penetrating Radar Theory and Applications* (pp. 271–297). Elsevier. <https://doi.org/10.1016/B978-0-444-53348-7.00009-0>
- Busby, J. P., Merritt, J. W. (1999). Quaternary deformation mapping with ground penetrating radar. *Journal of Applied Geophysics*, 41(1), pp. 75–91. [https://doi.org/10.1016/S0926-9851\(98\)00050-0](https://doi.org/10.1016/S0926-9851(98)00050-0)
- Busby, J.P., Cuss, R.J., Raines, M.G., Beamish, D. (2004). Application of ground penetrating radar to geological investigations. British Geological Survey. Internal report IR/04/212004.
- Buynevich, I. V., Jol, H. M., FitzGerald, D. M. (2009). Coastal Environments. In Jol, H. M. (Ed.), *Ground Penetrating Radar Theory and Applications* (pp. 299–322). Elsevier. <https://doi.org/10.1016/B978-0-444-53348-7.00010-7>
- Campbell, S., Affleck, R. T., Sinclair, S. (2018). Ground-penetrating radar studies of permafrost, periglacial, and near-surface geology at McMurdo Station, Antarctica. *Cold Regions Science and Technology*, 148, pp. 38–49. <https://doi.org/10.1016/j.coldregions.2017.12.008>
- Carless, D., Kulesa, B., Booth, A. D., Drocourt, Y., Sinnadurai, P., Street-Perrott, F. A., Jansson, P. (2021). An integrated geophysical and GIS based approach improves estimation of peatland carbon stocks. *Geoderma*, 402, 115176. <https://doi.org/10.1016/j.geoderma.2021.115176>
- Cassidy, N. J. (2009a). Electrical and Magnetic Properties of Rocks, Soils and Fluids. In Jol, H. M. (Ed.), *Ground Penetrating Radar Theory and Applications* (pp. 41–72). Elsevier. <https://doi.org/10.1016/B978-0-444-53348-7.00002-8>
- Cassidy, N. J. (2009b). Ground Penetrating Radar Data Processing, Modelling and Analysis. In Jol, H. M. (Ed.), *Ground Penetrating Radar Theory and Applications* (pp. 141–176). Elsevier. <https://doi.org/10.1016/B978-0-444-53348-7.00005-3>
- Chamberlain, A. T., Sellers, W., Proctor, C., Coard, R. (2000). Cave Detection in Limestone using Ground Penetrating Radar. *Journal of Archaeological Science*, 27(10), pp. 957–964. <https://doi.org/10.1006/jasc.1999.0525>
- Chang, P.-Y., Alumbaugh, D., Brainard, J., Hall, L. (2006). Cross-borehole ground-penetrating radar for monitoring and imaging solute transport within the vadose zone: XBGPR for monitoring solute transport. *Water Resources Research*, 42(10). <https://doi.org/10.1029/2004WR003871>
- Chen, H., Cohn, A. G. (2010). Probabilistic robust hyperbola mixture model for interpreting ground penetrating radar data. In *The 2010 International Joint Conference on Neural Networks (IJCNN)* (pp. 1–8). Barcelona, Spain: IEEE. <https://doi.org/10.1109/IJCNN.2010.5596298>
- Choi, K. H., Choi, J.-H., Kim, J. W. (2014). Reconstruction of Holocene coastal progradation on the east coast of Korea based on OSL dating and GPR surveys of beach-foredune ridges. *The Holocene*, 24(1), pp. 24–34. <https://doi.org/10.1177/0959683613515728>

- Clemmensen, L. B., Murray, A. S., Nielsen, L. (2012). Quantitative constraints on the sea-level fall that terminated the Littorina Sea stage, southern Scandinavia. *Quaternary Science Reviews*, 40, pp. 54–63.
<https://doi.org/10.1016/j.quascirev.2012.03.001>
- Comas, X., Slater, L., Reeve, A. (2005). Geophysical and hydrological evaluation of two bog complexes in a northern peatland: Implications for the distribution of biogenic gases at the basin scale: Geophysical and hydrological evaluation. *Global Biogeochemical Cycles*, 19(4). <https://doi.org/10.1029/2005GB002582>
- Comas, X., Terry, N., Slater, L., Warren, M., Kolka, R., Kristiyono, A., ... Darusman, T. (2015). Imaging tropical peatlands in Indonesia using ground-penetrating radar (GPR) and electrical resistivity imaging (ERI): implications for carbon stock estimates and peat soil characterization. *Biogeosciences*, 12(10), pp. 2995–3007.
<https://doi.org/10.5194/bg-12-2995-2015>
- Comas, X., Terry, N., Hribljan, J. A., Lilleskov, E. A., Suarez, E., Chimner, R. A., Kolka, R. K. (2017). Estimating belowground carbon stocks in peatlands of the Ecuadorian páramo using ground-penetrating radar (GPR): Estimating Carbon Stocks in the Páramo. *Journal of Geophysical Research: Biogeosciences*, 122(2), pp. 370–386.
<https://doi.org/10.1002/2016JG003550>
- Conyers, L. B. (2016). *Ground-Penetrating Radar for Geoarchaeology: Conyers/ Ground-Penetrating Radar for Geoarchaeology*. Chichester, UK: John Wiley & Sons, Ltd. <https://doi.org/10.1002/9781118949993>
- Corradini, E., Wilken, D., Zanon, M., Groß, D., Lübke, H., Panning, D., ... Rabbel, W. (2020). Reconstructing the palaeoenvironment at the early Mesolithic site of Lake Duvensee: Ground-penetrating radar and geoarchaeology for 3D facies mapping. *The Holocene*, 30(6), pp. 820–833. <https://doi.org/10.1177/0959683620902234>
- Costall, A. R., Harris, B. D., Teo, B., Schaa, R., Wagner, F. M., Pigois, J. P. (2020). Groundwater Throughflow and Seawater Intrusion in High Quality Coastal Aquifers. *Scientific Reports*, 10(1), 9866. <https://doi.org/10.1038/s41598-020-66516-6>
- Cunningham, A. C., Bakker, M. A. J., van Heteren, S., van der Valk, B., van der Spek, A. J. F., Schaart, D. R., Wallinga, J. (2011). Extracting storm-surge data from coastal dunes for improved assessment of flood risk. *Geology*, 39(11), pp. 1063–1066.
<https://doi.org/10.1130/G32244.1>
- Dagallier, G., Laitinen, A. I., Malartre, F., Van Campenhout, I. P. A. M., Veeken, P. C. H. (2000). Ground penetrating radar application in a shallow marine Oxfordian limestone sequence located on the eastern flank of the Paris Basin, NE France. *Sedimentary Geology*, 130(3–4), pp. 149–165. [https://doi.org/10.1016/S0037-0738\(99\)00105-0](https://doi.org/10.1016/S0037-0738(99)00105-0)
- Daniels, D. J. (Ed.). (2004). *Ground Penetrating Radar*. Institution of Engineering and Technology. <https://doi.org/10.1049/PBRA015E>
- Davis, J. L., Annan, A. P. (1989). Ground-penetrating radar for high-resolution mapping of soil and rock stratigraphy. *Geophysical Prospecting*, 37(5), pp. 531–551.
<https://doi.org/10.1111/j.1365-2478.1989.tb02221.x>
- De Angeli, S., Serpetti, M., Battistin, F. (2022). A Newly Developed Tool for the Post-Processing of GPR Time-Slices in A GIS Environment. *Remote Sensing*, 14(14), 3459. <https://doi.org/10.3390/rs14143459>
- Dekeyser, L., Brunton, F.R., Endres, A.L., Armstrong, D.K., Coniglio, M., Tetreault, D. K. (2007). Ground-penetrating radar as a resource assessment tool for Silurian-age carbonate building stone quarries on the Bruce Peninsula, southern Ontario. Ontario Geological Survey, Open File Report6212, 54pp. <http://www.geologyontario.mndm.gov.on.ca/mndmfiles/pub/data/imaging/OFR6212/OFR6212.pdf>

- DELL. (2022). Jenson Atex Depot. Dell Latitude 7424 Extreme Rugged notebook, <https://cdn.webshopapp.com/shops/302128/files/350660886/image.jpg>. [Accessed 10.12.2022].
- Demant, D., Renardy, F., Vanneste, K., Jongmans, D., Camelbeeck, T., Meghraoui, M. (2001). The use of geophysical prospecting for imaging active faults in the Roer Graben, Belgium. *GEOPHYSICS*, 66(1), pp. 78–89. <https://doi.org/10.1190/1.1444925>
- Diallo, M. C., Cheng, L. Z., Rosa, E., Gunther, C., Chouteau, M. (2019). Integrated GPR and ERT data interpretation for bedrock identification at Cléricy, Québec, Canada. *Engineering Geology*, 248, pp. 230–241. <https://doi.org/10.1016/j.enggeo.2018.09.011>
- Diamanti, N., Elliott, E. J., Jackson, S. R., Annan, A. P. (2018). The WARR Machine: System Design, Implementation and Data. *Journal of Environmental and Engineering Geophysics*, 23(4), pp. 469–487. <https://doi.org/10.2113/JEEG23.4.469>
- Dmitrijeva, M., Plado, J., Oja, T. (2018). The Luusika potential field anomaly, eastern Estonia: modelling results. *Estonian Journal of Earth Sciences*, 67(4), pp. 228–237. <https://doi.org/10.3176/earth.2018.18>
- Doetsch, J., Linde, N., Pessognelli, M., Green, A. G., Günther, T. (2012). Constraining 3-D electrical resistance tomography with GPR reflection data for improved aquifer characterization. *Journal of Applied Geophysics*, 78, pp. 68–76. <https://doi.org/10.1016/j.jappgeo.2011.04.008>
- Doolittle, J. A., Collins, M. E. (1998). A comparison of EM induction and GPR methods in areas of karst. *Geoderma*, 85(1), pp. 83–102. [https://doi.org/10.1016/S0016-7061\(98\)00012-3](https://doi.org/10.1016/S0016-7061(98)00012-3)
- Doolittle, J. A., Jenkinson, B., Hopkins, D., Ulmer, M., Tuttle, W. (2006). Hydrogeological investigations with ground-penetrating radar (GPR): Estimating water-table depths and local ground-water flow pattern in areas of coarse-textured soils. *Geoderma*, 131(3–4), pp. 317–329. <https://doi.org/10.1016/j.geoderma.2005.03.027>
- Doolittle, J. A., Butnor, J. R. (2009). Soils, peatlands and biomonitoring. In: Jol, H.M. (Ed.), *Ground Penetrating Radar: Theory and Applications* (pp. 179–202). Elsevier. <http://doi.org/10.1016/B978-0-444-53348-7.00006-5>
- Dou, Q., Wei, L., Magee, D. R., Cohn, A. G. (2017). *Real-Time Hyperbola Recognition and Fitting in GPR Data*. *IEEE Transactions on Geoscience and Remote Sensing*, 55(1), pp. 51–62. <https://doi.org/10.1109/TGRS.2016.2592679>
- EGDB (2022). Engineering Geology Data Bank of Estonia. <https://geoportaal.maaamet.ee/eng/Spatial-Data/Geological-Data/Data-Bank-of-Engineering-Geology-p374.html>. [Accessed 16.12.2022].
- EGLD (2022). Estonian Geoscience Literature Database. georadar, <https://kirjandus.geoloogia.info/reference?isEstonianReference&query=georadar>. [Accessed 10.12.2022].
- Eilertsen, R. S., Corner, G. D., Aasheim, O., Hansen, L. (2011). Facies characteristics and architecture related to palaeodepth of Holocene fjord-delta sediments: Facies characteristics and architecture. *Sedimentology*, 58(7), pp. 1784–1809. <https://doi.org/10.1111/j.1365-3091.2011.01239.x>
- ELB (2022a). Estonian Land Board. Mineral Registry, <https://geoportaal.maaamet.ee/eng/Spatial-Data/Geological-Data/Mineral-Registry-p352.html>. [Accessed 01.12.2022].

- ELB (2022b). Estonian Land Board. Geological Base Map 1:50 000 (ELB representation model), compiled mostly by the Geological Survey of Estonia, <https://geoportaal.maaamet.ee/eng/Spatial-Data/Geological-Data/Geological-Base-Map-1-50-000-p351.html>. [Accessed 15.10.2022].
- ELB (2022c). Estonian Land Board. Download Elevation Data, <https://geoportaal.maaamet.ee/eng/Maps-and-Data/Elevation-data/Download-Elevation-Data-p664.html>. [Accessed 15.10.2022].
- ELB (2022d). Estonian Land Board. Geological Maps 1:400 000, compiled by the Geological Survey of Estonia, <https://geoportaal.maaamet.ee/eng/Spatial-Data/Geological-Data/Geological-Maps-1-400-000-p358.html>. [Accessed 15.10.2022].
- ELB (2022e). Estonian Land Board. An X-GIS2 shared link with Viru-Nigula GPR profiles, <https://xgis.maaamet.ee/xgis2/page/link/U5NatRZ9>. [Accessed 30.11.2022].
- ELB (2022f). Estonian Land Board. Geo3D strategy, <https://geoportaal.maaamet.ee/eng/Spatial-Data/Geo3D/Geo3D-strategy-p835.html>. [Accessed 05.12.2022].
- ELB (2022g). Estonian Land Board. Maa-amet 3D, <https://3d.maaamet.ee/kaart>. [Accessed 10.12.2022].
- ELB (2022h). Estonian Land Board. 3D Digital Twin from the whole Estonia, <https://www.youtube.com/watch?v=P8cOaAcxJ5o>. [In Estonian, accessed 10.12.2022].
- ELB (2022i). Estonian Land Board. An X-GIS2 shared link with GPR profiles, <https://xgis.maaamet.ee/xgis2/page/link/FOkNLsNp>. [Accessed 10.11.2022].
- ELB (2022j). Estonian Land Board. Uploading the Mineral Survey Data Points, and laboratory analyses, <https://geoportaal.maaamet.ee/est/Ruumiandmed/Geoloogilised-andmed/Maavarade-register/Uuringupunktide-ja-laboriandmete-esitamine-p730.html>. [In Estonian, accessed 10.11.2022].
- ELERMO (2022). Elermo Ltd. Georadar, <https://georadar.ee>. [In Estonian, accessed 10.12.2022].
- Elkarmoty, M., Tinti, F., Kasmaeeyazdi, S., Bonduà, S., Bruno, R. (2018). 3D modeling of discontinuities using GPR in a commercial size ornamental limestone block. *Construction and Building Materials*, 166, pp. 81–86. <https://doi.org/10.1016/j.conbuildmat.2018.01.091>
- Engelhardt, O.M.L von, Ulprecht E.M. (1830). Geologische Karte von Est- und Livland. 1:2 000 000. Umriss des Felsstructur Estlands und Livlands. Archiv für Mineralogie, Geognosie, Bergbau und Hüttenkunde (Karsten), 2.
- ENVIR (2022a). The Decree of the Estonian Environmental Ministry for regulating the mineral exploration, <https://www.riigiteataja.ee/akt/102032021016?leiaKehtiv>. [In Estonian, accessed 01.12.2022].
- ENVIR (2022b). Ministry of the Environment. Peat, <https://envir.ee/ringmajandus/maapou/turvas>. [In Estonian, accessed 01.12.2022].
- ENVIR (2022c). The Decree of the Estonian Environmental Ministry specifying the damaged peatlands, <https://www.riigiteataja.ee/akt/129122016064?dbNotReadOnly=true>. [In Estonian, accessed 01.12.2022].
- EU 2019/1024. (2019). European directive on open data and the re-use of public sector information, <https://eur-lex.europa.eu/legal-content/EN/TXT/HTML/?uri=CELEX:32019L1024&from=EN#d1e809-56-1>. [Accessed 01.12.2022].
- Forte, E., Pipan, M. (2017). Review of multi-offset GPR applications: Data acquisition, processing and analysis. *Signal Processing*, 132, pp. 210–220. <https://doi.org/10.1016/j.sigpro.2016.04.011>

- Francke, J. (2012). A review of selected ground penetrating radar applications to mineral resource evaluations. *Journal of Applied Geophysics*, 81, pp. 29–37. <https://doi.org/10.1016/j.jappgeo.2011.09.020>
- Franseen, E. K., Byrnes, A. P., Xia, J., Miller, R. D. (2007). Improving resolution and understanding controls on GPR response in carbonate strata: Implications for attribute analysis. *The Leading Edge*, 26(8), pp. 984–993. <https://doi.org/10.1190/1.2769554>
- Frigui, H., Gader, P. (2009). Detection and Discrimination of Land Mines in Ground-Penetrating Radar Based on Edge Histogram Descriptors and a Possibilistic K_S-Nearest Neighbor Classifier. *IEEE Transactions on Fuzzy Systems*, 17(1), pp. 185–199. <https://doi.org/10.1109/TFUZZ.2008.2005249>
- GA. (2022). Geological Archive of Estonia. georadar, <https://fond.egt.ee/fond/egf/otsing/4KtQC6Bf>. [Accessed 10.12.2022].
- Gigli, G., Casagli, N. (2011). Semi-automatic extraction of rock mass structural data from high resolution LIDAR point clouds. *International Journal of Rock Mechanics and Mining Sciences*, 48(2), pp. 187–198. <https://doi.org/10.1016/j.ijrmms.2010.11.009>
- GitHub. (2022a). Repositories referring to ground-penetrating radar. <https://github.com/search?p=5&q=ground-penetrating-radar&type=Repositories>. [Accessed 02.12.2022].
- GitHub. (2022b). JSONWellLogFormat. <https://github.com/JSONWellLogFormat/JSONWellLogFormat>. [Accessed 02.12.2022].
- Goodman, D., Piro, S. (2013). *GPR Remote Sensing in Archaeology*. Berlin, Heidelberg: Springer Berlin Heidelberg. <https://doi.org/10.1007/978-3-642-31857-3>
- Gorlach, A., Kalm, V., Hang, T. (2015). Thickness distribution of quaternary deposits in the formerly glaciated part of the East European plain. *Journal of Maps*, 11(4), pp. 625–635. <https://doi.org/10.1080/17445647.2014.954646>
- Gourry, J.-C., Vermeersch, F., Garcin, M., Giot, D. (2003). Contribution of geophysics to the study of alluvial deposits: a case study in the Val d’Avaray area of the River Loire, France. *Journal of Applied Geophysics*, 54(1–2), pp. 35–49. <https://doi.org/10.1016/j.jappgeo.2003.07.002>
- GPR (2022). Colorado School of Mines. 19th International Conference on Ground Penetrating Radar, <https://learn.mines.edu/gpr2022>. [Accessed 29.11.2022].
- GSE (2022a). Geological Survey of Estonia. Geological mapping, <https://egt.ee/en/fields-activity-and-objectives/geological-information/geological-mapping>. [Accessed 19.08.2022].
- GSE (2022b). Geological Survey of Estonia. Geological data 1:200 000, <https://egt.ee/maapouealane-teave/geoloogilised-andmed/ruumiandmed-ja-kaardid>. [Accessed 26.08.2022].
- GSE (2022c). Geological Survey of Estonia. Construction minerals, <https://www.egt.ee/en/fields-activity-and-objectives/resources-earths-crust/construction-minerals>. [Accessed 04.12.2022].
- Grasmueck, M., Weger, R., Horstmeyer, H. (2005). Full-resolution 3D GPR imaging. *GEOPHYSICS*, 70(1), K12–K19. <https://doi.org/10.1190/1.1852780>
- Grasmueck, M., Quintà, M. C., Pomar, K., Eberli, G. P. (2013). Diffraction imaging of sub-vertical fractures and karst with full-resolution 3D Ground-Penetrating Radar: Diffraction imaging of sub-vertical fractures and karst. *Geophysical Prospecting*, 61(5), pp. 907–918. <https://doi.org/10.1111/1365-2478.12004>
- GSF (2020). Service package with a ground-penetrating radar and a drone for peat research, <https://www.gtk.fi/en/current/service-package-with-a-ground-penetrating-radar-and-a-drone-for-peat-research>. [Accessed 13.11.2022].

- Habicht, H.-L., Rosentau, A., Jõeleht, A., Heinsalu, A., Kriiska, A., Kohv, M., Hang, T., Aunap, R. (2017). GIS-based multiproxy coastline reconstruction of the eastern Gulf of Riga, Baltic Sea, during the Stone Age. *Boreas*, 46(1), pp. 83–99. <https://doi.org/10.1111/bor.12157>
- Hänninen, P. (1992). Application of ground penetrating radar and radio wave moisture probe techniques to peatland investigations. Geological Survey of Finland, 361. https://tupa.gtk.fi/julkaisu/bulletin/bt_361.pdf
- Harkat, H., Ruano, A. E., Ruano, M. G., Bennani, S. D. (2019). GPR target detection using a neural network classifier designed by a multi-objective genetic algorithm. *Applied Soft Computing*, 79, pp. 310–325. <https://doi.org/10.1016/j.asoc.2019.03.030>
- Hausmann, H., Behm, M. (2011). Imaging the structure of cave ice by ground-penetrating radar. *The Cryosphere*, 5(2), pp. 329–340. <https://doi.org/10.5194/tc-5-329-2011>
- Hiiemaa, H., Mustasaar, M., Kohv, M., Hang, T., Jõeleht, A., Lasberg, K., Kalm, V. (2014). Geological settings of the protected Selisoo mire (northeastern Estonia) threatened by oil shale mining. *Estonian Journal of Earth Sciences*, 63(2), pp. 97–107. <https://doi.org/10.3176/earth.2014.09>
- Hints, L. (1997). Ordovician. Lasnamägi Stage. In Raukas, A., Teedumäe, A. (Eds.), *Geology and mineral resources of Estonia* (pp. 67–68). Estonian Academy Publishers. <https://geoloogia.info/geology>
- Hirsch, F., Schneider, A., Nicolay, A., Błaszczewicz, M., Kordowski, J., Noryskiewicz, A. M., ... Raab, T. (2015). Late Quaternary landscape development at the margin of the Pomeranian phase (MIS 2) near Lake Wygonin (Northern Poland). *CATENA*, 124, pp. 28–44. <https://doi.org/10.1016/j.catena.2014.08.018>
- Høyer, A.-S., Møller, I., Jørgensen, F. (2013). Challenges in geophysical mapping of glaciotectonic structures. *GEOPHYSICS*, 78(5), B287–B303. <https://doi.org/10.1190/geo2012-0473.1>
- Huisman, J. A., Hubbard, S. S., Redman, J. D., Annan, A. P. (2003). Measuring Soil Water Content with Ground Penetrating Radar: A Review. *Vadose Zone Journal*, 2(4), pp. 476–491. <https://doi.org/10.2136/vzj2003.4760>
- Ilomets, M. (1994). On the growth of peats in Estonia. In Mardiste, H., Roosaare, J. (Eds.), *YearBook of the Estonian Geographical Society*, 26, pp. 13–18. Estonian Academy Publishers, Tallinn. [In Estonian, with English summary].
- Janocha, J., Smyrak-Sikora, A., Senger, K., Birchall, T. (2021). Seeing beyond the outcrop: Integration of ground-penetrating radar with digital outcrop models of a paleokarst system. *Marine and Petroleum Geology*, 125, 104833. <https://doi.org/10.1016/j.marpetgeo.2020.104833>
- Jõeleht, A., Plado, J. (2010). Architecture of the northeastern rim of the Kärkla impact crater, Estonia, based on ground-penetrating radar studies. In: Gibson, R.; Reimold, W.U. (Eds.), *Large Meteorite Impacts and Planetary Evolution IV*, pp. 133–140. Geological Society of America. [https://doi.org/10.1130/2010.2465\(09\)](https://doi.org/10.1130/2010.2465(09))
- Jõeleht, A., Sibul, I., Mustasaar, M., Plado, J. (2022). Bedrock deformations in northeastern Estonia based on ground-penetrating radar data. *Estonian Journal of Earth Sciences*, 71(4), pp. 189–200. <https://doi.org/10.3176/earth.2022.13>
- Jorry, S. J., Bièvre, G. (2011). Integration of sedimentology and ground-penetrating radar for high-resolution imaging of a carbonate platform: High-resolution imaging of a carbonate platform. *Sedimentology*, 58(6), pp. 1370–1390. <https://doi.org/10.1111/j.1365-3091.2010.01213.x>

- Kalińska, E., Hang, T., Jõelett, A., Olo, S., Nartišs, M., Adamiec, G. (2019). Macro- and micro-scale study and chronology of Late Weichselian aeolian sediments in Estonia, north-eastern European Sand Belt. *International Journal of Earth Sciences*, 108(6), pp. 2021–2035. <https://doi.org/10.1007/s00531-019-01746-2>
- Kall, T., Kruusla, K., Liibus, A., Oja, T. (2021). New 3D velocity model of Estonia from GNSS measurements. *Estonian Journal of Earth Sciences*, 70(2), pp. 107–125. <https://doi.org/10.3176/earth.2021.08>
- Kalm, V. (2009). Outlines of the Quaternary geology of the region. In Kalm, V., Laumets, L., Hang, T. (Eds.), *Extent and Timing of the Weichselian Glaciation Southeast of the Baltic Sea: Abstracts & Guidebook. The INQUA Peribaltic Working Group Field Symposium in Southern Estonia and Northern Latvia, September 13–17, 2009*, pp. 53–56. <https://sisu.ut.ee/sites/default/files/inquaperibaltic/files/inquaperibaltic2009abstrguide.pdf>
- Kalm, V., Hang, T., Lasberg, K., Rosentau, A., Kohv, M. (2009). Stop 2: Glacio-tectonically dislocated Eemian interglacial deposits at Rõngu. In Kalm, V., Laumets, L., Hang, T. (Eds.), *Extent and Timing of the Weichselian Glaciation Southeast of the Baltic Sea: Abstracts & Guidebook. The INQUA Peribaltic Working Group Field Symposium in Southern Estonia and Northern Latvia, September 13–17, 2009*, pp. 60–64. <https://sisu.ut.ee/sites/default/files/inquaperibaltic/files/inquaperibaltic2009abstrguide.pdf>
- Kalm, V., Raukas, A., Rattas, M., Lasberg, K. (2011). Pleistocene Glaciations in Estonia. In *Developments in Quaternary Sciences*, 15, pp. 95–104. Elsevier. <https://doi.org/10.1016/B978-0-444-53447-7.00008-8>
- Kalm, V. (2012). Ice-flow pattern and extent of the last Scandinavian Ice Sheet southeast of the Baltic Sea. *Quaternary Science Reviews*, 44, pp. 51–59. <https://doi.org/10.1016/j.quascirev.2010.01.019>
- Karofeld, E., Kaasik, A., Vellak, K. (2020). Growth characteristics of three *Sphagnum* species in restored extracted peatland. *Restoration Ecology*, 28(6), 1574–1583. <https://doi.org/10.1111/rec.13245>
- Kask, J., Lepland, A., Perens, R. (1994). Geological history and present day of Ruhnu Island. (Raukas, A., Talvi, T., Eds.), pp. 1–48. Estonian Academy of Sciences. [In Estonian with English summary].
- Kelly, T. B., Angel, M. N., O'Connor, D. E., Huff, C. C., Morris, L. E., Wach, G. D. (2021). A novel approach to 3D modelling ground-penetrating radar (GPR) data – A case study of a cemetery and applications for criminal investigation. *Forensic Science International*, 325, 110882. <https://doi.org/10.1016/j.forsciint.2021.110882>
- Kennedy, C. D., Wilderotter, S., Payne, M., Buda, A. R., Kleinman, P. J. A., Bryant, R. B. (2018). A geospatial model to quantify mean thickness of peat in cranberry bogs. *Geoderma*, 319, pp. 122–131. <https://doi.org/10.1016/j.geoderma.2017.12.032>
- Kettridge, N., Binley, A., Comas, X., Cassidy, N. J., Baird, A. J., Harris, A., ... Waddington, J. M. (2012). Do peatland microforms move through time? Examining the developmental history of a patterned peatland using ground-penetrating radar. *Journal of Geophysical Research: Biogeosciences*, 117(G03030). <https://doi.org/10.1029/2011JG001876>
- Kim, N., Kim, S., An, Y.-K., Lee, J.-J. (2021). A novel 3D GPR image arrangement for deep learning-based underground object classification. *International Journal of Pavement Engineering*, 22(6), pp. 740–751. <https://doi.org/10.1080/10298436.2019.1645846>

- Kimmel, K., Kull, A., Salm, J.-O., Mander, Ü. (2010). The status, conservation and sustainable use of Estonian wetlands. *Wetlands Ecology and Management*, 18(4), pp. 375–395. <https://doi.org/10.1007/s11273-008-9129-z>
- Kirs, J., Puura, V., Soesoo, A., Klein, V., Konsa, M., Koppelmaa, H., Niin, M., Urtson, K. (2009). The crystalline basement of Estonia: rock complexes of the Palaeoproterozoic Orosirian and Statherian and Mesoproterozoic Calymmian periods, and regional correlations. *Estonian Journal of Earth Sciences*, 58(4), pp. 219–228. <https://doi.org/10.3176/earth.2009.4.01>
- Kirsimäe, K., Hints, O., Meidla, T. (2020). Two hundred years of geology education in Estonia. *Estonian Journal of Earth Sciences*, 69 (4), pp. 175–176. <https://doi.org/10.3176/earth.2020.22>
- Kleesment, A., Mark-Kurik, E. (1997). Middle Devonian. In Raukas, A., Teedumäe, A. (Eds.), *Geology and Mineral Resources of Estonia*, pp. 112–121. Estonian Academy Publishers. <https://geoloogia.info/geology>
- Klein, V. 2012. 75 years in the footprints of the Estonian Geological Survey. Bulletin of the Geological Survey of Estonia, pp. 5–14. [In Estonian].
- Knoph, K., Tsoflias, G., Franseen, E., Goldstein, R. (2010). Ground-Penetrating Radar Imaging of Facies Distribution in a Carbonate Reservoir Analog (expanded abstract). *Conference Proceedings, Kansas Geophysics in the 21st Century*, 5 pp.
- Koganti, T., Ghane, E., Martinez, L. R., Iversen, B. V., Allred, B. J. (2021). Mapping of Agricultural Subsurface Drainage Systems Using Unmanned Aerial Vehicle Imagery and Ground Penetrating Radar. *Sensors*, 21(8), 2800. <https://doi.org/10.3390/s21082800>
- Kriiska, A., Lõugas, L. (2005). Formation of Ruhnu Island and its early settlement history. *Estonia Maritima* 7, pp. 119–132.
- Kriiska, A., Tšugai-Tsyulnikova, A., Plado, J., Vunk, A., Kimber, A., Paavel, K. (2018). Ground-penetrating radar survey and test pitting on Mädara hill fort. *Archaeological Fieldwork in Estonia*, pp. 53–58.
- Kull, A. et al. (2013). Determining the buffer zones (which can reduce the long-term disturbances) for securing the ecological functioning of mires. University of Tartu, Institute of Ecology and Earth Sciences. <https://www.kik.ee/et/projekt/soode-okoloogilise-funktsionaalsuse-tagamiseks-vajalike-puhvertsoonide-maaratlemine-0>. [In Estonian, accessed 14.12.2021].
- Küttim, M., Küttim, L., Pajula, R. (2018). The current state and ecological restoration of peatlands in Estonia. *Dynamiques Environnementales*, (42), pp. 342–349. <https://doi.org/10.4000/dynenviron.2425>
- Lamsters, K., Karušs, J., Stürmane, A., Jeskins, J., Džeriņš, P. (2020). Mapping of large-scale diapir structures at the paleo-ice tongue bed in western Latvia from geophysical investigations and borehole data. *Quaternary International*. <https://doi.org/10.1016/j.quaint.2020.12.003>
- Lang, J., Sievers, J., Loewer, M., Igel, J., Winsemann, J. (2017). 3D architecture of cyclic-step and antidune deposits in glacial subaqueous fan and delta settings: Integrating outcrop and ground-penetrating radar data. *Sedimentary Geology*, 362, pp. 83–100. <https://doi.org/10.1016/j.sedgeo.2017.10.011>
- Leckebusch, J. (2003). Ground-penetrating radar: a modern three-dimensional prospecting method. *Archaeological Prospection*, 10(4), pp. 213–240. <https://doi.org/10.1002/arp.211>

- Leclerc, R. F., Hickin, E. J. (1997). The internal structure of scrolled floodplain deposits based on ground-penetrating radar, North Thompson River, British Columbia. *Geomorphology*, 21(1), pp. 17–38. [https://doi.org/10.1016/S0169-555X\(97\)00037-8](https://doi.org/10.1016/S0169-555X(97)00037-8)
- Lindhorst, S., Schutter, I. (2014). Polar gravel beach-ridge systems: Sedimentary architecture, genesis, and implications for climate reconstructions (South Shetland Islands/Western Antarctic Peninsula). *Geomorphology*, 221, pp. 187–203. <https://doi.org/10.1016/j.geomorph.2014.06.013>
- Lindhorst, S., Reimann, T. (2021). Residual dune ridges: Sedimentary architecture, genesis, and implications for palaeo-climate reconstructions. *Earth Surface Processes and Landforms*, 46(11), pp. 2177–2194. <https://doi.org/10.1002/esp.5167>
- Linford, N., Linford, P., Martin, L., Payne, A. (2010). Stepped frequency ground-penetrating radar survey with a multi-element array antenna: Results from field application on archaeological sites. *Archaeological Prospection*, 17(3), pp. 187–198. <https://doi.org/10.1002/arp.382>
- Liu, X., Chen, J., Cui, X., Liu, Q., Cao, X., Chen, X. (2019). Measurement of soil water content using ground-penetrating radar: a review of current methods. *International Journal of Digital Earth*, 12(1), pp. 95–118. <https://doi.org/10.1080/17538947.2017.1412520>
- Looms, M. C., Klotzsche, A., van der Kruk, J., Larsen, T. H., Edsen, A., Tuxen, N., ... Nielsen, L. (2018). Mapping sand layers in clayey till using crosshole ground-penetrating radar. *Geophysics*, 83(1), A21–A26. <https://doi.org/10.1190/geo2017-0297.1>
- Losiak, A., Jöeleht, A., Plado, J., Szyszka, M., Kirsimäe, K., Wild, E. M., Steier, P., Belcher, C. M., Jazwa, A. M., Helde, R. (2020). Determining the age and possibility for an extraterrestrial impact formation mechanism of the Ilumetsa structures (Estonia). *Meteoritics & Planetary Science*, 55(2), pp. 274–293. <https://doi.org/10.1111/maps.13431>
- Lowry, C. S., Fratta, D., Anderson, M. P. (2009). Ground penetrating radar and spring formation in a groundwater dominated peat wetland. *Journal of Hydrology*, 373(1–2), pp. 68–79. <https://doi.org/10.1016/j.jhydrol.2009.04.023>
- Lunt, I. A., Hubbard, S. S., Rubin, Y. (2005). Soil moisture content estimation using ground-penetrating radar reflection data. *Journal of Hydrology*, 307(1–4), pp. 254–269. <https://doi.org/10.1016/j.jhydrol.2004.10.014>
- Ma, C., Zhao, Q., Huo, J., Chang, X., Ran, L. (2016). Single Borehole Radar for Well Logging in a Limestone Formation: Experiments and Simulations. *Journal of Environmental and Engineering Geophysics*, 21(4), pp. 201–213. <https://doi.org/10.2113/JEEG21.4.201>
- Maierhofer, C. (2003). Nondestructive Evaluation of Concrete Infrastructure with Ground Penetrating Radar. *Journal of Materials in Civil Engineering*, 15(3), pp. 287–297. [https://doi.org/10.1061/\(ASCE\)0899-1561\(2003\)15:3\(287\)](https://doi.org/10.1061/(ASCE)0899-1561(2003)15:3(287))
- Martel, R., Castellazzi, P., Gloaguen, E., Trépanier, L., Garfias, J. (2018). ERT, GPR, InSAR, and tracer tests to characterize karst aquifer systems under urban areas: The case of Quebec City. *Geomorphology*, 310, pp. 45–56. <https://doi.org/10.1016/j.geomorph.2018.03.003>
- Martinez, A., Kruger, J. M., Franseen, E. K. (1998). Utility of Ground-Penetrating Radar in Near-Surface, High-Resolution Imaging of Lansing-Kansas City (Pennsylvanian) Limestone Reservoir Analogs. *Current Research in Earth Sciences*, pp. 43–59. <https://doi.org/10.17161/cres.v0i241.11830>

- Mauz, B., Hijma, M. P., Amorosi, A., Porat, N., Galili, E., Bloemendal, J. (2013). Aeolian beach ridges and their significance for climate and sea level: Concept and insight from the Levant coast (East Mediterranean). *Earth-Science Reviews*, 121, pp. 31–54. <https://doi.org/10.1016/j.earscirev.2013.03.003>
- McCuaig, S. J., Ricketts, J. (2004). How much gravel? Use of Ground Penetrating Radar for Aggregate Resource Evaluation. Newfoundland Department of Mines and Energy, *Geological survey, Report 04-1*, pp. 107–115, https://www.researchgate.net/publication/238023773_How_Much_Gravel_Use_of_Ground_Penetrating_Radar_for_Aggregate_Resource_Evaluation
- Meidla, T. (2014). Estonia – a Palaeozoic country. In Bauert, H., Hints, O., Meidla, T., Männik, P. (Eds.), *4th Annual Meeting of IGCP 591, Estonia, 10–19 June 2014. Abstracts and Field Guide*, pp. 111–113. University of Tartu.
- Mellet, J. S. (1995). Profiling of ponds and bogs using ground-penetrating radar. *Journal of Paleolimnology*, 14(3), pp. 233–240. <https://doi.org/10.1007/BF00682425>
- Merkle, D., Frey, C., Reiterer, A. (2021). Fusion of ground penetrating radar and laser scanning for infrastructure mapping. *Journal of Applied Geodesy*, 15(1), pp. 31–45. <https://doi.org/10.1515/jag-2020-0004>
- Miidel, A., Raukas, A. (2005). Slope processes at the North Estonian Klint. *Proceedings of the Estonian Academy of Sciences. Geology*, 54(4), pp. 209–224. https://kirj.ee/wp-content/plugins/kirj/pub/geol-4-2005-209-224_20211023131312.pdf
- Miidel, A., Raukas, A., Tavast, E., and Vaher, R. (2006). Influence of bedrock topography on oil shale mining in North-East Estonia. *Oil Shale*, 23, pp. 313–327. <https://www.kirj.ee/public/oilshale/oil-2006-4-3.pdf>
- Minasny, B., Berglund, Ö., Connolly, J., Hedley, C., de Vries, F., Gimona, A., ... Widyatmanti, W. (2019). Digital mapping of peatlands – A critical review. *Earth-Science Reviews*, 196, 102870. <https://doi.org/10.1016/j.earscirev.2019.05.014>
- Møller, I., Jakobsen, P. R. (2002). Sandy till characterized by ground-penetrating radar. In S. Koppenjan, H. Lee (Eds.), pp. 308–312. Presented at the Ninth International Conference on Ground Penetrating Radar (GPR2002), Santa Barbara, CA. <https://doi.org/10.1117/12.462300>
- Møller, I., Vosgerau, H. (2006). Testing ground-penetrating radar for resolving facies architecture changes – a radar stratigraphic and sedimentological analysis along a 30 km profile on the Karup Outwash Plain, Denmark. *Near Surface Geophysics*, 4(1), pp. 57–68. <https://doi.org/10.3997/1873-0604.2005032>
- Moorman, B. J., Robinson, S. D., Burgess, M. M. (2003). Imaging periglacial conditions with ground-penetrating radar. *Permafrost and Periglacial Processes*, 14(4), pp. 319–329. <https://doi.org/10.1002/ppp.463>
- Moorman, B. J., Robinson, S. D., Burgess, M. M. (2007). Imaging near-surface permafrost structure and characteristics with Ground-Penetrating Radar. *CSEG Recorder* 32(2), pp. 1–8. <https://csegrecorder.com/articles/view/imaging-near-surface-permafrost-structure-and-characteristics>
- Mount, G. J., Comas, X. (2014). Estimating porosity and solid dielectric permittivity in the Miami Limestone using high-frequency ground penetrating radar (GPR) measurements at the laboratory scale. *Water Resources Research*, 50(10), pp. 7590–7605. <https://doi.org/10.1002/2013WR014947>

- Muru, M., Rosentau, A., Preusser, F., Plado, J., Sibul, I., Jõelet, A., Bjursäter, S., Aunap, R., Kriiska, A. (2018). Reconstructing Holocene shore displacement and Stone Age palaeogeography from a foredune sequence on Ruhnu Island, Gulf of Riga, Baltic Sea. *Geomorphology*, 303, pp. 434–445. <https://doi.org/10.1016/j.geomorph.2017.12.016>
- Mustasaar, M., Plado, J., Jõelet, A. (2012). Determination of Electromagnetic Wave Velocity in Horizontally Layered Sedimentary Target: A ground-penetrating radar study from Silurian limestones, Estonia. *Acta Geophysica*, 60(2), pp. 357–370. <https://doi.org/10.2478/s11600-011-0068-3>
- Mustasaar, M., Plado, J., Jõelet, A. (2013). A ground-penetrating radar study of the Vaidasoo bog (Estonia): no crater structure exists. *Geological Quarterly*, 57 (2), pp. 357–360. <https://doi.org/10.7306/gq.1093>
- Nakashima, Y., Zhou, H., Sato, M. (2001). Estimation of groundwater level by GPR in an area with multiple ambiguous reflections. *Journal of Applied Geophysics*, 47(3–4), pp. 241–249. [https://doi.org/10.1016/S0926-9851\(01\)00068-4](https://doi.org/10.1016/S0926-9851(01)00068-4)
- Neal, A. (2004). Ground-penetrating radar and its use in sedimentology: principles, problems and progress. *Earth-Science Reviews*, 66(3–4), pp. 261–330. <https://doi.org/10.1016/j.earscirev.2004.01.004>
- Nielsen, L., Møller, I., Nielsen, L. H., Johannessen, P. N., Pejrup, M., Andersen, T. J., Korshøj, J. S. (2009). Integrating ground-penetrating radar and borehole data from a Wadden Sea barrier island. *Journal of Applied Geophysics*, 68(1), pp. 47–59. <https://doi.org/10.1016/j.jappgeo.2009.01.002>
- Nirgi, T., Rosentau, A., Habicht, H.-L., Hang, T., Jonuks, T., Jõelet, A., Kihno, K., Kriiska, A., Mustasaar, M., Risberg, J., Suuroja, S., Talviste, P., Tõnisson, H. (2020). Holocene relative shore-level changes and Stone Age palaeogeography of the Pärnu Bay area, eastern Baltic Sea. *The Holocene* 30(1), pp. 37–52. <https://doi.org/10.1177/0959683619865603>
- Noviello, C., Gennarelli, G., Esposito, G., Ludeno, G., Fasano, G., Capozzoli, L., ... Catapano, I. (2022). An Overview on Down-Looking UAV-Based GPR Systems. *Remote Sensing*, 14(14), 3245. <https://doi.org/10.3390/rs14143245>
- Oliver, T. S. N., Tamura, T., Hudson, J. P., Woodroffe, C. D. (2017). Integrating millennial and interdecadal shoreline changes: Morpho-sedimentary investigation of two prograded barriers in southeastern Australia. *Geomorphology*, 288, pp. 129–147. <https://doi.org/10.1016/j.geomorph.2017.03.019>
- Orru, M. (1995). Estonian Mires. Estonian Geological Survey, Tallinn, 240 pp. [In Estonian, with English summary].
- Orru, M., Orru, H. (2008). Sustainable use of Estonian peat reserves and environmental challenges. *Estonian Journal of Earth Sciences*, 57(2), pp. 87–93. <https://doi.org/10.3176/earth.2008.2.04>
- Otvos, E. G. (2000). Beach ridges – definitions and significance. *Geomorphology*, 32(1–2), pp. 83–108. [https://doi.org/10.1016/S0169-555X\(99\)00075-6](https://doi.org/10.1016/S0169-555X(99)00075-6)
- Overgaard, T., Jakobsen, P. R. (2001). Mapping of glaciotectonic deformation in an ice marginal environment with ground penetrating radar. *Journal of Applied Geophysics*, 47(3–4), pp. 191–197. [https://doi.org/10.1016/S0926-9851\(01\)00064-7](https://doi.org/10.1016/S0926-9851(01)00064-7)
- Paal, J., Leibak, E. (2011). Estonian Mires: Inventory of habitats. Publication of the project “Estonian mires inventory completion for maintaining biodiversity”. Estonian Fund for Nature, Tartu. https://issuu.com/elfond/docs/estonian_mires_inventory

- Paal, J., Jürjendal, I., Kull, A. (2016). Impact of drainage on vegetation of transitional mires in Estonia. *Mires and Peat*, (18), pp. 1–19.
<https://doi.org/10.19189/MaP.2015.OMB.183>
- Paap, B. F., Bakker, M. A. J., Hoekstra, N. K., Oonk, H. (2011). Characterisation of landfills using a multidisciplinary approach. *Proceedings of the Institution of Civil Engineers – Waste and Resource Management*, 164(1), pp. 31–42.
<https://doi.org/10.1680/warm.900027>
- Paat, R., Jõelet, A., Kohv, M., Polikarpus, M. (2020). *Mire zoning within the oilshale district*. Report. Tartu University. GA No. 9432. [In Estonian].
<https://fond.egt.ee/fond/egf/9432>
- Park, Y., Guldmann, J.-M. (2019). Creating 3D city models with building footprints and LIDAR point cloud classification: A machine learning approach. *Computers, Environment and Urban Systems*, 75, pp. 76–89.
<https://doi.org/10.1016/j.compenvurbsys.2019.01.004>
- Parry, L. E., West, L. J., Holden, J., Chapman, P. J. (2014). Evaluating approaches for estimating peat depth. *Journal of Geophysical Research: Biogeosciences*, 119(4), pp. 567–576. <https://doi.org/10.1002/2013JG002411>
- Pellicer, X. M., Gibson, P. (2011). Electrical resistivity and Ground Penetrating Radar for the characterisation of the internal architecture of Quaternary sediments in the Midlands of Ireland. *Journal of Applied Geophysics*, 75(4), pp. 638–647.
<https://doi.org/10.1016/j.jappgeo.2011.09.019>
- Peters, L. P., Daniels, J. J., Young, J. D. (1994). Ground penetrating radar as a sub-surface environmental sensing tool. *Proceedings of the IEEE*, 82(12), pp. 1802–1822.
<https://doi.org/10.1109/5.338072>
- Pezdur, V., Čeru, T., Horn, B., Gosar, M. (2021). Investigating peatland stratigraphy and development of the Šijec bog (Slovenia) using near-surface geophysical methods. *Catena*, 206, 105484. <https://doi.org/10.1016/j.catena.2021.105484>
- Phelan, B. R., Sherbondy, K. D., Ranney, K. I., Narayanan, R. M. (2014). Design and performance of an ultra-wideband stepped-frequency radar with precise frequency control for landmine and IED detection. In *Proc. SPIE*, Baltimore, Maryland, USA.
<https://doi.org/10.1117/12.2050928>
- Pilecki, Z., Krzysztof, K., Elżbieta, P., Andrzej, K., Sylwia, T.-S., Tomasz, Ł. (2021). Identification of buried historical mineshaft using ground-penetrating radar. *Engineering Geology*, 294, 106400. <https://doi.org/10.1016/j.enggeo.2021.106400>
- Pirrus, E. (2007). Karst in Estonia, pp. 1–32. GeoGuide Baltoscandia. [In Estonian].
- Plado, J., Sibul, I., Mustasaar, M., Jõelet, A. (2011). Ground-penetrating radar study of the Rahivere peat bog, eastern Estonia. *Estonian Journal of Earth Sciences*, 60(1), pp. 31–42. <https://doi.org/10.3176/earth.2011.1.03>
- Plado, J., Preedon, U., Jõelet, A., Pesonen, L. J., Mertanen, S. (2016). Palaeomagnetism of Middle Ordovician Carbonate Sequence, Vaivara Sinimäed Area, Northeast Estonia, Baltica. *Acta Geophysica*, 64(5), pp. 1391–1411.
<https://doi.org/10.1515/acgeo-2016-0066>
- Plado, J., Kiik, K., Jokinen, J., Soesoo, A. (2020). Magnetic anomaly of the Jõhvi iron ore, northeastern Estonia, controlled by subvertical remanent magnetization. *Estonian Journal of Earth Sciences*, 69(4), pp. 189–199. <https://doi.org/10.3176/earth.2020.13>
- Põldsaar, K., Ainsaar, L. (2015). Soft-sediment deformation structures in the Cambrian (Series 2) tidal deposits (NW Estonia): Implications for identifying endogenic triggering mechanisms in ancient sedimentary record. *Palaeoworld*, 24(1–2), pp. 16–35.
<https://doi.org/10.1016/j.palwor.2014.12.003>

- Pöldvere, A. (Ed). (2003). Ruhnu (500) drill core. In *Ruhnu (500) drill core*, 5, pp. 1–76. Geological Survey of Estonia.
- Porsani, J. L., Sauck, W. A., Júnior, A. O. S. (2006). GPR for mapping fractures and as a guide for the extraction of ornamental granite from a quarry: A case study from southern Brazil. *Journal of Applied Geophysics*, 58(3), pp. 177–187.
<https://doi.org/10.1016/j.jappgeo.2005.05.010>
- Prado, J., Marques, L. (2015). Multi-sensor and multi-platform data fusion for buried objects detection and localization. In *2015 IEEE International Conference on Autonomous Robot Systems and Competitions*, pp. 186–191. Vila Real, Portugal: IEEE.
<https://doi.org/10.1109/ICARSC.2015.2>
- Prego, F. J., Solla, M., Puente, I., Arias, P. (2017). Efficient GPR data acquisition to detect underground pipes. *NDT & E International*, 91, pp. 22–31.
<https://doi.org/10.1016/j.ndteint.2017.06.002>
- Proulx-McInnis, S., St-Hilaire, A., Rousseau, A. N., Jutras, S. (2013). A review of ground-penetrating radar studies related to peatland stratigraphy with a case study on the determination of peat thickness in a northern boreal fen in Quebec, Canada. *Progress in Physical Geography: Earth and Environment*, 37(6), pp. 767–786.
<https://doi.org/10.1177/0309133313501106>
- Punning, J.-M., Koff, T. (1997). Application of ¹⁴C Data for the Estimation of Sphagnum Peat Increment in Estonian Ombrotrophic Mires. *Radiocarbon*, 40(2), 833–839.
<https://doi.org/10.1017/S0033822200018798>
- Puura, V., Vaher, R. (1997). Deep structure. In Raukas, A., Teedumäe, A. (Eds.), *Geology and mineral resources of Estonia*, p. 163. Estonian Academy Publishers.
<https://geoloogia.info/geology>
- Puura, V., Klein, V. (1997). Formation of the Earth's crust. In Raukas, A., Teedumäe, A. (Eds.), *Geology and mineral resources of Estonia*, pp. 181–183. Estonian Academy Publishers. <https://geoloogia.info/geology>
- Räängel, V. (1997). Sand and gravel. In Raukas, A., Teedumäe, A. (Eds.), *Geology and mineral resources of Estonia*, pp. 356–360. Estonian Academy Publishers.
<https://geoloogia.info/geology>
- Rattas, M., Kalm, V. (1999). Classification and areal distribution of glaciotectionic features in Estonia. *Geological Quarterly*, 43, 177–182.
<https://gq.pgi.gov.pl/article/view/8194>
- Rattas, M. (2004). Subglacial environments in the formation of drumlins – The case of the Saadjärve Drumlin Field. Doctoral thesis. In *Dissertationes Geologicae Universitatis Tartuensis*, 14, pp. 1–117. Tartu University Press.
<http://dspace.ut.ee/bitstream/handle/10062/624/Rattas.pdf>
- Rattas, M., Kalm, V. (2004). Glaciotectionic deformation patterns in Estonia. *Geological Quarterly*, 48(1), pp. 15–22. <https://gq.pgi.gov.pl/article/view/7329/5979>
- Rattas, M. (2007). Spatial distribution and morphological aspects of eskers and bedrock valleys in north Estonia: implications for the reconstruction of a subglacial drainage system under the Late Weichselian Baltic Ice Stream. *Applied Quaternary Research in the Central Part of Glaciated Terrain. Proceedings of the INQUA Peribaltic Group Field Symposium 2006 Oulanka Biological Research Station, Finland, September 11.–15.*, 46, pp. 63–68.
- Raukas, A., Tavast, E. (1987). About the morphology of the Estonian buried valleys. In *Year-book of the Estonian Geographical Society*, 20, pp. 5–15. Proceedings of Academy of Sciences of the Estonian SSR. [In Estonian].
<https://www.etera.ee/s/fa6TMBZwsg>

- Raukas, A., Kajak, K. (1995). Quaternary stratigraphy in Estonia. *Proceedings of the Estonian Academy of Sciences. Geology*, 44(3), pp. 149–162.
<https://books.google.ee/books?id=UIX1ySKoYBUC>
- Raukas, A., Kajak, K. (1997). Quaternary cover. In Raukas, A., Teedumäe, A. (Eds.), *Geology and mineral resources of Estonia*, pp. 125–136. Estonian Academy Publishers. <https://geoloogia.info/geology>
- Rautenberg, S., Schmitz, T., Lehné, R., Sibul, I. (2015). Challenges and chances of geological 3D-modelling – a case study for the northeastern part of Estonia. *GeoBerlin 2015 – Dynamic Earth from Alfred Wegener to Today and beyond – Abstracts. Annual Meeting of DGGV and DMG, 4-7 October 2015, Berlin*, p. 304.
https://epic.awi.de/id/eprint/38826/1/book_of_abstracts_geoberlin_2015.pdf
- Rey, J., Martínez, J., Vera, P., Ruiz, N., Cañadas, F., Montiel, V. (2015). Ground-penetrating radar method used for the characterisation of ornamental stone quarries. *Construction and Building Materials*, 77, pp. 439–447.
<https://doi.org/10.1016/j.conbuildmat.2014.12.076>
- RGPR (2022). RGPR: a free open-source software package for ground-penetrating radar (GPR) data processing, <https://emanuelhuber.github.io/RGPR>. [Accessed 05.12.2022].
- RIMFAX (2022). Mars 2020 Mission. Rimfax, <https://mars.nasa.gov/mars2020/spacecraft/instruments/rimfax>. [Accessed 10.11.2022].
- Rõõmusoks, A., Puura, V., Raukas, A., Mark-Kurik, E. (1997). History of geological research. In Raukas, A., Teedumäe, A. (Eds.), *Geology and mineral resources of Estonia*, pp. 15–26. Estonian Academy Publishers. <https://geoloogia.info/geology>
- Rosa, E., Larocque, M., Pellerin, S., Gagné, S., Fournier, B. (2009). Determining the number of manual measurements required to improve peat thickness estimations by ground penetrating radar. *Earth Surface Processes and Landforms*, 34(3), pp. 377–383. <https://doi.org/10.1002/esp.1741>
- Rosentau, A., Hang, T., Kalm, V. (2007). Water-level changes and palaeogeography of proglacial lakes in eastern Estonia: synthesis of data from the Saadjärve Drumlin Field area. *Estonian Journal of Earth Sciences*, 56(2), pp. 85–100. https://kirj.ee/public/Estonian_Journal_of_Earth_Sciences/2007/issue_2/earth_2007_2_2.pdf
- Rosentau, A., Harff, J., Meyer, M., Oja, T. (2012). Postglacial rebound and relative sea level changes in the Baltic Sea since the Litorina transgression. *Baltica*, 25(2), pp. 113–120. <https://doi.org/10.5200/baltica.2012.25.11>
- Rosentau, A., Jõelet, A., Plado, J., Aunap, R., Muru, M., Eskola, K. (2013). Development of the Holocene foredune plain in the Narva-Jõesuu area, eastern Gulf of Finland. *Geological Quarterly*, 57(1), pp. 89–100. <http://dx.doi.org/10.7306/gq.1077>
- Rosentau, A., Nirgi, T., Muru, M., Bjursäter, S., Hang, T., Preusser, F., ... Kriiska, A. (2020). Holocene relative shore level changes and Stone Age hunter-gatherers in Hiiumaa Island, eastern Baltic Sea. *Boreas*, 49(4), pp. 783–798.
<https://doi.org/10.1111/bor.12452>
- Rõuk, A.-M., Raukas, A. (1989). Drumlins of Estonia. *Sedimentary Geology*, 62(2–4), pp. 371–384. [https://doi.org/10.1016/0037-0738\(89\)90126-7](https://doi.org/10.1016/0037-0738(89)90126-7)
- Ruffell, A., Pringle, J. K., Forbes, S. (2014). Search protocols for hidden forensic objects beneath floors and within walls. *Forensic Science International*, 237, pp. 137–145. <https://doi.org/10.1016/j.forsciint.2013.12.036>
- Ruffell, A., Parker, R. (2021). Water penetrating radar. *Journal of Hydrology*, 597, 126300. <https://doi.org/10.1016/j.jhydrol.2021.126300>

- Rydin, H., Jeglum, J. K. (2006). Peatland succession and development. *The Biology of Peatlands*, pp. 119–137. Oxford University Press.
<https://doi.org/10.1093/acprof:oso/9780198528722.001.0001>
- Saarenketo, T., Scullion, T. (2000). Road evaluation with ground penetrating radar. *Journal of Applied Geophysics*, 43(2–4), 119–138.
[https://doi.org/10.1016/S0926-9851\(99\)00052-X](https://doi.org/10.1016/S0926-9851(99)00052-X)
- Saarse, L., Vassiljev, J. (2010). Holocene shore displacement in the surroundings of Tallinn, North Estonia. *Estonian Journal of Earth Sciences*, 59(3), pp. 207.
<https://doi.org/10.3176/earth.2010.3.03>
- Salm, J.-O., Kimmel, K., Uri, V., Mander, Ü. (2009). Global warming potential of drained and undrained peatlands in Estonia: a synthesis. *Wetlands*, 29 (4), 1081–1092.
- Sánchez-Aparicio, L. J., Bautista-De Castro, Á., Conde, B., Carrasco, P., Ramos, L. F. (2019). Non-destructive means and methods for structural diagnosis of masonry arch bridges. *Automation in Construction*, 104, pp. 360–382.
<https://doi.org/10.1016/j.autcon.2019.04.021>
- Sandersen, P. B. E., Jørgensen, F. (2003). Buried Quaternary valleys in western Denmark – occurrence and inferred implications for groundwater resources and vulnerability. *Journal of Applied Geophysics*, 53(4), pp. 229–248.
<https://doi.org/10.1016/j.jappgeo.2003.08.006>
- Saponaro, A., Dipierro, G., Cannella, E., Panarese, A., Galiano, A. M., Massaro, A. (2021). A UAV-GPR Fusion Approach for the Characterization of a Quarry Excavation Area in Falconara Albanese, Southern Italy. *Drones*, 5(2), 40.
<https://doi.org/10.3390/drones5020040>
- Satish Kumar, V., Dhakate, R., Amarender, B., Sankaran, S. (2016). Application of ERT and GPR for demarcating the saline water intrusion in coastal aquifers of Southern India. *Environmental Earth Sciences*, 75(5), 393.
<https://doi.org/10.1007/s12665-015-5207-8>
- Schellentrager, G. W., Doolittle, J. A., Calhoun, T. E., Wettstein, C. A. (1988). Using Ground-Penetrating Radar to Update Soil Survey Information. *Soil Science Society of America Journal*, 52(3), pp. 746–752.
<https://doi.org/10.2136/sssaj1988.03615995005200030027x>
- Schmidt, F. (1858). Charte der Silurischen Formation von Ebstland, Nord-Livland und Oesel. 1:1 000 000. Untersuchungen über die silurische Formation von Ebstland, Nord-Livland und Oesel. Dorpat. <https://kirjandus.geoloogia.info/reference/250>
- Sellmann, S., Quigley, M., Duffy, B., Moffat, I. (2022). Ground Penetrating Radar of Neotectonic Folds and Faults in South-Central Australia: Evolution of the Shallow Geophysical Structure of Fault-Propagation Folds with Increasing Strain. *Geosciences*, 12(11), 395. <https://doi.org/10.3390/geosciences12110395>
- Sibul, I.; Plado, J.; Jõelett, A. (2017). Ground-penetrating radar and electrical resistivity tomography for mapping bedrock topography and fracture zones: a case study in Viru-Nigula, NE Estonia. *Estonian Journal of Earth Sciences*, 66(3), pp. 142–151.
<https://doi.org/10.3176/earth.2017.11>
- Sigurdsson, T., Overgaard, T. (1998). Application of GPR for 3-D visualization of geological and structural variation in a limestone formation. *Journal of Applied Geophysics*, 40(1–3), 29–36. [https://doi.org/10.1016/S0926-9851\(98\)00015-9](https://doi.org/10.1016/S0926-9851(98)00015-9)
- Sjöberg, Y., Marklund, P., Pettersson, R., Lyon, S. W. (2015). Geophysical mapping of palsa peatland permafrost. *The Cryosphere*, 9(2), pp. 465–478.
<https://doi.org/10.5194/tc-9-465-2015>

- Slater, L. D., Reeve, A. (2002). Investigating peatland stratigraphy and hydrogeology using integrated electrical geophysics. *Geophysics*, 67(2), pp. 365–378. <https://doi.org/10.1190/1.1468597>
- Slob, E., Sato, M., Olhoeft, G. (2010). Surface and borehole ground-penetrating-radar developments. *Geophysics*, 75(5), pp. 75A103-75A120. <https://doi.org/10.1190/1.3480619>
- Smith, D. G., Jol, H. M. (1995). Ground penetrating radar: antenna frequencies and maximum probable depths of penetration in Quaternary sediments. *Journal of Applied Geophysics*, 33(1–3), pp. 93–100. [https://doi.org/10.1016/0926-9851\(95\)90032-2](https://doi.org/10.1016/0926-9851(95)90032-2)
- Soesoo, A., Nirgi, S., Plado, J. (2020). The evolution of the Estonian Precambrian basement: geological, geophysical and geochronological constraints. *Proceedings of the Karelian Research Centre of the Russian Academy of Sciences*, 2, pp. 18–33. <https://doi.org/10.17076/geo1185>
- Stivriņs, N., Ozola, I., Galka, M. (2017). Drivers of peat accumulation rate in a raised bog: impact of drainage, climate, and local vegetation composition. *Mires and Peat*, (19), pp. 1–19. <https://doi.org/10.19189/MaP.2016.OMB.262>
- Sutinen, R. (1992). Glacial deposits, their electrical properties and surveying by image interpretation and ground penetrating radar. *Geological survey of Finland Bulletin*, 359, pp. 1–123. https://tupa.gtk.fi/julkaisu/bulletin/bt_359.pdf
- Suuroja, K. (2006). *Baltic Klint in North Estonia as Symbol of Estonian Nature* (Miidel, A., Raukas, A., Eds.), pp. 1–224. Ministry of Environment.
- Suuroja, K., Ploom, K., Mardim, T., All, T., Otsmaa, M., Veski, A. (2006). The Explanatory Note to the Geological Maps of Rakvere (6434) Sheet. Geological Survey of Estonia, Tallinn, pp 1–117. [In Estonian]. <https://fond.egt.ee/fond/egf/7812>
- Suuroja, K., Ploom, K. (2016). About the origin of the Vaivara Sinimäed Hills and the Zone of Dislocations. *Bulletin of the Geological Survey of Estonia*, 12, pp. 37–56. [In Estonian]. <https://files.geocollections.info/ac/84/ac847701-0647-404a-bdde-cac2deb61119.pdf>
- Suursaar, Ü., Kall, T., Steffen, H., Tõnisson, H. (2019). Cyclicity in ridge patterns on the prograding coasts of Estonia. *Boreas*, 48(4), pp. 913–928. <https://doi.org/10.1111/bor.12398>
- Suursaar, Ü., Rosentau, A., Hang, T., Tõnisson, H., Tamura, T., Vaasma, T., ... Sugita, S. (2022). Climatically induced cyclicity recorded in the morphology of uplifting Tihu coastal ridgeplain, Hiiumaa Island, eastern Baltic Sea. *Geomorphology*, 404, 108187. <https://doi.org/10.1016/j.geomorph.2022.108187>
- Takahashi, K., Igel, J., Preetz, H., Kuro, S. (2012). Basics and Application of Ground-Penetrating Radar as a Tool for Monitoring Irrigation Process. In Kumar, M. (Ed.), *Problems, Perspectives and Challenges of Agricultural Water Management*. InTech. <https://doi.org/10.5772/29324>
- TALLINN (2019). Creation of a prototype of a technological solution for 3D data monitoring of underground facilities. Tallinn Urban Environment and Public Works Department. https://uuringud.tallinn.ee/file_download/1013. [Accessed 10.12.2022].
- Tamura, T. (2012). Beach ridges and prograded beach deposits as palaeoenvironment records. *Earth-Science Reviews*, 114(3–4), pp. 279–297. <https://doi.org/10.1016/j.earscirev.2012.06.004>
- Tamura, T., Nicholas, W. A., Oliver, T. S. N., Brooke, B. P. (2018). Coarse-sand beach ridges at Cowley Beach, north-eastern Australia: Their formative processes and potential as records of tropical cyclone history. *Sedimentology*, 65(3), pp. 721–744. <https://doi.org/10.1111/sed.12402>

- Tamura, T., Cunningham, A. C., Oliver, T. S. N. (2019). Two-dimensional chronostratigraphic modelling of OSL ages from recent beach-ridge deposits, SE Australia. *Quaternary Geochronology*, 49, pp. 39–44. <https://doi.org/10.1016/j.quageo.2018.03.003>
- Tanneberger, F., Tegetmeyer, C., Busse, S., Barthelmes, A., and 55 others. (2017). The peatland map of Europe. *Mires and Peat*, (19), pp. 1–17. <https://doi.org/10.19189/MaP.2016.OMB.264>
- Tanner, D. C., Buness, H., Igel, J., Günther, T., Gabriel, G., Skiba, P., ... Walter, T. R. (2020). Fault detection. In *Understanding Faults* (pp. 81–146). Elsevier. <https://doi.org/10.1016/B978-0-12-815985-9.00003-5>
- Tao, M., Chen, X., Cheng, Q., Binley, A. (2022). Evaluating the joint use of GPR and ERT on mapping shallow subsurface features of karst critical zone in southwest China. *Vadose Zone Journal*, 21(1). <https://doi.org/10.1002/vzj2.20172>
- Tavast, E., Raukas, A. (1982). *The bedrock relief of Estonia*, pp. 1–194. Valgus, Tallinn. [In Russian].
- TCER (2022). Technical Center of Estonian Roads Ltd. Maaradar <https://www.teed.ee/teenused/katsetamine-ja-mootmine/mootmine/maaradar>. [In Estonian, accessed 10.11.2022].
- Theimer, B. D., Nobes, D. C., Warner, B. G. (1994). A study of the geoelectrical properties of peatlands and their influence on ground-penetrating radar surveying. *Geophysical Prospecting*, 42(3), pp. 179–209. <https://doi.org/10.1111/j.1365-2478.1994.tb00205.x>
- TLU (2022). Tallinn University. Georadar, <https://www.exu.tlu.ee/lab-georadar>. [Accessed 10.12.2022].
- Topp, G. C., Davis, J. L., Annan, A. P. (1980). Electromagnetic determination of soil water content: Measurements in coaxial transmission lines. *Water Resources Research*, 16(3), pp. 574–582. <https://doi.org/10.1029/WR016i003p00574>
- Tosti, F., Slob, E. (2015). Determination, by Using GPR, of the Volumetric Water Content in Structures, Substructures, Foundations and Soil. In Benedetto, A., Pajewski, L. (Eds.), *Civil Engineering Applications of Ground Penetrating Radar*, pp. 163–194. Cham: Springer International Publishing. https://doi.org/10.1007/978-3-319-04813-0_7
- Tronicke, J., Blindow, N., Groß, R., Lange, M. A. (1999). Joint application of surface electrical resistivity- and GPR-measurements for groundwater exploration on the island of Spiekeroog – northern Germany. *Journal of Hydrology*, 223(1–2), pp. 44–53. [https://doi.org/10.1016/S0022-1694\(99\)00111-0](https://doi.org/10.1016/S0022-1694(99)00111-0)
- Tronicke, J., Dietrich, P., Wahlig, U., Appel, E. (2002). Integrating surface georadar and crosshole radar tomography: A validation experiment in braided stream deposits. *GEOPHYSICS*, 67(5), pp. 1516–1523. <https://doi.org/10.1190/1.1512747>
- Tšugai, A., Plado, J., Jõelett, A., Kriiska, A., Mustasaar, M., Raig, H., Risberg, J., Rosentau, A. (2014). Ground-penetrating Radar and Geological Study of the Kudruküla Stone Age Archaeological Site, Northeast Estonia. *Archaeological Prospection*, 21(3), pp. 225–234. <https://doi.org/10.1002/arp.1484>
- Turing, A. M. (1950). I.– Computing machinery and intelligence. *Mind*, LIX(236), pp. 433–460. <https://doi.org/10.1093/mind/LIX.236.433>
- Tuuling, I., Flodén, T. (2016). The Baltic Klint beneath the central Baltic Sea and its comparison with the North Estonian Klint. *Geomorphology*, 263, pp. 1–18. <https://doi.org/10.1016/j.geomorph.2016.03.030>

- Tuuling, I., Põldsaar, K. (2021). The role of the Leba Ridge–Riga–Pskov Fault Zone in the tectonic evolution of the deep-facies Livonian Tongue within the Baltic Ordovician–Silurian sedimentary basin: a review. *Estonian Journal of Earth Sciences*, 70(2), pp. 94–106. <https://doi.org/10.3176/earth.2021.07>
- UT. (2022). University of Tartu. DSpace, <https://dspace.ut.ee/discover?scope=%2F&query=%22ground+penetrating+radar%22&submit=&rpp=10>. [Accessed 10.12.2022].
- Vaher, R., Miidel, A., Raukas, A., Tavast, E. (2010). Ancient buried valleys in the city of Tallinn and adjacent area. *Estonian Journal of Earth Sciences*, 59(1), pp. 37–48. <https://doi.org/10.3176/earth.2010.1.03>
- Vaher, R., Miidel, A., Raukas, A. (2013). Structure and origin of the Vaivara Sinimäed hill range, Northeast Estonia. *Estonian Journal of Earth Sciences*, 62(3), pp. 160–170. <https://doi.org/10.3176/earth.2013.13>
- van Overmeeren, R. A. (1998). Radar facies of unconsolidated sediments in The Netherlands: A radar stratigraphy interpretation method for hydrogeology. *Journal of Applied Geophysics*, 40(1–3), pp. 1–18. [https://doi.org/10.1016/S0926-9851\(97\)00033-5](https://doi.org/10.1016/S0926-9851(97)00033-5)
- Vassiljev, J., Saarse, L., Grudzinska, I., Heinsalu, A. (2015). Relative sea-level changes and development of the Hiiumaa Island, Estonia, during the Holocene. *Geological Quarterly*, 59(3), pp. 517–530. <https://doi.org/10.7306/gq.1227>
- Veldre, M. (1994). Specifying the remnant reserves of the peat production areas in the Harju, Lääne-Viru, Lääne, Rapla, Järva, Jõgeva, Viljandi, Hiiu, Põlva, Saare, Valga and Võru Counties. Varudi Peat Deposit in the Lääne-Viru County. Geological Survey of Estonia, Keila, 47 pp. GA No. 4854. <https://fond.egt.ee/fond/egf/4854>. [In Estonian, accessed 22.11.2022].
- Vilumaa, K., Tõnisson, H., Kont, A., Ratas, U. (2013). Ground-penetrating radar studies along the coast of Estonia. *Journal of Coastal Research*, 65, pp. 612–617. <https://doi.org/10.2112/SI65-104.1>
- Vilumaa, K., Tõnisson, H., Sugita, S., Buynevich, I.V., Kont, A., Muru, M., Preusser, F., Bjursäter, S., Vaasma, T., Vandel, E., Molodkov, A., Järvelill, J.I. (2016). Past extreme events recorded in the internal architecture of coastal formations in the Baltic Sea region. *Journal of Coastal Research*, 75(sp1), pp. 775–779. <https://doi.org/10.2112/SI75-156.1>
- Vissak, R., Vunk, A. (1996). Archaeological surveys using ground penetrating radar in Pärnu and Tartu. *Proceedings of the Estonian Academy of Sciences. Humanities and Social Sciences*, 45, (3), pp. 338–361. [In Estonian, with English summary].
- Wai-Lok Lai, W., Dérobert, X., Annan, P. (2018). A review of Ground Penetrating Radar application in civil engineering: A 30-year journey from Locating and Testing to Imaging and Diagnosis. *NDT & E International*, 96, pp. 58–78. <https://doi.org/10.1016/j.ndteint.2017.04.002>
- Walter, J., Hamann, G., Lück, E., Kligenfuss, C., Zeitz, J. (2016). Stratigraphy and soil properties of fens: Geophysical case studies from northeastern Germany. *Catena*, 142, pp. 112–125. <https://doi.org/10.1016/j.catena.2016.02.028>
- Wang, H., Ouyang, S., Liu, Q., Liao, K., Zhou, L. (2022). Deep-Learning-Based Method for Estimating Permittivity of Ground-Penetrating Radar Targets. *Remote Sensing*, 14(17), 4293. <https://doi.org/10.3390/rs14174293>
- Warner, B. G., Nobes, D. C., Theimer, B. D. (1990). An application of ground penetrating radar to peat stratigraphy of Ellice Swamp, southwestern Ontario. *Canadian Journal of Earth Sciences*, 27(7), pp. 932–938.

- Weaver, W. (2006). Ground-penetrating radar mapping in clay: success from South Carolina, USA. *Archaeological Prospection*, 13(2), pp. 147–150.
<https://doi.org/10.1002/arp.281>
- WIKI. (2022a). Wikipedia. List of countries by length of coastline, https://en.wikipedia.org/wiki/List_of_countries_by_length_of_coastline. [Accessed 10.11.2022].
- WIKI. (2022b). Wikipedia. LAS file format, https://en.wikipedia.org/wiki/LAS_file_format. [Accessed 10.11.2022].
- Wilk, J., Zanetti, M., Losiak, A., Jöeleht, A., Välja, R., Wisniowski, T., Paavel, K., Kukko, A., Kaartinen, H., Plado, J., Zhu, M., Geppert, W.D. (2016). Kaali Impact Crater: A Structural Investigation of a Small Crater Based on 3D Laser Scanning, Strike and Dip Measurements, Ground Penetrating Radar, Electro-Resistivity Tomography and iSale-2D Numerical Modeling. *Meteoritics & Planetary Science*, 51: 79th Annual Meeting of the Meteoritical Society, Berlin, August 7–12, 2016. The Meteoritical Society, 6556. (S1).
- Wolfe, P. J., Richard, B. H. (1996). Integrated Geophysical Studies of Buried Valley Aquifers. *Journal of Environmental and Engineering Geophysics*, 1(1), pp. 75–84.
<https://doi.org/10.4133/JEEG1.1.75>
- Wu, K., Rodriguez, G. A., Zajc, M., Jacquemin, E., Clément, M., De Coster, A., Lambot, S. (2019). A new drone-borne GPR for soil moisture mapping. *Remote Sensing of Environment*, 235, 111456. <https://doi.org/10.1016/j.rse.2019.111456>
- Yamaguchi, T., Mizutani, T., Meguro, K., Hirano, T. (2022). Detecting Subsurface Voids From GPR Images by 3-D Convolutional Neural Network Using 2-D Finite Difference Time Domain Method. *IEEE Journal of Selected Topics in Applied Earth Observations and Remote Sensing*, 15, pp. 3061–3073.
<https://doi.org/10.1109/JSTARS.2022.3165660>
- Zajc, M., Pogačnik, Ž., Gosar, A. (2014). Ground penetrating radar and structural geological mapping investigation of karst and tectonic features in flyschoid rocks as geological hazard for exploitation. *International Journal of Rock Mechanics and Mining Sciences*, 67, pp. 78–87. <https://doi.org/10.1016/j.ijrmms.2014.01.011>
- Zajícová, K., Chuman, T. (2019). Application of ground penetrating radar methods in soil studies: A review. *Geoderma*, 343, pp. 116–129.
<https://doi.org/10.1016/j.geoderma.2019.02.024>
- Zanzi, L., Hojat, A., Ranjbar, H., Karimi-Nasab, S., Azadi, A., Arosio, D. (2019). GPR measurements to detect major discontinuities at Cheshmeh-Shirdoosh limestone quarry, Iran. *Bulletin of Engineering Geology and the Environment*, 78(2), pp. 743–752. <https://doi.org/10.1007/s10064-017-1153-x>
- Zhao, W., Forte, E., Pipan, M., Tian, G. (2013). Ground Penetrating Radar (GPR) attribute analysis for archaeological prospection. *Journal of Applied Geophysics*, 97, pp. 107–117. <https://doi.org/10.1016/j.jappgeo.2013.04.010>
- Zhao, Y., Ling, C., Zhang, K., Gao, Y., Sun, B., Wang, X. (2022). Detection of hidden mining-induced ground fissures via unmanned aerial vehicle infrared system and ground-penetrating radar. *International Journal of Rock Mechanics and Mining Sciences*, 160, 105254. <https://doi.org/10.1016/j.ijrmms.2022.105254>

SUMMARY IN ESTONIAN

Georadar Eestis: välitöödest avaandmete taaskasutuseni

Georadar on geofüüsikaline seade, mis võimaldab uurida pinnast seda otseselt häirimata. Erineva sagedusega (olenevalt seadmest 10–1000 MHz) elektromagnetilisi (EM) laineid maapinda suunates ja seejärel nende tagasipeegeldumise aega mõõtes on võimalik maapõuest koostada kahe- või kolmemõõtmeline läbilõige (radaripilt). Kuna radariga saab eristada eelkõige materjali elektrijuhtivusest ja poorsusest tingitud muutusi, pole radaripilt samaväärne otsese vaatluse (kaevand, paljand, puursüdamik) teel koostatud geoloogilise läbilõikega. Georadari trumbiks on pidev andmevoog suurel alal, mis on otsese mõõtmistega võimalik ainult paljandites. Kõige realistlikuma pildi maapõuest annab otsese ja kaudse meetodi kombinatsioon.

Doktoritöö üheks eesmärgiks seati erinevate settekeskkondade ja pinnase rikkestruktuuride iseloomustamine radaripildidel väljenduvate peegeldusmustrite abil. Autor osales neljal radariuuringul, mille põhjal valmisid teadusartiklid: Rahivere (Uuring I), Ruhnu (Uuring II), Viru-Nigula (Uuring III) ja Sillamäe-Narva (Uuring IV) piirkondade kohta. Töö annab ülevaate nimetatud uuringute olulisematest tulemustest.

Uuring I teostati Jõgevamaal maavarade registrisse kantud Rahivere turba-maardlas, mida profileeriti risti objekti väljavenitatus suunale. EM lainete levikukiiruse täpsustamiseks ja radaripildi peegelduste interpreteerimiseks rajati profiilidele 13 puurauku. Kuna radari abil oli turba ja mineraalpinnase kontakt hästi jälgitav, võimaldas kogutud paksusandmestik arvutada turba mahu maardla piires. Selget madaloo- ja rabaturba piiri ei suudetud radaripildil tuvastada, seega oli võimalik hinnata ainult turba kogumahtu. Võttes arvesse turba aluspinna reljeefi liigestatust, on radariga saadud maht tõenäoliselt täpsem ainult puuraukude alusel arvatud tulemusest.

Uuring II viidi läbi Ruhnu saarel koostöös geograafide ja arheoloogidega, hankimaks uut teavet saare laienemise ja varajase inimasustuse kohta. Kuna radariprofiilidel teostati puurimised koos vanusemäärangutega, oli võimalik uuritud ala pinnavormid paigutada nii ajalisse kui litoloogilisse konteksti. Pärast-jääaegse maakerke tulemusel on saare pindala üha suurenenud, varem rannikul asunud rannavallid (eelluided) on nüüd tekkeaja järgi reastatuna sisemaal. Olulisim radariprofiil kirjeldab katkematult ühe eelluidete jada siseehitust 6900–2500 aastat tagasi. Radaripildidel tuvastati neli peamist settetüüpi: (a) Devoni liivakivi, (b) moreen, (c) rannavööndi liiv-kruus ja (d) tuulesetted.

Uuring III teostati Lääne-Virumaal Viru-Nigula aleviku lähistel. Eesmärgiks oli koguda täiendavat infot geoloogilisel kaardistamisel leitud Varudi mattunud oru kuju ja võimalike tekkepõhjuste kohta. Georadariga profileeriti erinevaid setendeid: (a) Ordoviitsiumi lubjakivi, (b) moreen, (c) liiv-kruus, (d) turvas. Karbonaatset aluspõhja oli võimalik tuvastada kuni 4 m sügavuseni maapinnast. Radaripildidel pakkusid eelkõige huvi korrapärased muutused aluspõhja reljeefis. Sügavamatest nähtustest ülevaate saamiseks kaasati täiendav geofüüsikaline

tööriist – eritakistuse tomograafia. Meetodite kombineerimisel tuvastati kaks lähestikust rikkevööndit, mis löidki soodsa pinnase mattunud oru tekkeks.

Uuring IV toimus Ida-Virumaal, peamiselt Balti klindi vahetus läheduses asuvas Vaivara deformatsioonide vööndis. Sinimägede piirkonda on varem korduvalt geoloogiliselt-geofüüsikaliselt uuritud, kuid seni puudus detailsem ülevaade mandriliustike tekitatud deformatsioonide iseloomust ja ruumilisest levikust. Ida suunas hangiti georadariga teavet kuni Narva kesklinnani. Radaripildidel grupeeriti deformatsioonid intensiivsuse järgi, alates vaevumärgatavatest lainetustest kuni rikete ja kurdudeni. Kui deformatsioonid sellise jaotuse põhjal kaardile lisati, hakkasid kohati ilmema erikujuliste aluspõhjaliste plokkide kontuurid. Nende selgemaks eristamiseks on tarvis kaasata täiendavaid uurimismeetodeid.

Autori isiklike kogemuste ja kirjandusallikate alusel antakse töös soovitusi georadari kasutamiseks rakenduslikel uuringutel. Radarit saab edukalt tarvitada turba, liiva, kruusa, moreeni ja lubjakivi leviku ning aluspõhja reljeefi kaardistamisel, mitmesuguste aluspõhjaliste rikete ja deformatsioonide kirjeldamisel. Kuna meetod tugineb suuresti setendite veesisalduse ja poorsuse erinevustele, pakub ta tuge ka hüdroteoloogidele, piiritlemaks näiteks karstinähtusi, põhjaveekomplekse, veetaset ja reostuse ulatust pinnases.

Töös analüüsitakse georadari potentsiaali turba, liiva, kruusa ja karbonaatkivimite varude piiritlemisel ja mahtude hindamisel. Õigusaktide kohaselt tuleb maavarauuringute käigus võtta nõutud tihedusega proove, seega ei saa ainult radariandmete põhjal arvutada kaevandatavaid maavaravarusid. Kuid seadet on mõistlik kasutada näiteks (a) proovivõtupunktide asukoha täpsustamiseks, (b) kvaliteetsema maavara ja geoloogiliste takistuste (karstivormid, rikkevööndid jt) leidmiseks nii uuringu käigus kui kaevandamise ajal, (c) radaripildil eristuva settekeha kogumahu arvutamiseks. Keerulisemas geoloogilises situatsioonis võimaldab radar säästa puurtöödele kuluvat aega ja raha. Olenemata uuringu eesmärgist, tuleks radari läbilõiked alati siduda otseste vaatlusandmetega.

Doktoritöö teiseks eesmärgiks seati Eesti seniste georadari kasutamiskogemuste ülevaate koostamine, tutvustades seejärel uusi võimalusi välitöö aparatuuri valikuks ning tulemuslikumaks andmete järeltöötamiseks. Varasem praktika on liigitatud nelja kategooriasse: (a) turba-, (b) rannasetete-, (c) karbonaatkivimite- ja (d) muud uuringud. Pindalaliselt on Eestis seni kõige rohkem käsitletud soid, enim teadusartikleid on publitseeritud rannavormide arengu kohta. Uurimus on valdavalt geoloogilise suunitlusega, kuid põgusalt käsitletakse ka teisi radari kasutusvaldkondi – arheoloogiat, ehitust, teede ja maa-aluste tehnovõrkude käitamist.

Aeganõudev radariandmete töötlus ajendas autorit tegema ettepanekuid selle etapi lihtsustamiseks. Osa neist ideedest võiks huvi pakkuda ka radariseadmete ja -tarkvarade arendajatele. Geoinfosüsteemidest tuntud võimaluste juurutamine radariprogrammides lihtsustaks välitöö planeerimist ning andmete järeltöötlust. Radaripilte saaks kiiremini interpreteerida masinõppe algoritmide abil. Usaldusväärsete automaatsete tulemuste saamine eeldab rohkelt treeningandmeid erinevatest piirkondadest ja geoloogilistest nähtustest. Autori osalusel toimunud radariuuringute (I–IV) profiilid on kättesaadavad Maa-ameti geoportaalil. Seal

võiks olla hulk teisigi profiile koos radaripiltide interpretatsioonidega. Alates 2021. aastast saab iga uuringu teostaja oma tõlgendused uuringupunktidenä üles laadida Maa-ameti maardlate veebileideses.

Lähiaastatel plaanib Maa-amet võtta kasutusele kaardistusplatvormi Geo3D, kus lisaks maapealsetele objektidele hakatakse ka maapõue kujutama ruumiliselt ning võimalikult realistlikult. Avaandmetena aitaks iga radariuuringu interpretatsioonid värskendada Geo3D maa-alust moodulit. Koos teiste geoloogiliste andmetega muutuvad nad järgnevate uuringute kõige täpsemaks ja ajakohasemaks sisendiks. Parim teadmus maapõuest peab olema kõigile lihtsalt ja tasuta kättesaadav – nii saavad sündida parimad otsused, alates uue välitöö asukoha valikust kuni riiklikult oluliste teemadeni.

ACKNOWLEDGEMENTS

I express the utmost thanks to my supervisor Jüri Plado. You have guided me on my academic path as a reliable and inspiring mentor. I am sincerely happy about our common routes over the past decades. Argo Jõelet is highly appreciated for the fruitful instructions and discussions. Your expertise in the Estonian ground-penetrating radar research is invaluable. Since my first hesitant steps in the UT, Prof. Tõnu Meidla has consistently planted geological knowledge in me. Your support and honest feedback earn my full respect. I am also very grateful to all the fellow students participating in the fieldworks. The contribution of Mario Mustasaar must be especially underlined.

The probability to resolve geological puzzles rises considerably with financial backup. The four case studies described in the thesis were supported by the following projects: SF0180069s08, ETF9011, PUT456, IUT20-7, IUT20-34, and ETF7860.

Estonian Journal of Earth Sciences is recommended as an excellent output medium for applied geophysics.

The Department of Geology in the Land Board deserves eternal gratitude for balancing my workload at the critical moments. Reet, your continuous encouragement and competent advice have been absolutely essential.

Finally, special thanks to my beloved wife Kai and our fantastic daughters Merli, Kadri, and Roosli. I would not be at this point without the curiosity, energy, and love you all passed on to me.

PUBLICATIONS

CURRICULUM VITAE

Name Ivo Sibul
Date of birth 9 June 1979
E-mail ivo.sibul@maaamet.ee, ivo.sibul@gmail.com

Education

2012–2022 University of Tartu, doctoral studies in geology
2009 University of Tartu, MSc in geology
2002 University of Tartu, BSc in geology
1996 Tartu Miina Härma Gymnasium

Work experiences

2016–... Estonian Land Board, Department of Geology, advisor
2005–2016 Estonian Land Board, Department of Geology, chief specialist
2002–2005 Columbia-Kivi Ltd., technologist

Field of activity

Land Board's geological databases and services: data management, sharing, and analysis, participation in developments

Organisational affiliation

Geological Society of Estonia
Estonian Commission on Stratigraphy
Estonian Geoinformatics Society

Publications

- Plado, J., Sibul, I., Mustasaar, M., Jõelet, A. 2011. Ground-penetrating radar study of the Rahivere peat bog, eastern Estonia. *Estonian Journal of Earth Sciences*, 60(1), pp. 31–42.
- Sibul, I., Plado, J., Jõelet, A. 2017. Ground-penetrating radar and electrical resistivity tomography for mapping bedrock topography and fracture zones: a case study in Viru-Nigula, NE Estonia. *Estonian Journal of Earth Sciences*, 66(3), pp. 142–151.
- Muru, M., Rosentau, A., Preusser, F., Plado, J., Sibul, I., Jõelet, A., Bjursäter, S., Aunap, R., Kriiska, A. 2018. Reconstructing Holocene shore displacement and Stone Age palaeogeography from a foredune sequence on Ruhnu Island, Gulf of Riga, Baltic Sea. *Geomorphology*, 303, pp. 434–445.
- Jõelet, A., Sibul, I., Mustasaar, M., Plado, J. 2022. Bedrock deformations in northeastern Estonia based on ground-penetrating radar data. *Estonian Journal of Earth Sciences*, 71(4), pp. 189–200.

Conference abstracts

- Jõelet, A., Plado, J., Sibul, I. (2009). Ground-penetrating radar investigation of peatlands: Selisoo and Rahivere case studies. In Kalm, V., Laumets, L., Hang, T. (Eds.), *Extent and timing of the Weichselian Glaciation southeast of the Baltic Sea: Abstracts & Guidebook: The INQUA Peribaltic Working Group Field symposium in southern Estonia and northern Latvia, September 13–17, 2009*. Tartu University Press, Tartu, pp. 20–22.
- Sibul, I. (2014). The present and future of the Geological Base Map. In Suuroja, K., Põldvere, A. (Eds.), *From Geology to Society: XXII April Conference Abstracts*. Geological Survey of Estonia, Tallinn, pp. 35–38 [In Estonian].
- Sibul, I., Pruulmann, O. (2015). The living geological map: possible input data and usage potential. In Suuroja, K., Põldvere, A., Kaljuläte, K. (Eds.), *About the Estonian Subsurface Strategy: XXIII April Conference Abstracts*. Geological Survey of Estonia, Tallinn, pp. 25–27 [In Estonian].
- Sibul, I., Plado, J., Jõelet, A. (2016). Location of the Varudi Valley (Viru-Nigula) according to the ground-penetrating radar and electrical measurements. In Suuroja, K., Põldvere, A., Kaljuläte, K. (Eds.), *Exploiting the Subsurface vs. Environmental Protection: XXIV April Conference Abstracts*. Geological Survey of Estonia, Tallinn, pp. 22–23 [In Estonian].

ELULOOKIRJELDUS

Nimi Ivo Sibul
Sünniaeg 9. juuni 1979
E-post ivo.sibul@maaamet.ee, ivo.sibul@gmail.com

Haridus

2012–2022 Tartu Ülikooli geoloogia eriala doktorantuur
2009 Tartu Ülikooli geoloogia eriala magister (MSc)
2002 Tartu Ülikool, geoloogia eriala bakalaureus (BSc)
1996 Tartu Miina Härma Gümnaasium

Töökogemus

2016–... Maa-ameti geoloogia osakond, nõunik
2005–2016 Maa-ameti geoloogia osakond, peaspetsialist
2002–2005 AS Columbia-Kivi, tehnoloog

Töövaldkond

Maa-ameti geoloogilised andmebaasid ja -teenused: andmete haldamine ja levitamine, analüüsid, arendustes osalemine

Liikmesus erialaühendustes

Eesti Geoloogia Selts
Eesti Stratigraafia Komisjon
Eesti Geoinformaatika Selts

Publikatsioonid

- Plado, J., Sibul, I., Mustasaar, M., Jõelet, A. 2011. Ground-penetrating radar study of the Rahivere peat bog, eastern Estonia. *Estonian Journal of Earth Sciences*, 60(1), 31–42.
- Sibul, I., Plado, J., Jõelet, A. 2017. Ground-penetrating radar and electrical resistivity tomography for mapping bedrock topography and fracture zones: a case study in Viru-Nigula, NE Estonia. *Estonian Journal of Earth Sciences*, 66(3), 142–151.
- Muru, M., Rosentau, A., Preusser, F., Plado, J., Sibul, I., Jõelet, A., Bjursäter, S., Aunap, R., Kriiska, A. 2018. Reconstructing Holocene shore displacement and Stone Age palaeogeography from a foredune sequence on Ruhnu Island, Gulf of Riga, Baltic Sea. *Geomorphology*, 303, 434–445.
- Jõelet, A., Sibul, I., Mustasaar, M., Plado, J. 2022. Bedrock deformations in northeastern Estonia based on ground-penetrating radar data. *Estonian Journal of Earth Sciences*, 71(4), 189–200.

Konverentsiteesid

- Jõelett, A., Plado, J., Sibul, I. (2009). Ground-penetrating radar investigation of peatlands: Selisoo and Rahivere case studies. *Extent and timing of the Weichselian Glaciation southeast of the Baltic Sea: Abstracts & Guidebook: The INQUA Peribaltic Working Group Field symposium in southern Estonia and northern Latvia, September 13–17, 2009*, toim. Kalm, V., Laumets, L., Hang, T. Tartu Ülikooli Kirjastus, Tartu, 20–22.
- Sibul, I. (2014). Geoloogilise baaskaardi olevik ja tulevik. *Geoloogialt ühiskonnale: XXII Aprillikonverentsi teesid*, toim. Suuroja, K., Põldvere, A. Eesti Geoloogiakeskus, Tallinn, 35–38.
- Sibul, I., Pruulmann, O. (2015). Elav geoloogiline kaart: võimalikud sisendandmed ja kasutamise potentsiaal. *Eesti maapõue strateegiast: XXIII Aprillikonverentsi teesid*, toim. Suuroja, K., Põldvere, A., Kaljuläte, K. Eesti Geoloogiakeskus, Tallinn, 25–27.
- Sibul, I., Plado, J., Jõelett, A. (2016). Varudi oru (Viru-Nigula) asend georadari ja elektrometria abil. *Maapõuekasutus ja keskkonnahoid: XXIV Aprillikonverentsi teesid*, toim. Suuroja, K., Põldvere, A., Kaljuläte, K. Eesti Geoloogiakeskus, Tallinn, 22–23.

DISSERTATIONES GEOLOGICAE UNIVERSITATIS TARTUENSIS

1. **Пээп Мянник.** Конодонты в верхнеордовикских и нижнесилурийских отложениях Эстонии. Тарту, 1992, 355 с.
2. **Elvi Tavast.** Fennoskandia kilbi lõunanõlva ja sellega piirnevate alade alus- põhja reljeef. Tartu, 1992, 357 lk.
3. **Kaarel Orviku.** Characterisation and evolution of Estonian seashores. Tartu, 1992, 19 p.
4. **Анатолий Молодьков.** ЭПР-анализ скелетного вещества моллюсков в хроностратиграфических исследованиях позднего кайнозоя. Тарту, 1992, 33 с.
5. **Jaan Lutt.** Late- and postglacial deposits on the Estonian shelf. Tartu, 1993, 31 p.
6. **Reet Karukäpp.** Gotiglatsiaalne morfogenees Skandinaavia mandriliustiku kagusektoris. Tartu, 1997, 181 p.
7. **Argo Jõelett.** Geothermal studies of the Precambrian basement and Phanerozoic sedimentary cover in Estonia and Finland. Tartu, 1998, 125 p.
8. **Jüri Nemliher.** Mineralogy of Phanerozoic skeletal and sedimentary apatites: an XRD study. Tartu, 1999, 134 p.
9. **Kalle Kirsimäe.** Clay mineral diagenesis on the Lower Cambrian “Blue Clay” in the northern part of the Baltic Paleobasin. Tartu, 1999, 113 p.
10. **Jüri Plado.** Gravity and magnetic signatures of meteorite impact structures. Tartu, 2000, 87 p.
11. **Olev Vinn.** Morphogenesis and phylogenetic relationships of Clitambonitidines, Ordovician Brachiopods. Tartu, 2001, 127 p.
12. **Leho Ainsaar.** The middle Caradoc facies and faunal turnover in the late Ordovician Baltoscandian palaeobasin: sedimentological and carbon isotope aspects. Tartu, 2001, 109 p.
13. **Oive Tinn.** Early Ostracode evolution and Palaeoenvironmental application in the Ordovician of Baltoscandia. Tartu, 2002, 145 p.
14. **Maris Rattas.** Subglacial environments in the formation of drumlins — The case of the Saadjärve Drumlin Field, Estonia. Tartu, 2004, 117 p.
15. **Ene Kadastik.** Upper-Pleistocene stratigraphy and deglaciation history in northwestern Estonia. Tartu, 2004, 129 p.
16. **Helje Pärnaste.** Early Ordovician trilobites of suborder Cheirurina in Estonia and NW Russia: systematics, evolution and distribution. Tartu, 2004, 138 p.
17. **Mari-Ann Mõtus.** Silurian (Llandovery-Wenlock) tabulate corals of Baltoscandia: taxonomy, palaeoecology, distribution. Tartu, 2005, 167 p.
18. **Alar Rosentau.** Development of proglacial lakes in Estonia. Tartu, 2006, 114 p.
19. **Evelin Verš.** Development of impact-induced hydrothermal system at Kärddla impact structure. Tartu, 2006, 96 p.

20. **Sigitas Radzevičius.** The genus *Pristiograptus* in wienlock of East Baltic and the Holy Cross Mountains. Tartu, 2007, 133 p.
21. **Andres Marandi.** Natural chemical composition of groundwater as a basis for groundwater management in the Cambrian-Vendian aquifer system in Estonia. Tartu, 2007, 116 p.
22. **Eve Niinemets.** Vegetation and land-use history of the Haanja Heights (SE-Estonia) during the holocene. Tartu, 2008, 146 p.
23. **Kalle-Mart Suuroja.** Geology and lithology of the early palaeozoic marine impact structures Kärddla and Neugrund (Estonia). Tartu, 2008, 234 p.
24. **Rutt Hints.** Early diagenesis of Ordovician and Silurian Bentonites in the Northern Baltic Palaeobasin. Tartu, 2009, 90 p.
25. **Peeter Somelar.** Illitization of K-bentonites in the Baltic Basin. Tartu, 2009, 118 p.
26. **Ulla Preeden.** Remagnetizations in sedimentary rocks of Estonia and shear and fault zone rocks of southern Finland. Tartu, 2009, 121 p.
27. **Kati Tänavsuu-Milkeviciene.** Transgressive to regressive turnaround in the Middle Devonian Baltic Basin. Tartu, 2009, 106 p.
28. **Valle Raidla.** Chemical and isotope evolution of groundwater in the Cambrian-Vendian aquifer system in Estonia. Tartu, 2010, 134 p.
29. **Kadri Sohar.** Quaternary ostracods from Estonia and their application in palaeoenvironmental reconstruction. Tartu, 2010, 140 p.
30. **Kristjan Urtson.** Stepwise melt transport and accumulation: analogue and numerical modelling approach. Tartu, 2011, 83 p.
31. **Marko Kohv.** Landslides in clayey soils of western Estonia. Tartu, 2011, 116 p.
32. **Nele Muttik.** Post-impact alteration of impactites: Ries crater, Germany. Tartu, 2011, 78 p.
33. **Annette Sedman.** Strength and self-cementing properties of oil shale retorting wastes. Tartu, 2013, 82 p.
34. **Arkady Tsyrunnikov.** Complex seismo-acoustic and lithological study of the Lateglacial and postglacial sediments northern Gulf of Riga, eastern branch of the central Baltic Sea. Tartu, 2013, 102 p.
35. **Marge Uppin.** Geological sources and hydrochemistry of fluoride and boron in Silurian-Ordovician aquifer system. Tartu, 2013, 86 p.
36. **Peeter Talviste.** Temporal changes in weak natural and artificial soils – influence on geotechnical characteristics. Tartu, 2014, 204 p.
37. **Katrin Lasberg.** Chronology of the Weichselian Glaciation in the south-eastern sector of the Scandinavian Ice Sheet. Tartu, 2014, 100 p.
38. **Sirle Liivamägi.** Neoproterozoic Baltic paleosol: geology and paleoenvironmental interpretation. Tartu, 2015, 94 p.
39. **Lauri Joosu.** Petrography and the rare earth element composition of apatite in 2 Ga Onega and Pechenga basins, Russia: the environmental settings for phosphogenesis. Tartu, 2015, 139 p.
40. **Liisa Lang.** Baculate shell structure in Early Palaeozoic linguliform brachiopods. Tartu, 2015, 114 p.

41. **Päärn Paiste.** Geopolymeric potential of the Estonian oil shale processing waste. Tartu, 2017, 125 p.
42. **Mikk Gaškov.** Stable isotope and fluid inclusion evidence of multistage fluidal activity in Baltic paleobasin: Silurian carbonate sequence in Kalana, Estonia. Tartu, 2017, 104 p.
43. **Viirika Mastik.** Silurian noncalcified macroscopic algal fossils from the Kalana *Lagerstätte*, Estonia. Tartu, 2018, 91 p.
44. **Kairi Põldsaar.** Soft-sediment deformation and gravity flow structures in the Lower Palaeozoic successions of the Baltic Basin. Tartu, 2019, 105 p.
45. **Timmu Kreitsmann.** Application of carbon isotope and rare earth elements as recorders of environmental conditions in the aftermath of the Paleoproterozoic Lomagundi-Jatuli Event. Tartu, 2020, 163 p.
46. **Triine Nirgi.** Holocene relative shore-level changes and geoarchaeology of the prehistoric sites in western Estonia. Tartu, 2020, 161 p.
47. **Kristjan Leben.** Long-term diagenetic transformation and carbon sequestration potential of Ca-rich oil shale ash waste deposit sediments. Tartu, 2021, 117 p.
48. **Karin Truuver.** Ostracod associations of the ordovician–silurian boundary interval in baltoscandia. Tartu, 2021, 132 p.
49. **Kaarel Lumiste.** Phosphogenesis and REE+Y diagenesis of Recent and Paleozoic phosphorites. Tartu, 2021, 174 p.
50. **Sigrid Soomer.** Palaeoweathering record of the Archaean–Proterozoic transition in the Imandra–Varzuga Greenstone Belt, north-western Russia. Tartu, 2022, 114 p.